Topics in large scale clustering statistics in cosmology

by

Milad Noorikuhani

A dissertation submitted in partial fulfillment

of the requirements for the degree of

Doctor of Philosophy

Department of Physics

New York University

May, 2024

Professor Roman Scoccimarro

Acknowledgments

First and foremost, I would like to thank my advisor Professor Roman Scoccimarro for his guidance and patience over the past several years. He is also a wonderful teacher and I learned many things from him.

I'm grateful to Professor Jeremy Tinker for the opportunity to work with him on a Machine Learning project which was very educational and useful for me.

I would also like to thank Professor Michael Blanton for his detailed comments on the thesis manuscript which helped improve its language and content.

Finally, I would like to thank my family and dedicate this work to them as they have been the greatest source of inspiration and love for me throughout my PhD years.

Abstract

Recent and upcoming surveys of galaxies at large scales provide a wealth of information about cosmological physics and its underlying fundamental theories. To ensure efficient and maximal extraction of such information, we need accurate modeling of galaxy clustering at those scales and also an estimate of systematic errors that can be caused by simplifying assumptions in such models. Whatever factors that affect the redshift and trajectory of observed light rays from galaxies will also impact our inference of clustering features from observations. One of these factors is the pattern of peculiar velocities of galaxies that alter their measured redshift. These type of effects are generally referred to as"redshift space distortions" (RSD) and can be modeled by attributing galaxy velocities to a large scale "bulk motion" of bound dark matter halos plus a virialized contribution from motions within halos. Each of these are modeled differently and have different effects on the statistics of observed galaxy density fluctuations. One simplifying assumption that is usually made in statistical analyses of the clustering data in Fourier space is that all line-of-sight vectors (vectors that connect observers on Earth to a point/galaxy in the sky) are parallel. Corrections beyond this assumption are usually called "wide-angle effects." Another factor is the perturbed space-time background of the universe, which impacts both redshifts and trajectories of observed light rays. This is usually considered as part of the "relativistic corrections". In the first two parts of this thesis we investigate the impact of wide-angle effects on statistics like galaxy power spectrum and bispectrum and provide simple methods to incorporate them. We also compare the magnitude of these effects with that of the relativistic corrections.

In the third part of this thesis we provide a simple model for the galaxy bispectrum in redshift space that incorporates the so-called Fingers-of-God (FoG) contributions which are part of the above-mentioned RSD. FoG is a term that refers to an apparent weakening of the observed galaxy clustering signal that emanates from the virial velocities of galaxies within gravitationally bound structures like clusters.

Contents

List of Figures

List of Appendices

1 Introduction

Physical cosmology is a branch of science that deals with understanding the origin of the universe and aims to describe its large-scale structure. The standard model of cosmology, referred to as ΛCDM, is a mathematical theory of the universe that assumes the energy momentum budget of the universe can be allocated to a constant dark energy component (Λ), cold dark matter (CDM), ordinary matter (baryons) and radiation (photons and neutrinos). The universe at large scales can be considered as approximately homogeneous and isotropic and the dynamics of its background spacetime can be described by Friedmann–Lemaître–Robertson–Walker (FLRW) models [89, 7].

However we know that perfect homogeneity will not permit formation of structures, because by structure we mean some kind of clumpiness that deviates from homogeneity. Theories like inflation (a period of accelerated expansion in the early universe) provide a mathematical model for seeding primordial inhomogeneities in the space-time of the universe through amplification of quantum fluctuations. After inflation, matter in the universe will co-evolve with this perturbed background, leading to the formation of structures by gravitational instability. According to ΛCDM, the dominant component of matter in the universe is cold dark matter, which can be considered as a pressureless "dust". The ratio of the ordinary (visible) matter density to dark matter density is about 0.2 according to observations of the cosmic microwave background and big-bang nucleosynthesis [70].

Within this picture, studying the inhomogeneities in the universe can provide a myriad of constraints on cosmological theories. The dark matter overdensity, or density fluctuation ampli-

tude, can be simply defined as:

$$\delta(\vec{x},\tau) = \frac{\rho(\vec{x},\tau) - \bar{\rho}(\tau)}{\bar{\rho}(\tau)}\,, \tag{1.1}$$

which quantifes the deviation from homogeneity. Here $\bar{\rho}(\tau)$ is the average density at a given time, $\vec{x}$ is a comoving vector position of a point and τ is the conformal time (the conformal time, τ, is related to the "cosmic" time, t, via the relation $\mathrm{d}\tau = \mathrm{dt/a(t)}$ where a is the scale factor of the universe). An important statistic that can be built out of this quantity is the two-point correlation function defined as:

$$\zeta(\vec{r}) = \langle \delta(\vec{x})\delta(\vec{x}+\vec{r})\rangle \tag{1.2}$$

for overdensities separated by $\vec{r}$. For an isotropic universe , $\zeta(\vec{r}) = \zeta(r)$, i.e it only depends on the magnitude of the separation vector. The Fourier transform of this quantity is called the power spectrum, $P(\vec{k})$, and is defined as:

$$\delta_D(\vec{k}_1 + \vec{k}_2)P(\vec{k}_1) = \langle \delta(\vec{k}_1)\delta(\vec{k}_2)\rangle \tag{1.3}$$

where $\delta(\vec{k})$ is the Fourier transform of the overdensity and δ_D is the Dirac delta function. Again, for an isotropic universe, $P(\vec{k}) = P(k)$.

The dynamics of the density fluctuation is in general complicated. However when we are interested in overdensities at large scales , i.e. large separations in Eq (1.2) or equivalently small $k's$ in Eq. (1.3), dark matter can be approximated as a pressureless fluid obeying the continuity

and Euler equations in an expanding universe:

$$\dot{\delta} + \nabla \cdot [(1+\delta)\vec{v}] = 0, \tag{1.4}$$

$$\dot{\vec{v}} + (\vec{v} \cdot \nabla)\vec{v} = -\mathcal{H}\vec{v} - \nabla\phi, \tag{1.5}$$

$$\nabla^2\phi = 4\pi G a^2 \bar{\rho}\delta \tag{1.6}$$

where a dot is a derivative with respect to the conformal time $(\partial/\partial\tau)$, ∇ is the gradient with respect to comoving coordinates $(\vec{x})$ and $\vec{v} = \mathrm{d}x/\mathrm{d}\tau$ is the peculiar velocity of the fluid particles. For these equations we have assumed that the corresponding separation scales are still much smaller than the Hubble horizon of the universe and therefore we can use Newtonian gravity to incorporate the effects of space-time perturbations (gravitational instabilities) . This allows us to use the Poisson equation with gravitational potential ϕ where ϕ is originally seeded during inflation and is later sourced by density fluctuations. The other parameter is the conformal Hubble parameter, $\mathcal{H} = aH = (da/d\tau)/a$ where a is the scale factor of the universe and H is the Hubble parameter. We also assume no vorticity here such that $\vec{v}$ is curl free and can be described by its divergence, $\theta_v = \nabla \cdot \vec{v}$.

We can then take Fourier transform of δ (δ_k) and θ_v $(\theta_{v,k})$ and find their evolution in Fourier space by solving the equations above. At very large scales, e.g. when $k < 0.1$ h/Mpc, we are in the "linear" regime, meaning that we can neglect δ^2 or θ^2 terms. In this regime the evolution of the dark matter overdensities from those equations is simply given by:

$$\delta(\vec{k},\tau) = D_+(\tau)\delta(\vec{k},\tau_0) + D_-(\tau)\delta(\vec{k},\tau_0), \quad \theta_v(\vec{k},\tau) = -\mathcal{H}f\delta(\vec{k},\tau) \tag{1.7}$$

where D_+ is called the linear growth factor that depends on cosmological parameters, D_- is a decaying factor that can usually be neglected and $f \equiv \mathrm{d}\left(\ln D_+\right)/\mathrm{d}\left(\ln a\right)$ quantifies the growth rate.

This simple picture starts to break down as we enter smaller scales, $k \gtrsim 0.1$ h/Mpc, where nonlinear gravitational effects become important. At these scales, one needs to solve nonlinear coupled Eqs. (1.4)-(1.6). One approach to solve these equations that is relatively successful at "quasi-linear" scales (roughly $0.1\,\mathrm{h/Mpc} \lesssim k \lesssim 0.3\,\mathrm{h/Mpc}$) is to expand the fields (δ_k, $\theta_{v,k}$) in terms of their linear counterparts and solve the equations perturbatively. This is the practice of Standard Perturbation Theory (SPT) which we also use in this dissertation. The non-linear (or quasi-linear) density and velocity divergence fields can be expanded as:

$$\delta_k(\tau) = \sum_{n=1}^{\infty} \int d^3q_1 ... \int d^3q_n \delta^D(\vec{k} - \sum_{i=1}^{n} \vec{q}_i)\, F_n(\vec{q}_1, \vec{q}_2, ..., \vec{q}_n, \tau)\, \delta_{\rm lin}(\vec{q}_1, \tau) ... \delta_{\rm lin}(\vec{q}_n, \tau) \tag{1.8}$$

$$\theta_k(\tau) = \tag{1.9}$$
$$-\mathcal{H}(\tau) f(\tau) \sum_{n=1}^{\infty} \int d^3q_1 ... \int d^3q_n \delta^D(\vec{k} - \sum_{i=1}^{n} \vec{q}_i)\, G_n(\vec{q}_1, \vec{q}_2, ..., \vec{q}_n, \tau)\, \delta_{\rm lin}(\vec{q}_1, \tau) ... \delta_{\rm lin}(\vec{q}_n, \tau)$$

where the evolution of $\delta_{\rm lin}(\vec{q}, \tau)$ can be described by Eq (1.7) and SPT density and velocity kernels F_n and G_n (symmetrized under exchange of $\vec{q}$'s) are calculated from the equations of motion.

Returning to the definition of dark matter power spectrum, Eq (1.3), whenever we use linear density fluctuations, we refer to the power spectrum as the linear power spectrum. The corrections to the linear power spectrum coming from higher order terms (higher powers of $\delta_{\rm lin}$'s) are usually referred to as "loop corrections." We can immediately see that the linear power spectrum is proportional to D_+^2 and measuring it will provide information about D_+, which itself depends on cosmological parameters.

Most models of inflation predict that primordial space-time fluctuations have a Gaussian distribution with zero mean. This also makes the linear density fluctuation, $\delta_{\rm lin}$, Gaussian distributed. This implies that the linear power spectrum alone will contain all the statistical information. However, from the two equations above, we can see that nonlinear evolution leads to "non-Gaussianity" of matter and velocity fluctuations as they are expanded in terms of higher powers of $\delta_{\rm lin}$. This leads to non-vanishing three-point correlation functions of these fields. Therefore,

the Bispectrum, defined as:

$$B(\vec{k}_1, \vec{k}_2)\, \delta_D(\vec{k}_1 + \vec{k}_2 + \vec{k}_3) = \langle \delta(\vec{k}_1)\delta(\vec{k}_2)\delta(\vec{k}_3) \rangle \,, \tag{1.10}$$

is another important statistic that "complements" the power spectrum and contains information about nonlinear gravitational evolution. Also to explain some terminology, the leading order bispectrum is usually called "tree-level" and higher order corrections to it are called loop corrections.

To study structure in the universe, we observe the visible matter, which leads to the following challenges: First we need to relate the density fluctuations of the visible matter to those of the dark matter. This is in general a challenging task, especially in the nonlinear regime. However, at larger scales, we can do this with the help of "bias" parameters. In the linear regime, the simplest form of bias relates the linear density fluctuations of the visible matter to those of the dark matter with the simple linear relation:

$$\delta_g = b\, \delta \tag{1.11}$$

where b is an order one constant. The subscript g here refers to galaxies, because we usually observe the clustering of galaxies and they represent clustering of visible matter at large scales. In this dissertation and elsewhere, we also use the term "tracer," which simply means the objects that trace dark matter. In the nonlinear regime, several other bias parameters are also introduced to relate galaxy overdensity to nonlinear combinations of dark matter overdensities.

Another challenge comes from the fact that the redshifts and trajectories of light rays from tracers that are observed on Earth have undergone changes compared to what would be expected if they simply traveled in a perfectly homogeneous FLRW expanding universe. In that case, the light will simply be redshifted due to Hubble expansion. But in the presence of inhomogeneity, tracers will have peculiar velocities, and those velocities add an extra redshift/blueshift contribution to the Hubble redshift of the light ray that is emitted from them. These changes in redshift

impact our inference of comoving distances, because we rely on redshift measurements to calculate the comoving distance to tracers. Consequently, these changes in our inference of distances leads to changes in our inference of overdensities. These effects are usually referred to as redshift space distortions (RSD).

The comoving position of a tracer/galaxy in redshift space (measured from the observed redshift) is given by:

$$\vec{s} = \vec{x} + \hat{x}\,(\vec{v}_g \cdot \hat{x})/\mathcal{H} \tag{1.12}$$

where $\vec{s}$ represents the vector of comoving coordinates in redshift space, $\vec{x}$ is the vector of comoving coordinates in "real space" and $\vec{v}_g$ is the peculiar velocity of the galaxy. It can be shown that this change in coordinates leads to the following modified relation for the redshift space density fluctuation at a comoving position $\vec{x}$ [103]:

$$\delta_{g,s}(\vec{x}) = \int \frac{d^3x'd^3k}{(2\pi)^3} e^{i\vec{k}\cdot(\vec{x}-\vec{x}')} \{e^{-i\frac{1}{\mathcal{H}}(\vec{k}\cdot\hat{x}')(\vec{v}_g(\vec{x}')\cdot\hat{x}')}[1+\delta_g(\vec{x}')] - 1\}\,. \tag{1.13}$$

Here a subscript s signifies the redshift space parameter. We can see that if $\vec{v}_g = 0$, then $\delta_{g,s}(\vec{x}) = \delta_g(\vec{x})$.

This effect can have two types of consequences depending on the source of $\vec{v}_g$. The component of the peculiar velocity that is attributed to the large scale evolution, the one whose divergence can be studied from equations like (1.4)-(1.6), leads to an enhancement in clustering (or clumpiness) along the line-of sight. This phenomenon is usually referred to as the Kaiser effect [67]. The other component which originates from virial equilibrium at smaller gravitationally bound systems like galaxy clusters results in a weakening (elongation) of the clustering signal along the line-of-sight. This is usually referred to as the Fingers-of-God (FoG) effect.

In addition to RSD, the perturbed spacetime background also causes the redshift and trajectory of light rays to change. As an example, a light ray traveling towards us can, on its way, fall in a gravitational potential well and climb out of it. However due to the expansion of the universe, the

gravitational potential well gets more "shallow" as the light emerges out of it compared to when the ray entered it. This phenomenon, which is part of the “Integrated Sachs Wolfe effect,” leads to a net blueshift or redshift of the light ray (depending on whether the ray enters a potential well or hill) [97]. Similarly, gravitational lensing causes the trajectories of light rays to bend and change. All these effects are usually referred to as relativistic corrections and when separations of interest become comparable to the Hubble horizon of the universe, they can become important.

When we calculate the power spectrum and bispectrum of galaxies in redshift space, by properly Fourier transforming $\langle \delta_{g,s}(\vec{x}_1)\delta_{g,s}(\vec{x}_2)\rangle$ and $\langle \delta_{g,s}(\vec{x}_1)\delta_{g,s}(\vec{x}_2)\delta_{g,s}(\vec{x}_3)\rangle$, one simplifying assumption that is made is that all line-of-sight vectors are parallel. In other words, it is assumed that $\hat{x}_1 = \hat{x}_2 = \dots$. This simplification is usually called the plane-parallel approximation. In addition, it is assumed that galaxies are effectively at "infinity", neglecting any term proportional to $1/x$.

In Chapter 2 we show that evolution of density fluctuations in a relativistic context (necessary for calculating relativistic effects mentioned before) can be calculated from a simple method. Then we relax the plane-parallel approximation and investigate the corrections beyond that (wide-angle effects) on the galaxy power spectrum in the linear and nonlinear regime and how it impacts the inference of some of cosmological parameters. We also compare these corrections with those of relativistic origin. In Chapter 3 we perform a similar study for the galaxy bispectrum and compare wide-angle and relativistic corrections on the galaxy bispectrum. In Chapter 4 we provide a model for the galaxy bispectrum in redshift space that incorporates both aforementioned FoG effect and also approximately the nonlinear evolution of the overdensities, resulting in a simple method with promising accuracy at quasi linear scales. Chapters 2 and 3 are based on a previously published work [81]. Chapter 4 is based on a paper that will be submitted for publication in the near future.

2 | Wide-angle and relativistic effects on the galaxy power spectrum

2.1 Introduction

Dark matter inhomogeneities at large scales obey simple conservation laws, which can be described by matter overdensities and peculiar velocities responding to gravity. Evolution of the matter density contrast and velocity fields at large scales has been extensively studied at both linear and weakly nonlinear regimes (see e.g. [88, 9, 4]). Biased tracers like galaxies follow the peculiar motions of dark matter leading to the addition of a redshift/blueshift term to their Hubble redshift along the line-of-sight (LOS). This results in distortion of their observed number density contrast and anisotropies in their clustering statistics in galaxy redshift surveys [67, 61].

In fact, the redshift-space comoving distance of an object, $\vec{s}$, differs from that in real space, $\vec{x}$, by $\vec{s} = \vec{x} + \hat{x}\,(\vec{v}_o \cdot \hat{x})/\mathcal{H}$ where $\vec{v}_o$ is the peculiar velocity of the object, $\mathcal{H}$ is the conformal Hubble parameter ($\mathcal{H} = aH$) and $\hat{x}$ denotes the LOS direction. Tracers follow the large scale bulk motion of dark matter with almost the same peculiar velocity due to the equivalence principle [39], ($\vec{v}_0 \approx \vec{v}_{DM}$). Then one can write $\vec{v}_{DM} = -\mathcal{H} f \vec{u}$ and study $\nabla \cdot \vec{u}$, which is a scalar quantity that, assuming negligible vorticity, contains all the information about the velocity field and equals density perturbation δ in linearized standard perturbation theory (SPT [9]). In such a context, the growth rate is defined as $f \equiv d\ln D_+/d\ln a$, where D_+ represents the linear growth factor of

perturbations.

The distortion of observed distances breaks the translational symmetry due to being dependent on the LOS direction. At linear level in SPT, assuming uniform selection function, it can be shown that the leading redshift space distortion (RSD) contribution to observed galaxy number density contrast is:

$$\delta_{g,s}(\vec{x}) = \delta_g(\vec{x}) + f\,\hat{x}\cdot\nabla_x(\vec{u}_g\cdot\hat{x}) + \dots\,, \tag{2.1}$$

where subscript "s" labels redshift space quantities and the ellipsis denotes nonlinear/higher-order terms and other subleading corrections. The well known Kaiser multipoles [67, 61] can be obtained from this equation in the so-called *plane-parallel* limit where all $\hat{x}$ vectors are assumed to be parallel, i.e $\hat{x} \equiv \hat{z} \approx$ const. In this limit the linear galaxy power spectrum in redshift space becomes: $P^{\rm lin}_{g,s}(k,\mu) = (1+\beta\mu^2)^2 P^{\rm lin}_g(k)$ where $P^{\rm lin}_g(k)$ is the linear (isotropic) power in absence of RSD: $\langle\delta_g(\vec{k})\,\delta_g(\vec{k'})\rangle = P^{\rm lin}_g(k)\,\delta_D(\vec{k}+\vec{k'})$, $\mu \equiv \hat{k}\cdot\hat{z}$ and $\beta \equiv f/b_1$ with b_1 being the linear bias coefficient. This expression can be expanded in terms of Legendre polynomials, $\mathcal{L}_\ell(\mu)$, giving rise to Kaiser multipoles.

The analysis of RSD provides opportunities for testing cosmological and gravitational models [20, 37, 92, 94, 16, 31, 99, 100, 6, 128, 55] because they have different predictions for the growth rate of perturbations. In addition, RSD impact our cosmological inferences based on N-point correlation functions of galaxy overdensities from redshift surveys. These applications often use the *plane-parallel/infinite-observer* approximations (hereafter simply referred to as plane-parallel approximation) in which the line of sight (LOS) is a constant direction and next-to-leading-order inverse distance corrections (proportinal to the inverse of the distance to the structures observed) are neglected. In this thesis, we use the terms *wide-angle* and *inverse-distance* for those contributions beyond plane-parallel and infinite-distance limit respectively.

In addition to RSD, there are sub-leading corrections to the observed galaxy number density contrast including those with *relativistic* origins [122, 124, 123, 29, 22, 65, 127, 11, 44, 42] which

stem from the change in redshift, light trajectories, volume elements, etc. because of the perturbed background space-time. Taking these into account in statistical analyses can lead to constraints on relativistic parameters. Usually, inverse-distance contributions are calculated along with other relativistic corrections but the plane-parallel approximation is still considered. However, wide-angle effects can be as large as other relativistic corrections and in some cases even larger (as we will explicitly show below).

Wide-angle and inverse-distance contributions to two-point statistics at linear level have been extensively studied so far [112, 17, 76, 113, 84, 93, 126, 95, 26, 28, 108]. Also the impact of a combination of full sky (angular) or wide-angle effects with relativistic terms on galaxy/halo two-point functions have also been studied in configuration space [12, 91, 114, 15]. Furthermore, there have been recent works on the investigation of relativistic effects (including observer terms) [58] and also relativistic, wide-angle and observer effects [25, 51] on multipoles of galaxy power spectrum at linear level. Evaluations of such corrections to galaxy two-point functions in Fourier space are often done numerically. It is also useful to do similar evaluations with analytic or simple relations which make it easier to compare different contributions separately and also have a quick idea about dependence of each contribution on various parameters. In this thesis, we provide a procedure for obtaining such relations.

It is also well known that local primordial non-Gaussianities (PNG) can lead to scale dependent corrections to power spectrum [35, 110] that scale similarly with relativistic and wide-angle effects (see e.g. [23, 65, 24, 69, 72, 34, 8, 119, 74, 117] for an investigation of the bias on local PNG parameter caused by ignoring relativistic corrections). Therefore, it is useful to have a simple and fast modeling of wide-angle and relativistic effects on redshift space correlation functions as it can make cosmological inferences more accurate. This is especially motivated in the era of precision cosmology with upcoming redshift surveys covering larger patches of sky with increased precision [38, 47, 3, 111, 1, 45].

It is worth noting that although angular power spectra (based on redshifts and angles of

tracers) use the observables in the most direct way, the estimators in the Fourier basis are simplest from the theoretical point of view and are enough to illustrate the size of the effects we are interested in. In addition, the vast majority of measurements have so far been done in this basis, although as the surveys probe larger scales it is more natural to change to a more suitable basis.

One useful approach for this purpose is to first perform perturbative expansions based on appropriate parameters that quantify wide-angle effects in configuration space and then take the Fourier transform of the result [95, 26]. In this work, we also use a perturbative procedure but in a way that makes calculations simpler and, more importantly, easily extendable to nonlinear regimes and higher-order statistics. For the galaxy power spectrum at linear level, we utilize this procedure to find simple formulas for leading order wide-angle corrections and compare them with "non-integrated" and integrated relativistic terms at large scales. In this work, we also provide a simple procedure for finding the evolution of dark matter density contrast and other fluctuations in a relativistic context. This procedure can be extended to other situations, e.g. including large-distance modifications of gravity.

At the nonlinear level for two-point statistics, wide-angle corrections have been investigated in the Zel'dovich approximation (first order in Lagrangian perturbation theory) [27, 115]. Also nonlinear RSD effects have been studied in spherical harmonic space [56]. However, to the best of our knowledge, wide-angle corrections to nonlinear power spectra in SPT have not been calculated so far. The perturbative procedure to deal with wide-angle corrections used in this work can significantly simplify such calculations to any order. As an example, we keep the galaxy number density contrast and velocity fields up to third order in SPT and find leading order wide-angle and inverse-distance corrections to one-loop galaxy power spectrum around BAO scales and larger, assuming a ΛCDM cosmology. We also compare, approximately, the size of *Fingers-of-God* (FoG) contributions with that of wide-angle effects at those scales. From these results, we draw a conclusion about the importance of wide-angle and relativistic corrections at large scales in the presence of non-linearities.

Throughout this chapter, we adopt the following conventions for integrals in configuration and Fourier spaces:

$$\int_{\vec{x}} \equiv \int \frac{d^3x}{(2\pi)^3}, \qquad \int_{\vec{k}} \equiv \int d^3k \tag{2.2}$$

2.2 General Strategy

Calculation of anisotropic N-point correlation functions in Fourier space beyond the plane-parallel approximation can become involved due to broken translational symmetry. However, a helpful approach is to define "local" quantities such as the local power spectrum, $P_g(\vec{k},\vec{x})$, and bispectrum, $B_g(\vec{k}_1,\vec{k}_2,\vec{k}_3,\vec{x})$, which are defined at each position $\vec{x}$ (a suitable choice of LOS) by taking the Fourier transform with respect to the relative position vectors of galaxies [104] (see also [95]). Then, these local quantities can be inserted into estimators which integrate over position vectors and yield the final multipoles in Fourier space [120, 104].

Definition of the LOS in these local quantities is not unique. For the power spectrum it can be defined as the bisector or midpoint of two galaxy displacement vectors or can also be chosen to be aligned with one of the galaxy position vectors (end-point LOS) [21, 16, 98]. The latter makes it possible to evaluate estimators via Fast Fourier transform techniques [104, 19]. In this work we use the midpoint for the power spectrum and centroid for the bispectrum which are symmetric under exchange.

To illustrate the main ideas, consider the general formula for calculating the galaxy power spectrum multipoles from the density perturbations:

$$P_g^\ell(k) = \frac{(2\pi)^3}{V_s}(2\ell+1)\int \frac{d\Omega_k}{4\pi}\int_{\vec{x}_1}\int_{\vec{x}_2} e^{-i\vec{k}\cdot\vec{x}_{12}} W(\vec{x}_1)W(\vec{x}_2)\mathcal{L}_\ell(\hat{k}\cdot\hat{x}_c)\left\langle \delta_g(\vec{x}_1)\,\delta_g(\vec{x}_2)\right\rangle. \tag{2.3}$$

where $\vec{x}_1$ and $\vec{x}_2$ integrals can be taken over an infinite volume with window functions $W(\vec{x})$

appropriately defined to force the integrals to be confined to the survey region with volume V_s. Here $\vec{x}_c = (\vec{x}_1 + \vec{x}_2)/2$ is the midpoint of the pair which is chosen to define the LOS. This vector is measured with respect to the observer, i.e $x_c = 0$ at the observer's location. We have: $\vec{x}_1 = \vec{x}_c + \vec{x}_{12}/2$ and $\vec{x}_2 = \vec{x}_c - \vec{x}_{12}/2$. The above integral can be re-written as:

$$P_g^\ell(k) = \frac{(2\pi)^3}{V_s}(2\ell+1)\int \frac{d\Omega_k}{4\pi}\int_{\vec{x}_c} \mathcal{L}_\ell(\hat{k}\cdot\hat{x}_c)\int_{\vec{x}_{12}} e^{-i\vec{k}\cdot\vec{x}_{12}} W(\vec{x}_1)W(\vec{x}_2)\left\langle \delta_g(\vec{x}_1)\,\delta_g(\vec{x}_2)\right\rangle \tag{2.4}$$

In general, it is a tedious task to evaluate this integral including all relevant contributions. In this work we aim to provide a straightforward way to calculate this expression. Especially, we aim to determine the importance of different contributions and their relative sizes. This can help one to decide which contribution should be kept and which can be neglected.

The window function in Eq. (2.4) enforces the limitations in volume (and its shape). Therefore, we can always take $\vec{x}_{12}$ integral over infinity and take the $\vec{x}_c$ integral over the survey volume. Since we mainly do the calculations for scales that are well within the survey volume, we can just set the window function to unity for those modes. In Section 2.6, we will discuss how our results can be generalized to include effects of the window function and non-trivial survey geometries. Let us start from the definition of the "local" power spectrum, which sets the stage for the rest of calculations in this section. It describes the power at position $\vec{x}_c$ contributed by Fourier modes $\vec{k}$ and is given by [104]:

$$P_{g,n}^{\rm loc}(\vec{k},\vec{x}_c) = \int_{\vec{x}_{12}} e^{-i\vec{k}\cdot\vec{x}_{12}}\left\langle \delta_{g,n}(\vec{x}_1)\,\delta_{g,n}(\vec{x}_2)\right\rangle \tag{2.5}$$

where $\delta_g(\vec{x})$ is the observed galaxy density contrast, measured at comoving position $\vec{x}$. The index n is a label that denotes the type of contribution, e.g. RSD, relativistic, etc. Note that in the most general case, for scales comparable to the survey size, Eq. (2.5) must be generalized to its windowed form, the innermost integral in Eq. (2.4). We will discuss this in section 2.6.

The relevant geometry under consideration is shown in Figure 2.1. Since we are integrating

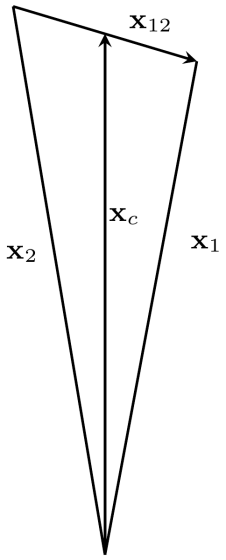

Figure 2.1: Relevant geometry for local power spectrum calculations. The vector $\vec{x}_c$ is the midpoint which we take to define the local line-of-sight and $\vec{x}_{12} = \vec{x}_1 - \vec{x}_2$.

over $\vec{x}_{12}$, the final local power spectrum is only a function of $\vec{x}_c$. We assume the time-dependence of fields implicitly, i.e. $\delta_{g,n}(\vec{x}) = \delta_{g,n}(\vec{x}, \tau)$, but for brevity do not write it.

The local power spectrum can be expanded in terms of Legendre polynomials as:

$$P^{\rm loc}_{g,n}(\vec{k}, \vec{x}_c) = \sum_\ell \mathcal{P}^{(\ell)}_{g,n}(k, x_c)\ \mathcal{L}_\ell(\hat{k} \cdot \hat{x}_c) \tag{2.6}$$

which reproduces plane-parallel multipoles in the limit $x_c \to \infty$ and constant $\hat{x}_c$. In this equation, $\mathcal{P}^{(\ell)}_{g,n}(k, x_c)$ can be considered as the "local" power spectrum multipole which is calculated as:

$$\mathcal{P}^{(\ell)}_{g,n}(k, x_c) \equiv (2\ell + 1) \int \frac{d\Omega_k}{4\pi} \mathcal{L}_\ell(\hat{k} \cdot \hat{x}_c)\, P^{\rm loc}_{g,n}(\vec{k}, \vec{x}_c) \tag{2.7}$$

The full power spectrum multipoles are obtained by summing over all LOS vectors [104]:

$$\begin{aligned} P^{(\ell)}_{g,n}(k) \equiv \quad & \int_{V_s} \frac{d^3\vec{x}_c}{V_s}\, \mathcal{P}^{(\ell)}_{g,n}(k, x_c) = \\ & \int_{V_s} \frac{d\Omega_s}{V_s} \int_{V_s} x_c^2 dx_c \mathcal{P}^{(\ell)}_{g,n}(k, x_c), \end{aligned} \tag{2.8}$$

which depends on the geometry of the survey volume V_s.

2.3 Galaxy density fluctuations with RSD and inverse-distance terms only

We start from the simplest case, where we implement the mapping from real to redshift space, excluding corrections emanating from the effects of the perturbed background on light ray trajectories (observed angles and redshifts). Assuming uniform selection function ($\bar{n}(\vec{x}) = \bar{n}(\vec{s})$), here and throughout this dissertation, conservation of galaxy numbers in real and redshift spaces implies:

$$[1 + \delta_{g,s}(\vec{s})]\, d^3\vec{s} = [1 + \delta_g(\vec{x})]\, d^3\vec{x} \tag{2.9}$$

Using the RSD map $\vec{s} = \vec{x} + \hat{x}\,(\vec{v}_g \,.\, \hat{x})/\mathcal{H}$ and Eq. (2.9), one finds

$$\delta_{g,s}(\vec{k}) = \int_{\vec{x}} e^{-i\vec{k}\cdot\vec{x}} \left\{ e^{-i\frac{1}{\mathcal{H}}(\vec{k}\cdot\hat{x})(\vec{v}_g(\vec{x})\cdot\hat{x})} \left[1 + \delta_g(\vec{x})\right] - 1 \right\} \tag{2.10}$$

which can be used to obtain δ_s at any comoving position,

$$\delta_{g,s}(\vec{x}) = \int_{\vec{x}',\vec{k}} e^{i\vec{k}\cdot(\vec{x}-\vec{x}')} \left\{ e^{-i\frac{1}{\mathcal{H}}(\vec{k}\cdot\hat{x}')(\vec{v}_g(\vec{x}')\cdot\hat{x}')} \left[1 + \delta_g(\vec{x}')\right] - 1 \right\} . \tag{2.11}$$

The exponential factor inside the curly braces can be expanded to any desired order. Doing so, products involving Cartesian components of $\vec{k}$ will have the general form k_j^m with m being the power and $j = 1, 2, 3$ representing x, y, z components. These can be turned into derivatives with respect to x_j, $(-i\partial_j)^m$, which can then be pulled out of the integral. This results in:

$$\delta_{g,s} = \delta_g + \sum_{m=1}^{\infty} \frac{(-1)^m}{m!\,\mathcal{H}^m} \partial_{j_1} \ldots \partial_{j_m} \left[(1 + \delta_g)\, \hat{x}_{j_1} \ldots \hat{x}_{j_m} (\vec{v}\cdot\hat{x})^m \right] \tag{2.12}$$

where all fields are evaluated at $\vec{x}$ and we have assumed that velocities are unbiased ($\vec{v}_g = \vec{v}$) with $\vec{v}$ being the dark matter velocity. This is valid at the large scales we are interested in. Now, when at least one derivative acts on the unit vectors, it generates the *inverse-distance corrections* (absent for a fixed LOS) since

$$\partial_i \hat{x}_j = \frac{\delta_{ij} - \hat{x}_i \hat{x}_j}{|\vec{x}|}, \tag{2.13}$$

whereas when *all* derivatives act on the fields (like δ_g and $\vec{v}$), they generate the usual plane-parallel result for $\delta_{g,s}(\vec{x})$ where the fixed LOS is replaced by the true varying LOS $\hat{x}$: expanding these type of terms around a fixed direction generates the strict plane-parallel results and their *wide-angle corrections*, as we discuss below.

2.4 RSD, inverse-distance, relativistic and wide-angle corrections to the linear galaxy power spectrum

At linear level, one only needs the first two terms in Eq. (2.12) and should add to that relativistic terms that come from perturbed angles and redshifts of the received light due to background spacetime perturbations. The coefficient of the inverse-distance term should also be modified by gravitational lensing (e.g. a term proportional to magnification bias). Here we only consider metric perturbations caused by scalar modes in an otherwise flat metric. Therefore, for the perturbed flat FLRW metric, in conformal Newtonian gauge (CNG), we have:

$$ds^2 = a^2\big[-(1+2\Phi)d\tau^2 + (1-2\Psi)\delta_{ij}dx^i dx^j\big]\,. \tag{2.14}$$

The linear, leading order relativistic calculation has received a fair amount of attention [122, 124, 123, 29, 22, 65]. Here, for the linear galaxy density fluctuation, $\delta_{g,L}(\vec{x})$, we follow in particular [29]

(see their Eq. 37) and add observer terms (contributions that are evaluated at the location of the observer) to that expression using the results from [102, 58, 25] and write:

$$\begin{aligned}\delta_{g,L}(\vec{x}) \;=\; & \delta_g - \frac{1}{\mathcal{H}}\hat{x}_i\partial_i(\vec{v}\cdot\hat{x}) + \left[\frac{2-5s}{\mathcal{H}x} + 5s - b_e + \frac{\dot{\mathcal{H}}}{\mathcal{H}^2}\right][\Psi - \Psi_o + (\vec{v}_o - \vec{v})\cdot\hat{x} + \mathcal{H}_0 V_o] + \\ & \frac{1}{\mathcal{H}}\dot{\Phi} + (5s-2)\Phi + \Psi - \frac{2-5s}{x}V_o + (2-5s)\vec{v}_o\cdot\hat{x} + \\ & \frac{(5s-2)}{2}\int_{\tau_0}^{\tau} d\tau' \frac{\tau-\tau'}{(\tau_0-\tau)(\tau_0-\tau')}\nabla^2_{\hat{x}'}(\Phi+\Psi) + \\ & + \frac{2-5s}{x}\int_{\tau}^{\tau_0} d\tau'(\Phi+\Psi) + \left[\frac{2-5s}{\mathcal{H}x} + 5s - b_e + \frac{\dot{\mathcal{H}}}{\mathcal{H}^2}\right]\int_{\tau}^{\tau_0} d\tau'(\dot{\Phi}+\dot{\Psi})\,.\end{aligned} \tag{2.15}$$

All parameters here are in CNG . We will relate δ_g to the dark matter density contrast later. In this equation, terms with a subscript o are evaluated at the observer's location and a dot refers to a partial derivative with respect to the conformal time. The remaining parameters in Eq. (2.15) are as follows. The magnification bias is $s \equiv -(2/5)(\partial \ln \bar{n}_g/\partial \ln L)|_{\bar{L}}$, with $\bar{n}_g$ being the background galaxy number density and $\bar{L}$ the threshold luminosity. The parameter $b_e \equiv \partial \ln[\bar{n}_g a^3]/\partial \ln a$ measures the evolution of the galaxy comoving number density (evolution bias) and the velocity potential, V, is related to the peculiar velocity via $\vec{v} = -\nabla V$. Also, the integrated terms are integrated along the LOS ($\hat{x}' = \hat{x}$).

2.4.1 Relativistic evolution of fluctuations

In this section, we relate the Fourier modes of fluctuation fields appearing in Eq. (2.15), δ_g, Φ, $\vec{v}$, ... to the dark matter density contrast, δ_m, and its derivatives, and then find the evolution of δ_m in a relativistic context. While such calculations have been done before (see e.g. [125]), the emphasis here is to find the evolution using a simple method that can be applied to more general situations.

Denoting the perturbed density of cold dark matter in the CNG by $\bar{\rho}_m\,(1+\delta_m)$, we aim to find the evolution of $\delta_m(\vec{k})$ starting at $\tau = \tau_\star$ long after the radiation-dominated era. Here we ignore

contributions of massless neutrinos and photons given the eras we are interested in. Also, since at the end we focus on the power spectrum at large scales ($k \lesssim 0.01$h/Mpc) we can ignore the contribution of massive neutrinos because these mostly impact smaller scales. We also neglect anisotropic stress; this choice leads to $\Phi = \Psi$ from Einstein equations. Under these assumptions, at the linear level, the continuity and Euler equations for the non-relativistic dark matter fluid lead to the following equations for fluctuations in Fourier space (in CNG):

$$\dot{\delta}_m(\vec{k}) - 3\dot{\Phi}(\vec{k}) + \Theta_v(\vec{k}) = 0 \tag{2.16}$$

$$\dot{\Theta}_v(\vec{k}) + \mathcal{H}\Theta_v(\vec{k}) = k^2\Phi(\vec{k}) \tag{2.17}$$

where $\Theta_v(x) = \nabla \cdot \vec{v}(x)$ with $v^i = \mathrm{dx^i}/\mathrm{d}\tau$ as the peculiar velocity. The velocity potential in Fourier space can also be written as $V(\vec{k}) = \Theta_v(\vec{k})/k^2$. Also all quantities depend on proper time, but we do not write the dependence explicitly for brevity.

Assuming the fluctuations are sourced by adiabatic (curvature) perturbations, we have $\delta_m(\vec{k}) = \delta_b(\vec{k})$ where b refers to baryons. We also assume that $\Theta_{v,m}(\vec{k}) = \Theta_{v,b}(\vec{k}) = \Theta_v(\vec{k})$, which is a good approximation at large scales. Then, the Einstein equations for the Einstein tensors $G^0_{\ 0}$, $G^0_{\ i}$ and $G^i_{\ i}$ lead to the following relations for fluctuations in Fourier space (in units where $c = 1$):

$$\Phi(\vec{k}) + 3\frac{\mathcal{H}}{k^2}\dot{\Phi}(\vec{k}) + 3\frac{\mathcal{H}^2}{k^2}\Phi(\vec{k}) = -\frac{4\pi G a^2}{k^2}\left[\bar{\rho}_m\delta_m(\vec{k}) + \bar{\rho}_b\delta_b(\vec{k})\right] = -\frac{3}{2}\frac{\mathcal{H}^2}{k^2}\Omega_M\delta_m(\vec{k}) \tag{2.18}$$

$$\dot{\Phi}(\vec{k}) + \mathcal{H}\Phi(\vec{k}) = 4\pi G a^2(\bar{\rho}_m + \bar{\rho}_b)\frac{\Theta_v(\vec{k})}{k^2} = \frac{3}{2}\frac{\mathcal{H}^2}{k^2}\Omega_M\Theta_v(\vec{k}) \tag{2.19}$$

$$\ddot{\Phi}(\vec{k}) + 3\mathcal{H}\dot{\Phi}(\vec{k}) + (2\dot{\mathcal{H}} + \mathcal{H}^2)\Phi(\vec{k}) = 0 \tag{2.20}$$

where for the last equalities in Eq. (2.18) and Eq. (2.19) we have used Friedmann equations with $\Omega_M = \Omega_m + \Omega_b$ the total matter (dark + baryon) density parameter. Taking a time derivative of the continuity equation, Eq. (2.16), and making use of a combination of Euler equation, Eq. (2.17), and equations above, one finds the following second order equation for the evolution of dark matter

density contrast:

$$\ddot{\delta}_m(\vec{k}) + 3\mathcal{H}\dot{\Phi}(\vec{k}) + 6\dot{\mathcal{H}}\Phi(\vec{k}) + \mathcal{H}\dot{\delta}_m(\vec{k}) - \frac{3}{2}\mathcal{H}^2\Omega_M\delta_m(\vec{k}) = 0\,. \tag{2.21}$$

Now we need to express $\dot{\Phi}(\vec{k})$ and $\Phi(\vec{k})$ in terms of $\delta_m(\vec{k})$, $\dot{\delta}_m(\vec{k})$. To this end, we can take Eqs. (2.16), (2.18) and (2.19) as a system of three equations, three unknows ($\Phi(\vec{k})$, $\dot{\Phi}(\vec{k})$, $\Theta(\vec{k})$) and solve for these in terms of other parameters. The result is:

$$\Phi(\vec{k}) = \frac{3\mathcal{H}^2\left(6\mathcal{H}\,\Omega_M\dot{\delta}_m(\vec{k}) - 2k^2\Omega_M\delta_m(\vec{k}) + 9\mathcal{H}^2\Omega_M^2\delta_m(\vec{k})\right)}{2(2k^4 - 27\mathcal{H}^4\Omega_M - 9\mathcal{H}^2k^2\Omega_M)} \tag{2.22}$$

$$\dot{\Phi}(\vec{k}) = \frac{3\left(-3\mathcal{H}^4\Omega_M\dot{\delta}_m(\vec{k}) - \mathcal{H}^2k^2\Omega_M\dot{\delta}_m(\vec{k}) + \mathcal{H}^3k^2\Omega_M\delta_m(\vec{k})\right)}{2k^4 - 27\mathcal{H}^4\Omega_M - 9\mathcal{H}^2k^2\Omega_M} \tag{2.23}$$

$$\Theta_v(\vec{k}) = -\frac{2k^4\dot{\delta}_m(\vec{k}) - 9\mathcal{H}^3k^2\Omega_M\delta_m(\vec{k})}{2k^4 - 27\mathcal{H}^4\Omega_M - 9\mathcal{H}^2k^2\Omega_M}\,. \tag{2.24}$$

After inserting these expressions into Eq. (2.21), one can factor out the common denominator (multiplied by $2k^4$) to get:

$$\frac{2k^4}{(2k^4 - 27\mathcal{H}^4\Omega_M - 9\mathcal{H}^2k^2\Omega_M)}\,(\cdots) = 0\,. \tag{2.25}$$

For non-zero k, the only solution to this equation is $(\cdots) = 0$. Therefore, the equation for the relativistic evolution of δ_m takes the following form:

$$\begin{aligned}
&\ddot{\delta}_m(\vec{k}) + \dot{\delta}_m(\vec{k}) - \frac{3}{2}\mathcal{H}^2\Omega_M\delta_m(\vec{k}) - \left(\frac{9\mathcal{H}^2}{2k^2} + \frac{27\mathcal{H}^4}{2k^4}\right)\Omega_M\ddot{\delta}_m(\vec{k}) \\
&- \left(\frac{9\mathcal{H}^3}{k^2} + \frac{27\mathcal{H}^5}{k^4}(1 - \frac{\dot{\mathcal{H}}}{\mathcal{H}^2})\right)\Omega_M\dot{\delta}_m(\vec{k}) \\
&+ \left(\frac{9\mathcal{H}^4}{2k^2}(1 + \frac{3}{2}\Omega_M - 2\frac{\dot{\mathcal{H}}}{\mathcal{H}^2}) + \frac{81\mathcal{H}^6}{4k^4}\Omega_M(1 + 2\frac{\dot{\mathcal{H}}}{\mathcal{H}^2})\right)\Omega_M\delta_m(\vec{k}) = 0\,.
\end{aligned} \tag{2.26}$$

The first three terms above constitute the well-known equation for the evolution of dark

matter density fluctuations in the absence of relativistic corrections. The rest are such corrections which are suppressed by powers of $\mathcal{H}/k$ and can be omitted for modes far below the (conformal) Hubble scale. The first piece has two solutions, $D_+(\tau)C^+_{\tau_\star}(\vec{k})$ (growing mode) and $D_-(\tau)C^-_{\tau_\star}(\vec{k})$ (decaying mode) where $C^\pm_{\tau_\star}(\vec{k})$ are determined from initial conditions at $\tau = \tau_\star$ and:

$$D_+(\tau) = \frac{5}{2}\Omega_M\mathcal{H}^3\int_0^a \frac{da'}{\mathcal{H}(a')^3}, \qquad D_-(\tau) = \frac{H(\tau)}{H_0} \tag{2.27}$$

To find two solutions of Eq. (2.26) that include relativistic corrections we can postulate that

$$\delta^+_m(\vec{k}) = D_+(\tau)\left(1 + \frac{\mathcal{H}^2}{k^2}\xi(\tau)\right)\mathcal{A}^+_{\tau_\star}(\vec{k}), \tag{2.28}$$

$$\delta^-_m(\vec{k}) = D_-(\tau)\left(1 + \frac{\mathcal{H}^2}{k^2}\gamma(\tau)\right)\mathcal{A}^-_{\tau_\star}(\vec{k}), \tag{2.29}$$

which are inspired by the form of relativistic suppression factors, and plug them into Eq. (2.26) to find ξ and γ. The quantities $\mathcal{A}^\pm_{\tau_\star}(\vec{k})$ will be determined later. After doing so and making use of

$$\dot{D}_+ = \frac{\Omega_M}{2}(5a - 3D_+)\mathcal{H}, \tag{2.30}$$

$$\dot{\mathcal{H}} = (1 - \frac{3}{2}\Omega_M)\mathcal{H}^2, \tag{2.31}$$

$$\dot{\Omega}_M = 3\mathcal{H}\,\Omega_M(\Omega_M - 1), \tag{2.32}$$

the equation for growing and decaying modes take the following general forms:

$$\frac{\mathcal{H}^2}{k^2}\Psi^+_1(\xi,\dot{\xi},\ddot{\xi}) + \frac{\mathcal{H}^4}{k^4}\Psi^+_2(\xi,\dot{\xi},\ddot{\xi}) + \frac{\mathcal{H}^6}{k^6}\Psi^+_3(\xi,\dot{\xi},\ddot{\xi}) = 0,$$
$$\frac{\mathcal{H}^2}{k^2}\Psi^-_1(\gamma,\dot{\gamma},\ddot{\gamma}) + \frac{\mathcal{H}^4}{k^4}\Psi^-_2(\gamma,\dot{\gamma},\ddot{\gamma}) + \frac{\mathcal{H}^6}{k^6}\Psi^-_3(\gamma,\dot{\gamma},\ddot{\gamma}) = 0$$

where the Ψ^+'s are also functions of D_+, Ω_M, a and $\mathcal{H}$ and Ψ^-'s have the same functionality except for D_+. To find ξ and γ we can use a simple trick inspired by the fact that any solution

for ξ and γ needs to be valid at all scales in tandem with the fact that Ψ's in the equations above are suppressed at sub-Hubble scales by different powers of $\mathcal{H}/k$. This implies that one can find solutions for ξ and γ by requiring the Ψ's to be separately zero for each of the equations above. For example, for the growing mode, requiring $\Psi_m^+ = 0$ ($m = 1, 2, 3$), leaves us with a system of three equations with three unknowns (ξ, $\dot{\xi}$, $\ddot{\xi}$) from which ξ can be found. A similar procedure can be used for finding γ. One can also show that direct first and second order derivatives of ξ and γ are consistent with $\dot{\xi}$, $\ddot{\xi}$ and $\dot{\gamma}$, $\ddot{\gamma}$ respectively. The final results are:

$$\xi(\tau) = \frac{3(5a - 3D_+)\Omega_M}{2D_+} = 3\frac{d\ln D_+}{d\ln a} \equiv 3f \tag{2.33}$$

$$\gamma(\tau) = -\frac{9}{2}\Omega_M \tag{2.34}$$

which show that unlike γ, ξ is proportional to the growth rate parameter f, as one expects for the growing mode. Therefore, to sum the results up, the full solution for the relativistic evolution of dark matter fluctuations is given by the simple expression:

$$\begin{aligned}\delta_m(\vec{k}) \;\; = \;\; & D_+(\tau)\,(1 + 3f\frac{\mathcal{H}^2}{k^2})\,\mathcal{A}^+_{\tau_\star}(\vec{k}) \;\; + \\ & D_-(\tau)\,(1 - \frac{9}{2}\Omega_M\frac{\mathcal{H}^2}{k^2})\,\mathcal{A}^-_{\tau_\star}(\vec{k})\,.\end{aligned} \tag{2.35}$$

Since we are interested in $\tau \gg \tau_*$ at which time the decaying mode can be neglected, we can set $\delta_m \approx \delta_{m,+}$ and define $\mathcal{A}^+_{\tau_\star}(\vec{k}) \equiv \mathcal{A}_{\tau_\star}(\vec{k})$. Finally, one can plug this result into Eqs. (2.22)-(2.24) to find the other parameters. After some algebra one gets:

$$\delta_m(\vec{k}) = D_+(1 + 3f\frac{\mathcal{H}^2}{k^2})\mathcal{A}_{\tau_\star}(\vec{k}) \tag{2.36}$$

$$\Phi(\vec{k}) = -\frac{3}{2}\frac{\mathcal{H}^2}{k^2}D_+\Omega_M\mathcal{A}_{\tau_\star}(\vec{k}) \tag{2.37}$$

$$\dot{\Phi}(\vec{k}) = -\frac{3}{2}\frac{\mathcal{H}^3}{k^2}D_+\Omega_M(f-1)\mathcal{A}_{\tau_\star}(\vec{k}) \tag{2.38}$$

$$\Theta_v(\vec{k}) = -\mathcal{H}fD_+\mathcal{A}_{\tau_\star}(\vec{k}) \tag{2.39}$$

The relations above are for fluctuation modes in CNG at $\tau \gg \tau_\star$. However, comparison between the dark matter density contrast in CNG and its analogue in synchronous gauge gives us a better insight about $\mathcal{A}_{\tau_\star}(\vec{k})$. The density contrast and velocity divergence in CNG can be related to those in synchronous gauge at linear level via the standard gauge transformation (see e.g. [73]):

$$\tilde{\delta}_m(\vec{k}) = \delta_m(\vec{k}) - \alpha\frac{\dot{\bar{\rho}}_m}{\bar{\rho}_m} \tag{2.40}$$

$$\tilde{\Theta}_v(\vec{k}) = \Theta_v(\vec{k}) - \alpha k^2 \tag{2.41}$$

where a tilde signifies synchronous gauge quantity. Now we can work in synchronous/comoving gauge (SCG) in which comoving coordinates are defined by free falling dark matter particles with $\tilde{v}^i = 0$. Therefore $\tilde{\Theta}_v = 0$ in SCG and from Eqs. (2.40), (2.41) one finds:

$$\tilde{\delta}_m(\vec{k}) = \delta_m(\vec{k}) + 3\frac{\mathcal{H}}{k^2}\Theta_v(\vec{k}) \tag{2.42}$$

where we have used $\bar{\rho}_m \propto a^{-3}$. Now we can make use of Eqs. (2.36) and (2.39) to obtain:

$$\begin{aligned}\tilde{\delta}_m(\vec{k}) &= D_+(1+3f\frac{\mathcal{H}^2}{k^2})\mathcal{A}_{\tau_\star}(\vec{k}) - 3\frac{\mathcal{H}}{k^2}(\mathcal{H}fD_+\mathcal{A}_{\tau_\star}(\vec{k})) \\ &= D_+\mathcal{A}_{\tau_\star}(\vec{k}).\end{aligned} \tag{2.43}$$

This result implies that one can replace $\mathcal{A}_{\tau_\star}(\vec{k})$ in Eqs. (2.36)-(2.39) by $\tilde{\delta}_m(\vec{k})/D_+$ to find:

$$\delta_m(\vec{k}) = \left(1+3f\frac{\mathcal{H}^2}{k^2}\right)\tilde{\delta}_m(\vec{k}) \tag{2.44}$$

$$\Phi(\vec{k}) = -\frac{3}{2}\frac{\mathcal{H}^2}{k^2}\Omega_M\tilde{\delta}_m(\vec{k}) \tag{2.45}$$

$$\dot{\Phi}(\vec{k}) = -\frac{3}{2}\frac{\mathcal{H}^3}{k^2}\Omega_M(f-1)\tilde{\delta}_m(\vec{k}) \tag{2.46}$$

$$\Theta_v(\vec{k}) = -\mathcal{H}f\tilde{\delta}_m(\vec{k})\,. \tag{2.47}$$

This relates the quantities in CNG to the density fluctuation in SCG (with linear power spectrum $\simeq k^{n_s}$ as $k \longrightarrow 0$, where n_s is the scalar spectral index) which will make calculations much easier.

The final step for calculating the observed galaxy power spectrum from Eq. (2.15) is relating δ_g to δ_m via an appropriate bias relation. In a relativistic context, galaxy density fluctuation is most easily related to the dark matter fluctuation in the SCG [29, 65], via $\tilde{\delta}_g = b_1\tilde{\delta}_m$ at linear level. This bias relation is also gauge invariant [65], allowing one to find the corresponding bias relation in other gauges. The gauge transformation for the galaxy density fluctuation and velocity modes are similar to Eqs. (2.40) and (2.41) except $\dot{\bar{\rho}}_g/\bar{\rho}_g = (-3 + b_e)\mathcal{H}$. Assuming zero velocity bias at large scales ($\Theta_{v,g} = \Theta_v, \tilde{\Theta}_{v,g} = 0$) one finds $\tilde{\delta}_g(\vec{k}) = \delta_g(\vec{k}) + (3 - b_e)\mathcal{H}\Theta_v(\vec{k})/k^2$. Now, using $\tilde{\delta}_g(\vec{k}) = b_1\tilde{\delta}_m(\vec{k})$ and Eq. (2.47) one obtains:

$$\delta_g(\vec{k}) = b_1\tilde{\delta}_m(\vec{k}) + (3 - b_e)\frac{\mathcal{H}^2}{k^2}f\tilde{\delta}_m(\vec{k}) \tag{2.48}$$

2.4.2 The full linear galaxy density contrast

Using equations (2.44)-(2.48), one can rewrite the linear galaxy density fluctuation in Eq. (2.15) by expressing its constituents in terms of inverse Fourier integrals. We have:

$$\delta_{g,L}(\vec{x}) = \delta^{\mathrm{RSD}}(\vec{x}) + \delta^{\mathrm{NI}}(\vec{x}) + \delta^{\mathrm{I}}(\vec{x}) \tag{2.49}$$

where we have ignored observer terms. It has been shown in [58, 25] that the inclusion of observer terms renders the variance of the observed galaxy density fluctuations free of IR-divergences and is also necessary for a gauge invariant expression of the observed galaxy density contrast. It is also shown that when all relativistic terms including observer contributions are included, relativistic effects in cosmological observable statistics become infrared insensitive at linear and nonlinear levels [79]. However, for modes well within survey volume, observer effects on Fourier space correlation functions should be negligible because these are evaluated at a single position of the

observer. For modes comparable to the survey size when the window function is included (see section 2.6), the convolution with the window function and the mixing between window and correlation function multipoles can make observer terms relevant. For example, contributions like the observer's velocity induce a kinematic dipole in the measured galaxy density contrast that can affect the measured galaxy power spectrum multipoles in realistic situations (see e.g. [51]). However, for the scales we are interested in, we can omit these contributions. Therefore, we will only focus on other terms. In the equation above, $\delta^{\rm NI}(\vec{x})$ is comprised of all relativistic and inverse-distance terms that are evaluated at the source position. This also includes the second term in Eq. (2.48). The $\delta^{\rm I}(\vec{x})$ terms are integrated relativistic contributions. The total linear galaxy density fluctuation in Eq. (2.49) can be written in the instructive form:

$$\begin{aligned}\delta_{g,L}(\vec{x}) = &\int_{\vec{k}'} e^{i\vec{k}'\cdot\vec{x}}(\mathrm{F}^{\rm RSD}+\mathrm{F}^{\rm NI})(\vec{k}',\vec{x})\,\tilde{\delta}_{m0}(\vec{k}') \\ &+ \int_{\vec{k}'}\int_0^x dx' e^{i\vec{k}'\cdot\vec{x}'}\mathrm{F}^{\rm I}(\vec{k}',\vec{x},\vec{x}')\tilde{\delta}_{m0}(\vec{k}')\end{aligned} \tag{2.50}$$

where the F functions are:

$$\mathrm{F}^{\rm RSD}(\vec{k}',\vec{x}) = \left(b_1 + f(\hat{k}'\cdot\hat{x})^2\right)\tilde{\mathcal{D}}_+(\tau_x) \tag{2.51}$$

$$\begin{aligned}\mathrm{F}^{\rm NI}(\vec{k}',\vec{x}) = &\left\{(3-b_e)f\frac{\mathcal{H}^2}{k'^2} + \frac{3}{2}\frac{\mathcal{H}^2}{k'^2}\Omega_M\left[\frac{5s-2}{\mathcal{H}x} - 10s + b_e + \frac{3}{2}\Omega_M - f + 1\right]\right. \\ &\left. -f\frac{i(\hat{k}'\cdot\hat{x})\mathcal{H}}{k'}\left[5s - b_e + 1 - \frac{3}{2}\Omega_M - \frac{5s-2}{\mathcal{H}x}\right]\right\}\tilde{\mathcal{D}}_+(\tau_x)\end{aligned} \tag{2.52}$$

$$\begin{aligned}\mathrm{F}^{\rm I}(\vec{k}',\vec{x},\vec{x}') = 3H_0^2\Omega_{M0}(1+z_{x'})&\left\{(5s-2)\frac{(x-x')x'}{2x}\left[1-(\hat{k}'\cdot\hat{x}')^2 + 2i\frac{(\hat{k}'\cdot\hat{x}')}{k'x'}\right]\right. \\ &\left. + \left[\frac{2-5s}{\mathcal{H}x} + 5s - b_e + 1 - \frac{3}{2}\Omega_M\right]\frac{(1-f_{x'})\mathcal{H}(x')}{k'^2} + \frac{5s-2}{k'^2x}\right\}\tilde{\mathcal{D}}_+(\tau_{x'})\end{aligned} \tag{2.53}$$

where $\tilde{\mathcal{D}}_+(\tau_x) \equiv \tilde{D}_+(\tau_x)/\tilde{D}_+(\tau_0)$ represents the normalized growth factor of the SCG density fluctuation and $\tilde{D}_+$ can be obtained from Eq.(2.27). For these results we have used $\nabla^2_{\hat{x}'}\phi = x'^2\vec{\nabla}^2\phi -$

$\partial_{x'}(x'^2\partial_{x'}\phi)$ and $\mathcal{H}^2\Omega_M = H_0^2\Omega_{M0}(1+z)$. Also for calculating integrated contributions in Eq. (2.15) proper time differences are converted to comoving distances, e.g. $\tau_0 - \tau' = x'$. Now we can construct the corresponding local power spectrum defined in Eq. (2.5). This becomes:

$$P_{g,L}^{\rm loc}(\vec{k},\vec{x}_c) = \int_{\vec{x}_{12}} e^{-i\vec{k}\cdot\vec{x}_{12}}\,\langle\delta_{g,L}(\vec{x}_c+\vec{x}_{12}/2)\,\delta_{g,L}(\vec{x}_c-\vec{x}_{12}/2)\rangle \tag{2.54}$$

where we have used that $\vec{x}_{1,2} = \vec{x}_c \pm \vec{x}_{12}/2$, following the geometry of Fig. 2.1. In the following we will also use $\langle\tilde{\delta}_{m0}(\vec{k}_1)\tilde{\delta}_{m0}(\vec{k}_2)\rangle = \delta_D(\vec{k}_1+\vec{k}_2)\tilde{P}_{m0}(k)$ with $\tilde{P}_{m0}(k)$ being the linear dark matter power spectrum in the SCG at the corresponding redshift.

2.4.3 Wide-angle corrections

We now illustrate, with an example, how wide-angle effects can be easily calculated using perturbative expansions. Let's consider, for instance, the RSD-RSD contribution (which comes from the $\mathrm{F}^{\rm RSD}\times\mathrm{F}^{\rm RSD}$ contribution) to the local power spectrum in Eq. (2.54) which, from Eqs (2.50) and (2.51), takes the form:

$$\int_{\vec{x}_{12},\vec{k}'} e^{-i(\vec{k}-\vec{k}')\cdot\vec{x}_{12}}\,[b_1+f\,(\hat{k}'\cdot\hat{x}_1)^2]\,[b_1+f\,(\hat{k}'\cdot\hat{x}_2)^2] \times\tilde{P}_m(k'). \tag{2.55}$$

Wide-angle corrections arise when one relaxes the assumption that $\hat{x}_1$ and $\hat{x}_2$ are equal to $\hat{x}_c$. Here we ignore the variation of f itself and assume it is evaluated at x_c. Similarly, $\tilde{P}_m(k')$ is evaluated at x_c. In general, calculation of wide-angle corrections can be complicated but for sufficiently small ratio of $\vec{x}_{12}/x_c$ one can compute them perturbatively.

Perturbative methods for calculation of leading order wide-angle corrections to two-point correlation functions have been used in [95, 26] by choosing $\vec{x}_{12}/x_c$ or other suitable choices (like

the bisector instead of the midpoint in the denominator) for quantifying the magnitudes of the corrections. Here our approach for perturbative calculations is relatively different as we find analytic relations in Cartesian Fourier space that can be easily extended to the nonlinear regime and also to higher-order statistics like bispectrum.

Let's again consider the geometry of Fig. 2.1 as a sketch of galaxy pair positions and our choice of LOS. We define the perturbation parameter vector to be:

$$\boldsymbol{\epsilon} \equiv \frac{\vec{x}_{12}}{x_c} \tag{2.56}$$

with $\vec{x}_{12} = \vec{x}_1 - \vec{x}_2$. We can assume that pairs are within spherical bins with mean radius at redshift $\bar{z}$ and depth Δz. For most surveys $\Delta z/\bar{z} < 1$. Therefore, the sample volume can be written as:

$$V_s = \frac{4\pi}{3} f_{\rm sky} \left[\left(\bar{r} + \frac{\Delta r}{2} \right)^3 - \left(\bar{r} - \frac{\Delta r}{2} \right)^3 \right] \tag{2.57}$$

where $f_{\rm sky} \equiv \Omega_s/\Omega_{\rm tot}$ is the fraction of the sky covered by the survey ($\Omega_{\rm tot} \simeq 41253$ deg^2) and $\bar{r}$ and Δr correspond to the comoving distances at $\bar{z}$ and Δz. We assume for most galaxy pairs within the bin, the ratio of Eq. (2.56) is small. It is also worth noting that, looking at Eq. (2.4), the results that will be obtained in the following can be windowed by any survey-specific window function (see Section 2.6). Also, there can be pairs for which (2.56) is larger than one. However, their corresponding separations are most of the time much larger than k^{-1} for the scales we are interested in. Therefore, these have negligible contributions and one can still use the entire survey volume.

To evaluate integrals such as Eq. (2.55), one can expand $\hat{x}_1$, $\hat{x}_2$ and any scalar function made

out of them in terms of $\vec{\epsilon}$ to any desired order. For example:

$$\hat{x}_1 = \frac{\vec{x}_c + \vec{x}_{12}/2}{|\vec{x}_c + \vec{x}_{12}/2|} = \hat{x}_c + \frac{1}{2}\boldsymbol{\epsilon} + ... + O(\epsilon^3)\,,$$
$$\frac{1}{x_1} = \frac{1}{x_c}(1 - \frac{1}{2}\boldsymbol{\epsilon}\cdot\hat{x}_c + ...) \tag{2.58}$$

and similar expansions for $\hat{x}_2$, $1/x_2$. Here we keep terms up to second order to compute leading order contributions. But in general, these help us separate wide-angle corrections in a perturbative manner to any desired order.

After these expansions, we can decompose $\boldsymbol{\epsilon}$ into its Cartesian components, with the "z"-direction defined to be along the LOS unit vector, $\hat{x}_c$. Doing so, Eq. (2.55) can be expressed as a sum of integrals that have the following general form:

$$\mathcal{I}^L_{m,n,l} = \int_{\vec{x}_{12},\vec{k}'} e^{i(\vec{k}'-\vec{k})\cdot\vec{x}_{12}} C_{m,n,l}(\vec{k}', \hat{x}_c, x_c)(\boldsymbol{\epsilon}_x)^m(\boldsymbol{\epsilon}_y)^n(\boldsymbol{\epsilon}_z)^l \tag{2.59}$$

where C contains all corresponding terms apart from perturbation factors and (m, n, l) can be 0, 1 and 2 such that $(m + n + l) \leq 2$ (for terms up to second order). Now, according to Eq. (2.56), all $(\boldsymbol{\epsilon}_j)^a$ terms turn into the a-th derivative of the exponential factor with respect to $\vec{k}_j$ and can be pulled out of the integral. This results in no $\vec{x}_{12}$ factor being left inside and the integral over $\vec{x}_{12}$ becomes delta function, $\delta_D(\vec{k}' - \vec{k})$, which results in:

$$\mathcal{I}^L_{m,n,l} = \left(\frac{i^{(m+n+l)}}{x_c^m\, x_c^n\, x_c^l}\right)\left(\frac{\partial^m}{\partial k_x^m}\,\frac{\partial^n}{\partial k_y^n}\,\frac{\partial^l}{\partial k_z^l}\right)\; C_{m,n,l}(\vec{k}, \hat{x}_c, x_c) \tag{2.60}$$

and we sum over all such terms:

$$\mathcal{I}^L(k, \hat{k}.\hat{x}_c, x_c) = \sum_{(m+n+l)\leq 2} \mathcal{I}^L_{m,n,l}(k, \hat{k}.\hat{x}_c, x_c) \tag{2.61}$$

This result depends only on $\vec{k}$ and $\vec{x}_c$, as expected. Also with our symmetric choice of LOS there is no imaginary term and, therefore, no $1/(kx_c)$ contribution. The leading order wide-angle corrections to the power spectrum are therefore suppressed by $1/(kx_c)^2$ or $(1/(kx_c))(\mathcal{H}/k)$ where the latter corresponds to mixing with relativistic corrections.

2.4.4 Non-integrated relativistic corrections

The procedure explained above for wide-angle effects involves computing the mixing between wide-angle and relativistic contributions. Therefore, to find non-integrated relativistic terms one can evaluate the corresponding contributions to $P^{\rm loc}_{g,L}$ with the plane-parallel assumption.

Finally, it is worth mentioning that in previous parts, we assumed that parameters like f, $\tilde{\mathcal{D}}_+$, Ω_M, etc. are evaluated at x_c. As an example, we assumed $f(x_1)f(x_2) \approx f(x_c)^2$. While one would expect that this is a good approximation for surveys that are radially narrow, it is strightforward to obtain corrections to this assumption by performing an expansion around x_c. This will result in terms that are suppressed by $\mathcal{H}^2/k^2$ where $\mathcal{H}$ is evaluated at x_c. Then, the result is integrated over, as in Eq. (2.8), to yield the final multipoles.

2.4.5 Integrated relativistic corrections

To find the leading order correction from integrated contributions to the local power spectrum, one should start from Eq. (2.54) and, considering Eq. (2.50), cross correlate Eq. (2.53) with the RSD term, Eq. (2.51). This results in:

$$\int_{\vec{x}_{12},\vec{k}'} e^{-i\vec{k}\cdot\vec{x}_{12}} \left(\int_0^{x_1} dx' e^{i\vec{k}'\cdot(\vec{x}'-\vec{x}_2)}\, \mathrm{F}^{\rm I}(k', x_1, x', \hat{k}'\cdot\hat{x}')\, \mathrm{F}^{\rm RSD}(-\hat{k}'\cdot\hat{x}_2) \right.$$
$$\left. + \int_0^{x_2} dx' e^{i\vec{k}'\cdot(\vec{x}_1-\vec{x}')}\, \mathrm{F}^{\rm I}(k', x_2, x', -\hat{k}'\cdot\hat{x}')\, \mathrm{F}^{\rm RSD}(\hat{k}'\cdot\hat{x}_1) \right) \tilde{P}_{m0}(k') \tag{2.62}$$

Now we can make use of the fact that $\hat{x}' = \hat{x}_1 = \vec{x}_1/x_1$ in the first integral and $\hat{x}' = \hat{x}_2 = \vec{x}_2/x_2$ in the second one (at linear level in fluctuations) and also perform the coordinate transformation $y = x' x_c/x_1$ and $y = x' x_c/x_2$ in the first and second integrals respectively. Then, using that $\vec{x}_{1,2} = \vec{x}_c \pm \vec{x}_{12}/2$ one obtains:

$$\int_{\vec{x}_{12},\vec{k}'} e^{-i(\vec{k}-\frac{x_c+y}{2x_c}\vec{k}')\cdot\vec{x}_{12}} \left(\int_0^{x_c} dy \left(\frac{x_1}{x_c}\right) e^{i\vec{k}'\cdot\left(\frac{y}{x_c}-1\right)\cdot\vec{x}_c} \mathrm{F}^{\mathrm{I}}\left(k', x_1, \frac{x_1}{x_c}y, \hat{k}'\cdot\hat{x}_1\right) \mathrm{F}^{\mathrm{RSD}}(-\hat{k}'\cdot\hat{x}_2) \right.$$
$$\left. + \int_0^{x_c} dy \left(\frac{x_2}{x_c}\right) e^{-i\vec{k}'\cdot\left(\frac{y}{x_c}-1\right)\cdot\vec{x}_c} \mathrm{F}^{\mathrm{I}}\left(k', x_2, \frac{x_2}{x_c}y, -\hat{k}'\cdot\hat{x}_2\right) \mathrm{F}^{\mathrm{RSD}}(\hat{k}'\cdot\hat{x}_1) \right) \tilde{P}_{m0}(k') \,. \quad (2.63)$$

Now, to find the leading order contribution, we can ignore mixing with wide-angle corrections and set $\hat{x}_1 = \hat{x}_2 = \hat{x}_c$ in the equation above. In addition $x_{1,2}/x_c$ can also be set to one as any correction will produce subleading terms. The final result then becomes:

$$\int_0^{x_c} dy \quad \left(\frac{2x_c}{x_c+y}\right)^3 \left(e^{i2(\frac{y-x_c}{y+x_c})\vec{k}\cdot\vec{x}_c} \mathrm{F}^{\mathrm{I}}\left(\frac{2x_c k}{x_c+y}, x_c, y, \hat{k}\cdot\hat{x}_c\right) \mathrm{F}^{\mathrm{RSD}}(-\hat{k}\cdot\hat{x}_c) + \right.$$
$$\left. e^{-i2\left(\frac{y-x_c}{y+x_c}\right)\vec{k}\cdot\vec{x}_c} \mathrm{F}^{\mathrm{I}}\left(\frac{2x_c k}{x_c+y}, x_c, y, -\hat{k}\cdot\hat{x}_c\right) \mathrm{F}^{\mathrm{RSD}}(\hat{k}\cdot\hat{x}_c) \right) \tilde{P}_{m0}\left(\frac{2x_c k}{x_c+y}\right) \quad (2.64)$$

which is a simple 1D integral for numerical integration as will be discussed in the following.

Final Results

The final results for the local linear power spectrum with non-integrated relativistic (including inverse-distance) and wide-angle corrections take the following form:

$$P_{g,L}^{\mathrm{loc,\,NI}}(k,\eta,x_c) = P_{g,L}^{\mathrm{pp}}(k,\eta) + \frac{1}{(kx_c)^2}P_g^{\mathrm{R1}}(k,\eta) + \frac{\mathcal{H}^2}{k^2}P_g^{\mathrm{R2}}(k,\eta) + \frac{1}{(kx_c)}\frac{\mathcal{H}}{k}P_g^{\mathrm{R12}}(k,\eta) +$$
$$+\frac{1}{(kx_c)^2}P_g^{\mathrm{w1}}(k,\eta) + \frac{1}{(kx_c)}\frac{\mathcal{H}}{k}P_g^{\mathrm{w2}}(k,\eta) + O(\frac{1}{(kx_c)^4}) + \ldots \quad (2.65)$$

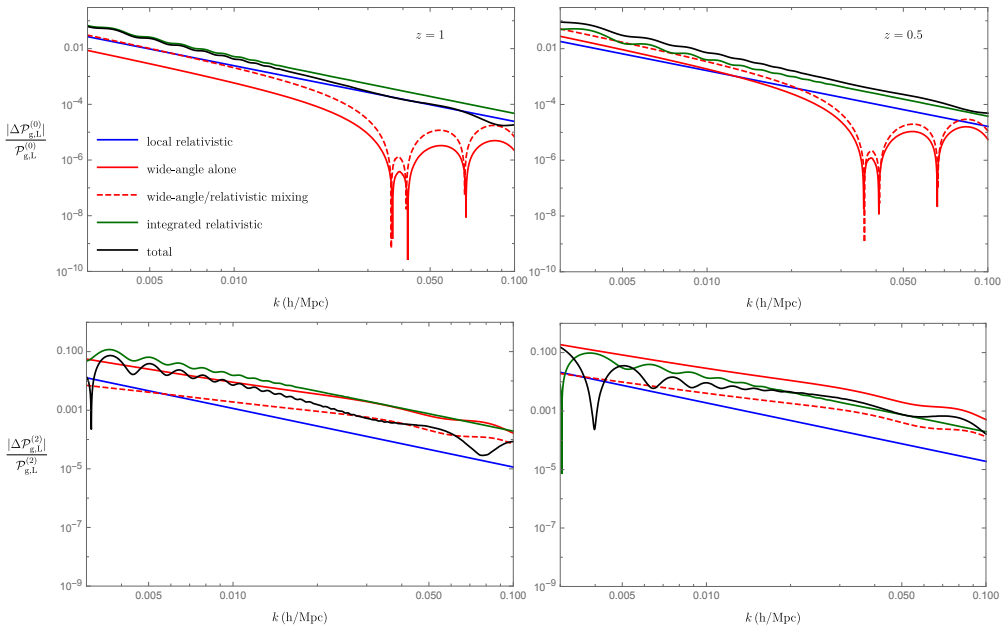

Figure 2.2: Absolute values of relative corrections to monopole and quadrupole of the plane-parallel linear local power spectrum from leading local (non-integrated) relativistic (corresponding to functions R_1, R_2 and R_{12} defined above), wide-angle alone (function $w1$ which also includes the mixing with inverse-distance corrections modified by magnification bias), wide-angle/relativistic mixing (function $w2$) and integrated relativistic corrections (based on the integral of (2.64)). The black line shows the sum of all these contributions. The linear bias is $b_1 = 1.5$, and magnification and evolution biases are set to $s = 1$ and $b_e = 0$ respectively.

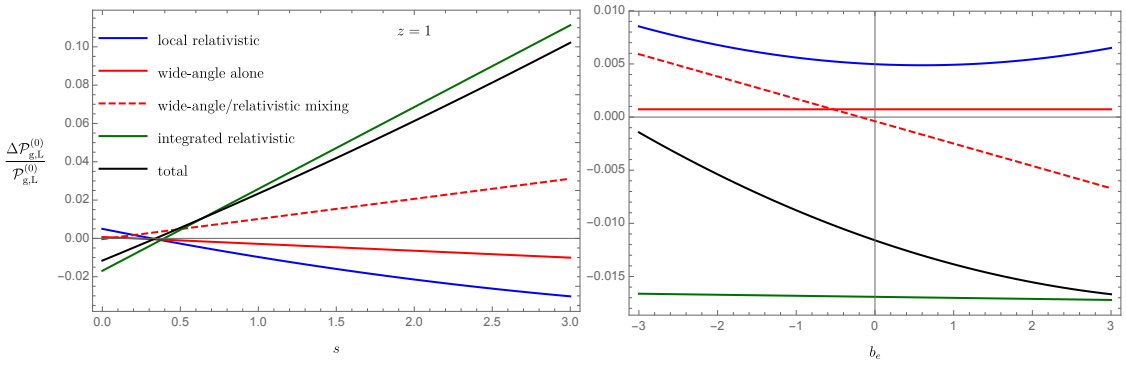

Figure 2.3: Similar plot as above (not absolute value) for monopole but at a fixed scale, $k = 0.005\ h/\text{Mpc}$ and varying magnification bias with $b_e = 0$ (left) and evolution bias with $s = 0$ (right) at redshift $z = 1$

where again $\eta = \hat{k} \cdot \hat{x}_c$. The first term is just the local plane-parallel approximation result:

$$P^{\rm pp}_{g,L}(k,\eta) = (b_1 + f\eta^2)^2\, \tilde{P}_L(k)\,. \tag{2.66}$$

The next three terms are non-integrated relativistic corrections which include inverse-distance (R_1) modified by magnification bias and other local (non-integrated) relativistic (R_2) contributions and the mixing between them (R_{12}). We have:

$$P^{\rm R_1}_{g}(k,\eta) = f^2\eta^2(2-5s)^2\, \tilde{P}_L(k) \tag{2.67}$$

and

$$\begin{aligned} P^{\rm R_2}_{g}(k,\eta) = \frac{1}{4}\Bigg[&-4b_1 f(-6+2b_e+3\Omega_M) + 6b_1\Omega_M(2+2b_e-20s+3\Omega_M) \\ &+f\eta^2\Big(6\Omega_M(2+2b_e-20s+3\Omega_M) + f(28+4b_e^2+40s+100s^2 \\ &-4b_e(4+10s-3\Omega_M) - 24\Omega_M - 60\,s\,\Omega_M + 9\,\Omega_M^2)\Big)\Bigg]\tilde{P}_L(k) \end{aligned} \tag{2.68}$$

$$P^{\rm R_{12}}_{g}(k,\eta) = (-2+5s)\left(3\,b_1\Omega_M + 3f\eta^2\Omega_M + f^2\eta^2(-2+2b_e-10s+3\Omega_M)\right)\tilde{P}_L(k) \tag{2.69}$$

The last two terms in Eq. (2.65) are the leading order wide-angle corrections which have mixing

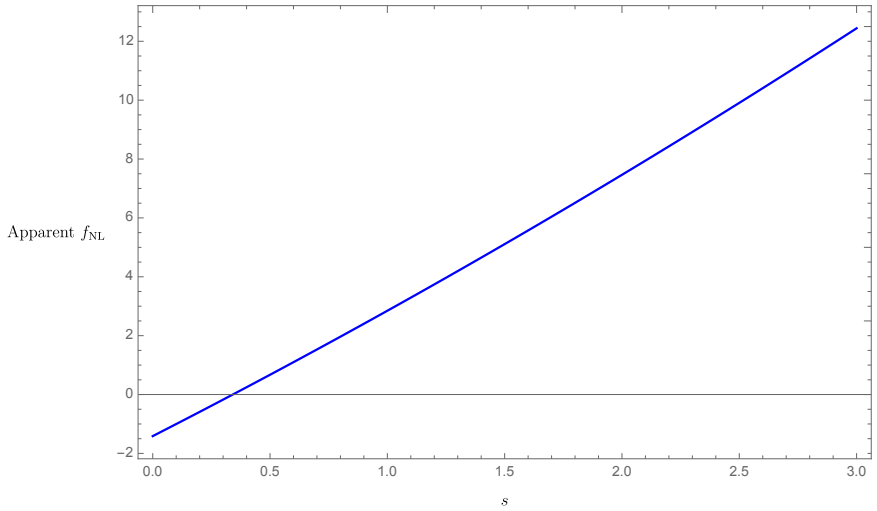

Figure 2.4: Apparent $f_{\rm NL}$ induced by deviations of the plane-parallel approximation for linear galaxy bias $b_1 = 1.5$ as a function of magnification bias at $k = 0.005$ h/Mpc and assuming $b_e = 0$.

with inverse-distance and other non-integrated relativistic terms. These two contributions vanish in the limit $\vec{x}_1 = \vec{x}_2$. We find:

$$\begin{aligned} P_g^{\rm w1}(k,\eta) &= f\left(b_1\left(-16\eta^4+17\eta^2+\left(5-20\,\eta^2\right)s-2\right)+f\eta^2\left(-24\,\eta^4+26\,\eta^2+5s-7\right)\right) \\ &\quad +f\left(b_1\left(10\,\eta^4-11\,\eta^2+5\left(2\eta^2-1\right)s+2\right)+f\eta^2\left(9\,\eta^4-8\,\eta^2+5s\right)\right)k\tilde{P}_L'(k) \\ &\quad -\frac{1}{2}f\left(\eta^2-1\right)\left(4b_1\eta^2-b_1+2f\eta^4+f\eta^2\right)k^2\tilde{P}_L''(k)\,. \end{aligned} \tag{2.70}$$

and

$$\begin{aligned} P_g^{\rm w2}(k,\eta) &= -f\eta^2\left(b_1-2f\eta^2+f\right)(2b_e-10s+3\,\Omega_M-2)\tilde{P}_L(k) \\ &\quad +\frac{1}{2}f\left(\eta^2-1\right)\left(b_1-f\eta^2\right)(2b_e-10s+3\Omega_M-2)k\tilde{P}_L'(k) \end{aligned} \tag{2.71}$$

with $\tilde{P}' = d\tilde{P}/dk$, etc. A similar procedure is followed for the integrated relativistic correction. In fact, the local power spectrum for these contributions can be found by inserting (2.64) into the integral of Eq. (2.72) and doing the integral over $\eta = \hat{k}\cdot\hat{x}_c$ first. This results in a straightforward one-dimensional integral over y.

From these results, one can insert them into Eq. (2.7) to find the local multipoles:

$$\mathcal{P}^{(\ell)}_{g,L}(k, x_c) \equiv \frac{(2\ell+1)}{2} \int_{-1}^{1} d\eta \, \mathcal{L}_\ell(\eta) P_{g,L}(k, \eta, x_c) \tag{2.72}$$

which can be used in Eq. (2.8) to obtain the power spectrum multipoles:

$$P^{(\ell)}_g(k) \equiv \int_{V_s} \frac{d^3\vec{x}_c}{V_s} \mathcal{P}^{(\ell)}_{g,L}(k, x_c), \tag{2.73}$$

where the integration is done within the volume of the galaxy sample, V_s, see Eq. (2.57).

Let us now illustrate these corrections and estimate their relative importance. Here we show plots of corrections to the local power spectrum and do not specify a survey bin. However, it is very straightforward to find the final power spectrum multipoles by performing the integration in Eq. (2.73) since the local power spectrum multipoles are functions of magnitude of $\vec{x}_c$ only. In addition, for bins with narrow depth, the results are close. Figure 2.2 shows our results at redshift $z = 1$ and linear bias $b_1 = 1.5$. For the cosmology, we assumed a flat ΛCDM model with $\Omega_M = 0.32$, $\sigma_8 = 0.828$, $n_s = 0.968$ and negligible radiation. For this plot, we also assumed $s = 1$ and $b_e = 0$ (i.e $n_g \propto 1/a^3$). In general, the relative importance of different contributions depends on redshift and total corrections scale almost like $1/k^2$ at these $k's$. Figure 2.3 shows the variation of monopole corrections at a fixed scale $k = 0.005$ h/Mpc. We can see here that there is much more sensitivity to magnification bias as compared with evolution bias.

Implications for local $f_{\rm NL}$ measurements

It is well known that local primordial non-Gaussianity (PNG) induces a scale-dependent bias with the following form [35, 110]:

$$\Delta b(k) = 3 f_{\rm NL} \delta_c (b_1 - 1) \frac{\Omega_M \mathcal{H}^2 a}{\tilde{D}_+(z) k^2 T(k)} \tag{2.74}$$

where $T(k)$ is the transfer function and $\delta_c \simeq 1.69$. This modifies the (plane-parallel) linear galaxy power spectrum as $P_g^{\rm pp,\,NG}(k,\eta) \rightarrow (b_1 + \Delta b(k) + f\eta^2)^2 \tilde{P}_L(k)$. At large scales ($k \lesssim 0.01$ h/Mpc) where $T(k) \rightarrow 1$, the $1/k^2$ scaling of Δb resembles that of wide-angle and relativistic contributions calculated already. This implies that such corrections can be mistaken with a true $f_{\rm NL}$ term if not taken into account in theoretical modeling. Comparing power spectrum monopoles, for example, we can find such apparent $f_{\rm NL}$. Figure 2.4 shows such a term as a function of magnification bias. It is estimated by comparing the PNG correction to the linear monopole power spectrum with the similar corrections from the total wide-angle and relativistic (integrated and non-integrated) contributions. It is smaller than current limits but not negligible compared to upcoming survey forecasts [129].

2.5 The One-loop Power Spectrum

2.5.1 Beyond Linear Theory

We now show how to apply the perturbative approach followed in the linear case to include non-linear effects. Here we keep terms up to third order in SPT (1-loop). For this case we neglect relativistic $\mathcal{H}/k$ contributions and consider inverse distance and wide-angle corrections only. This is because their inclusion is an unnecessary complication for our purpose of comparing the wide-angle corrections with other local effects as inverse-distance terms and other local relativistic terms are typically of the same order (see e.g. [63, 10] for an investigation of relativistic effects in the nonlinear regime). Therefore, hereafter we remove the "tilde" on top of SCG quantities for simplicity and, for example, use δ instead of $\tilde{\delta}$.

Equation (2.12) can be recast by writing δ_g and $\vec{v}$ in terms of their Fourier representations, and assuming negligible vorticity the velocity field can be rewritten in terms of its scalar mode, the divergence $\Theta_v = \boldsymbol{\nabla}\cdot\vec{v} \equiv -\mathcal{H}f\boldsymbol{\nabla}\cdot\vec{u} = -\mathcal{H}f\Theta$ which carries the same amount of information.

Therefore, Equation (2.12) can be rewritten as:

$$\begin{aligned}\delta_{g,s}(\vec{x}) &= \delta_g(\vec{x}) + f\int_{\vec{k}} e^{i\vec{k}\cdot\vec{x}} D_\theta(\vec{k},\vec{x})\,\Theta(\vec{k}) + f\int_{\vec{k}_1,\vec{k}_2} e^{i\vec{k}_{12}\cdot\vec{x}} D_{\theta\delta}(\vec{k}_1,\vec{k}_2,\vec{x})\,\Theta(\vec{k}_1)\delta_g(\vec{k}_2) + \\ & f^2\int_{\vec{k}_1,\vec{k}_2} e^{i\vec{k}_{12}\cdot\vec{x}} D_{\theta\theta}(\vec{k}_1,\vec{k}_2,\vec{x})\,\Theta(\vec{k}_1)\Theta(\vec{k}_2) \\ & + f^2\int_{\vec{k}_1,\vec{k}_2,\vec{k}_3} e^{i\vec{k}_{123}\cdot\vec{x}} D_{\theta\theta\delta}(\vec{k}_1,\vec{k}_2,\vec{k}_3,\vec{x})\,\Theta(\vec{k}_1)\Theta(\vec{k}_2)\delta_g(\vec{k}_3) + \\ & f^3\int_{\vec{k}_1,\vec{k}_2,\vec{k}_3} e^{i\vec{k}_{123}\cdot\vec{x}} D_{\theta\theta\theta}(\vec{k}_1,\vec{k}_2,\vec{k}_3,\vec{x})\,\Theta(\vec{k}_1)\Theta(\vec{k}_2)\Theta(\vec{k}_3) + \ldots\end{aligned} \tag{2.75}$$

where the D kernels collect terms proportional to δ_g and powers of Θ as denoted by their subindex, and we have displayed only the necessary terms for a 1-loop power spectrum calculation. These kernels are given by,

$$\begin{aligned}D_\theta(\vec{k},\vec{x}) &= \frac{(\vec{k}\cdot\hat{x})^2}{k^2} - \frac{2i}{x}\frac{\vec{k}\cdot\hat{x}}{k^2}, \\ D_{\theta\delta}(\vec{k}_1,\vec{k}_2,\vec{x}) &= \frac{(\vec{k}_{12}\cdot\hat{x})(\vec{k}_1\cdot\hat{x})}{k_1^2} - \frac{2i}{x}\frac{\vec{k}_1\cdot\hat{x}}{k_1^2}, \\ D_{\theta\theta}(\vec{k}_1,\vec{k}_2,\vec{x}) &= \frac{(\vec{k}_1\cdot\hat{x})(\vec{k}_2\cdot\hat{x})}{k_1^2k_2^2}\left(\frac{1}{2}(\vec{k}_{12}\cdot\hat{x})^2 - \frac{2i}{x}(\vec{k}_{12}\cdot\hat{x}) - \frac{1}{x^2}\right), \\ D_{\theta\theta\delta}(\vec{k}_1,\vec{k}_2,\vec{k}_3,\vec{x}) &= \frac{(\vec{k}_1\cdot\hat{x})(\vec{k}_2\cdot\hat{x})}{k_1^2k_2^2}\left(\frac{1}{2}(\vec{k}_{123}\cdot\hat{x})^2 - \frac{2i}{x}(\vec{k}_{123}\cdot\hat{x}) - \frac{1}{x^2}\right), \\ D_{\theta\theta\theta}(\vec{k}_1,\vec{k}_2,\vec{k}_3,\vec{x}) &= \frac{(\vec{k}_1\cdot\hat{x})(\vec{k}_2\cdot\hat{x})(\vec{k}_3\cdot\hat{x})}{k_1^2k_2^2k_3^2}\left(\frac{1}{6}(\vec{k}_{123}\cdot\hat{x})^3 - \frac{i}{x}(\vec{k}_{123}\cdot\hat{x})^2 - \frac{1}{x^2}(\vec{k}_{123}\cdot\hat{x})\right).\end{aligned} \tag{2.76}$$

where $\vec{k}_{12\ldots} = \vec{k}_1 + \vec{k}_2 + \ldots$. The first term in each of these kernels corresponds to the plane-parallel result where the fixed LOS is replaced by $\hat{x}$, the second and further terms correspond to inverse-distance corrections.

These expressions include all RSD contributions needed for the calculation of the tree-level bispectrum and one-loop galaxy power spectrum. These results can also be used to derive the

RSD perturbatiom theory (PT) kernels, after using the PT expansion for δ and Θ. We discuss them in Appendix A.

We start from Eq. (2.75) and plugging it into Eq. (2.5) we find

$$
\begin{aligned}
P^{loc}_{g,s}(\vec{k},\vec{x}_c) = & \int_{\vec{x}_{12},\vec{k}_1} e^{i(\vec{k}_1-\vec{k})\cdot\vec{x}_{12}}\Big\{P_{gg}(k_1) + f\Big(D_\theta(-\vec{k}_1,\vec{x}_2) + D_\theta(\vec{k}_1,\vec{x}_1)\Big)P_{g\theta}(k_1) \\
& + f^2 D_\theta(\vec{k}_1,\vec{x}_1)D_\theta(-\vec{k}_1,\vec{x}_2)P_{\theta\theta}(k_1)\Big\} + \\
& \int_{\{\vec{x}_{12},\vec{k}_1,\vec{k}_2\}} e^{i(\vec{k}_{12}-\vec{k})\cdot\vec{x}_{12}}\Big\{f^2 b_1^2 D_{\theta\delta}(\vec{k}_1,\vec{k}_2,\vec{x}_1)\Big(D_{\theta\delta}(-\vec{k}_1,-\vec{k}_2,\vec{x}_2) + D_{\theta\delta}(-\vec{k}_2,-\vec{k}_1,\vec{x}_2)\Big)\times \\
& \times P_L(k_1)P_L(k_2) + f^4 D_{\theta\theta}(\vec{k}_1,\vec{k}_2,\vec{x}_1)\Big(D_{\theta\theta}(-\vec{k}_1,-\vec{k}_2,\vec{x}_2) + D_{\theta\theta}(-\vec{k}_2,-\vec{k}_1,\vec{x}_2)\Big)P_L(k_1)P_L(k_2)\Big\} + \\
& + \Bigg[\Bigg(\int_{\vec{x}_{12},\vec{k}_1,\vec{k}_2} e^{i(\vec{k}_1-\vec{k})\cdot\vec{x}_{12}}\Big\{f D_{\theta\delta}(\vec{k}_2,-\vec{k}_{12},\vec{x}_2)B_{g\theta g}(\vec{k}_1,\vec{k}_2,-\vec{k}_{12}) \\
& + f^2 D_{\theta\theta}(\vec{k}_2,-\vec{k}_{12},\vec{x}_2)B_{g\theta\theta}(\vec{k}_1,\vec{k}_2,-\vec{k}_{12}) + f^2 D_\theta(\vec{k}_1,\vec{x}_1)D_{\theta\delta}(\vec{k}_2,-\vec{k}_{12},\vec{x}_2)B_{\theta\theta g}(\vec{k}_1,\vec{k}_2,-\vec{k}_{12}) \\
& + f^3 D_\theta(\vec{k}_1,\vec{x}_1)D_{\theta\theta}(\vec{k}_2,-\vec{k}_{12},\vec{x}_2)B_{\theta\theta\theta}(\vec{k}_1,\vec{k}_2,-\vec{k}_{12}) + f^2 b_1^2\Big(D_{\theta\theta\delta}(-\vec{k}_1,\vec{k}_2,-\vec{k}_2,\vec{x}_2) + \\
& D_{\theta\theta\delta}(\vec{k}_2,-\vec{k}_1,-\vec{k}_2,\vec{x}_2) + D_{\theta\theta\delta}(\vec{k}_2,-\vec{k}_2,-\vec{k}_1,\vec{x}_2)\Big)P_L(k_1)P_L(k_2) + f^3 b_1\Big(D_{\theta\theta\theta}(-\vec{k}_1,\vec{k}_2,-\vec{k}_2,\vec{x}_2) \\
& + D_{\theta\theta\theta}(\vec{k}_2,-\vec{k}_1,-\vec{k}_2,\vec{x}_2) + D_{\theta\theta\theta}(\vec{k}_2,-\vec{k}_2,-\vec{k}_1,\vec{x}_2)\Big)P_L(k_1)P_L(k_2) \\
& + f^3 b_1 D_\theta(\vec{k}_1,\vec{x}_1)\Big(D_{\theta\theta\delta}(-\vec{k}_1,\vec{k}_2,-\vec{k}_2,\vec{x}_2) + D_{\theta\theta\delta}(\vec{k}_2,-\vec{k}_1,-\vec{k}_2,\vec{x}_2) \\
& + D_{\theta\theta\delta}(\vec{k}_2,-\vec{k}_2,-\vec{k}_1,\vec{x}_2)\Big)P_L(k_1)P_L(k_2) + f^4 D_\theta(\vec{k}_1,\vec{x}_1)\Big(D_{\theta\theta\theta}(-\vec{k}_1,\vec{k}_2,-\vec{k}_2,\vec{x}_2) \\
& + D_{\theta\theta\theta}(\vec{k}_2,-\vec{k}_1,-\vec{k}_2,\vec{x}_2) + D_{\theta\theta\theta}(\vec{k}_2,-\vec{k}_2,-\vec{k}_1,\vec{x}_2)\Big)P_L(k_1)P_L(k_2)\Big\} \\
& + \int_{\vec{x}_{12},\vec{k}_1,\vec{k}_2} e^{i(\vec{k}_{12}-\vec{k})\cdot\vec{x}_{12}}\Big\{f^3 b_1 D_{\theta\delta}(\vec{k}_1,\vec{k}_2,\vec{x}_1)\Big(D_{\theta\theta}(-\vec{k}_1,-\vec{k}_2,\vec{x}_2) \\
& + D_{\theta\theta}(-\vec{k}_2,-\vec{k}_1,\vec{x}_2)\Big)P_L(k_1)P_L(k_2)\Big\}\Bigg) \qquad + \qquad (\vec{x}_1 \leftrightarrow \vec{x}_2)\Bigg].
\end{aligned}
\tag{2.77}
$$

where we have used that four-point functions can be treated in the Gaussian limit due to our

one-loop approximation, the D-functions are defined as in Eq. (2.76) and, as usual,

$$\left\langle \delta_g(\vec{k}_1)\,\delta_g(\vec{k}_2)\right\rangle = \delta_D(\vec{k}_1+\vec{k}_2)\,P_{gg}(k_1), \quad \left\langle \delta_g(\vec{k}_1)\,\Theta(\vec{k}_2)\right\rangle = \delta_D(\vec{k}_1+\vec{k}_2)\,P_{g\theta}(k_1), \tag{2.78}$$

$$\left\langle \Theta(\vec{k}_1)\,\Theta(\vec{k}_2)\right\rangle = \delta_D(\vec{k}_1+\vec{k}_2)\,P_{\theta\theta}(k_1)$$

$$\left\langle \delta_g(\vec{k}_1)\delta_g(\vec{k}_2)\Theta(\vec{k}_3)\right\rangle = \delta_D(\vec{k}_1+\vec{k}_2+\vec{k}_3)\;B_{gg\theta}(\vec{k}_1,\vec{k}_2,\vec{k}_3) \tag{2.79}$$

and similarly for other bispectra terms such as $B_{g\theta g}$, etc. To perform a one-loop calculation of the galaxy power spectrum in redshift space we need biased bispectra at tree-level and biased power spectra at one-loop. Therefore we include local bias terms up to second order (b_1, b_2) with non-local bias contributions from tidal fields at second and third order (γ_2 and γ_{21} in the parametrization of [30, 49, 48]). The bias expansion then reads,

$$\delta_g(\vec{x}) = \quad b_1\delta(\vec{x}) + \frac{b_2}{2}\delta^2(\vec{x}) + \gamma_2\,\mathcal{G}_2(\Phi_v|\vec{x}) + \gamma_{21}\,\mathcal{G}_2(\varphi_1,\varphi_2\,|\vec{x}) + \ldots$$

where "..." refers to higher order terms or those that enforce $\langle\delta_g\rangle = 0$. The latter don't change the power spectrum as long as $k \neq 0$. In this equation $\mathcal{G}_2(\Phi_v|\vec{x})$ is the second-order Galileon arising from tidal effects defined as:

$$\mathcal{G}_2(\Phi_v|\vec{x}) \equiv (\nabla_{ij}\Phi_v)^2 - (\nabla^2\Phi_v)^2 \tag{2.80}$$

with $\nabla^2\Phi_v = \Theta$. In addition, $\mathcal{G}_2(\varphi_1,\varphi_2\,|\vec{x})$ is a nonlocal third-order bias contribution that depends on the Lagrangian linear and quadratic potentials $\varphi_{1,2}$ [49]:

$$\mathcal{G}_2(\varphi_1,\varphi_2|\vec{x}) \equiv \nabla_{ij}\varphi_1\nabla_{ij}\varphi_2 - \nabla^2\varphi_1\nabla^2\varphi_2 \tag{2.81}$$

where $\nabla^2\varphi_1 = -\delta$ and $\nabla^2\varphi_2 = -\mathcal{G}_2(\varphi_1)$.

The galaxy-galaxy and matter-galaxy power spectra in this bias basis has been calculated in

[49, 48]. Using their formulas, one can also find galaxy-velocity power spectrum. We have:

$$\begin{aligned} P_{\rm gg}(k) = \; & b_1^2 P_{mm}(k) + 4\, b_1 P_L(k) \int_{\vec{q}} \Big[2\gamma_2 G_2(\vec{k}, -\vec{q}) + \gamma_{21} K(\vec{k}, \vec{q}) \Big] K(\vec{k} - \vec{q}, \vec{q}) P_L(|\vec{k} - \vec{q}|) \\ & + 2\, b_1 \int_{\vec{q}} \Big[b_2 + 2\gamma_2 K(\vec{k} - \vec{q}, \vec{q}) \Big] F_2(\vec{k} - \vec{q}, \vec{q}) P_L(|\vec{k} - \vec{q}|) P_L(q) \\ & + \frac{1}{2} \int_{\vec{q}} \Big[b_2^2 + 2 b_2 \gamma_2 K(\vec{k} - \vec{q}, \vec{q}) + 4\gamma_2^2 K(\vec{k} - \vec{q}, \vec{q})^2 \Big] P_L(|\vec{k} - \vec{q}|) P_L(q)\,, \end{aligned} \tag{2.82}$$

and

$$\begin{aligned} P_{\rm g\theta}(k) = \; & b_1 P_{m\theta}(k) + 2 P_L(k) \int_{\vec{q}} \Big[2\gamma_2 G_2(\vec{k}, -\vec{q}) + \gamma_{21} K(\vec{k}, \vec{q}) \Big] K(\vec{k} - \vec{q}, \vec{q}) P_L(|\vec{k} - \vec{q}|) \\ & + \int_{\vec{q}} \Big[b_2 + 2\gamma_2 K(\vec{k} - \vec{q}, \vec{q}) \Big] G_2(\vec{k} - \vec{q}, \vec{q}) P_L(|\vec{k} - \vec{q}|) P_L(q)\,. \end{aligned} \tag{2.83}$$

In these equations P_{mm} and $P_{m\theta}$ are the one-loop matter-matter and matter-velocity power spectra. These, along with $P_{\theta\theta}$, have the following well-known expressions [9]:

$$P_{mm}(k) = P_{\rm L}(k) + 2 \int_{\{\vec{q}\}} F_2(\vec{k} - \vec{q}, \vec{q})^2 P_{\rm L}(|\vec{k} - \vec{q}|) P_{\rm L}(q) + 6\, P_{\rm L}(k) \int_{\{\vec{q}\}} F_3(\vec{k}, -\vec{q}, \vec{q}) P_{\rm L}(q)\,,$$

$$\begin{aligned} P_{m\theta}(k) \; = \; & P_{\rm L}(k) + 2 \int_{\{\vec{q}\}} F_2(\vec{k} - \vec{q}, \vec{q}) G_2(\vec{k} - \vec{q}, \vec{q}) P_{\rm L}(|\vec{k} - \vec{q}|) P_{\rm L}(q) \\ & + 3\, P_{\rm L}(k) \int_{\{\vec{q}\}} (F_3(\vec{k}, -\vec{q}, \vec{q}) + G_3(\vec{k}, -\vec{q}, \vec{q})) P_{\rm L}(q)\,, \end{aligned}$$

$$P_{\theta\theta}(k) = P_{\rm L}(k) + 2 \int_{\{\vec{q}\}} G_2(\vec{k} - \vec{q}, \vec{q})^2 P_{\rm L}(|\vec{k} - \vec{q}|) P_{\rm L}(q) + 6\, P_{\rm L}(k) \int_{\{\vec{q}\}} G_3(\vec{k}, -\vec{q}, \vec{q}) P_{\rm L}(q) \tag{2.84}$$

where F_n and G_n represent SPT kernels [9], e.g. ($x_{12} \equiv \widehat{\vec{q}}_1 \cdot \widehat{\vec{q}}_2$)

$$F_2(\vec{q}_1,\vec{q}_2) = \frac{5}{7} + \frac{x_{12}}{2}\left(\frac{q_1}{q_2}+\frac{q_2}{q_1}\right) + \frac{2}{7}x_{12}^2, \quad G_2(\vec{q}_1,\vec{q}_2) = \frac{3}{7} + \frac{x_{12}}{2}\left(\frac{q_1}{q_2}+\frac{q_2}{q_1}\right) + \frac{4}{7}x_{12}^2,$$
$$K(\vec{q}_1,\vec{q}_2) = x_{12}^2 - 1. \tag{2.85}$$

For the bispectra appearing in Eq. (2.77) we have,

$$\begin{aligned} B_{g\theta g}(\vec{k}_1,\vec{k}_2,-\vec{k}_{12}) \;=\; & \Gamma_g^{(2)}(\vec{k}_1,\vec{k}_2)\Gamma_g^{(1)}(k_1)\Gamma_\theta^{(1)}(k_2)P_{\rm L}(k_1)P_{\rm L}(k_2) \\ & + \Gamma_\theta^{(2)}(\vec{k}_1,-\vec{k}_{12})\Gamma_g^{(1)}(k_1)\Gamma_g^{(1)}(k_{12})P_{\rm L}(k_1)P_{\rm L}(k_{12}) \\ & + \Gamma_g^{(2)}(\vec{k}_2,-\vec{k}_{12})\Gamma_g^{(1)}(k_2)\Gamma_\theta^{(1)}(k_{12})P_{\rm L}(k_2)P_{\rm L}(k_{12}) \end{aligned}$$

and similar expressions for other combinations $B_{g\theta\theta}$, $B_{\theta\theta g}$ and $B_{\theta\theta\theta}$, with Γ-functions up to the needed order given by [49, 48],

$$\Gamma_g^{(1)}(k) = b_1, \quad \Gamma_\theta^{(1)}(k) = 1, \quad \Gamma_g^{(2)}(\vec{k}_1,\vec{k}_2) = 2\,b_1 F_2(\vec{k}_1,\vec{k}_2) + b_2 + 2\,\gamma_2 K(\vec{k}_1,\vec{k}_2),$$
$$\Gamma_\theta^{(2)}(\vec{k}_1,\vec{k}_2) = 2\,G_2(\vec{k}_1,\vec{k}_2) \tag{2.86}$$

Now we turn to a discussion of the impact of going beyond the plane-parallel approximation from these one-loop expressions.

2.5.2 Inverse-distance and wide-angle effects

We proceed in the same way as done in linear theory. Considering the geometry of Fig. 2.1 again, the inverse-distance corrections come from $1/x_n$ terms in Eq. (2.77) by setting $x_1 = x_2 = x_c$ and $\hat{x}_1 = \hat{x}_2 = \hat{x}_c$. Then, since there will be no explicit dependence on $\vec{x}_1$ and $\vec{x}_2$ in the D-functions, the integral over $\vec{x}_{12}$ turns into a delta function and we are left with just one loop integral which can be easily evaluated numerically. At the end, these terms produce $1/(kx_c)^2$ corrections but without wide-angle contributions. For wide-angle corrections, before applying the perturbative method to evaluate the integrals in Eq. (2.77), it is instructive to highlight a few steps one can take to reduce the number of parameters involved and to make the expressions more amenable to perturbative expansion. As an example, let's consider the second and forth integrals in Eq. (2.77) (others are simpler) which take the following general form:

$$\mathcal{I}_{2,4} = \int_{\vec{x}_{12},\vec{k}_1,\vec{k}_2} e^{i(\vec{k}_{12}-\vec{k})\cdot\vec{x}_{12}}\, C(\vec{k}_1,\vec{k}_2,\vec{x}_1,\vec{x}_2) \tag{2.87}$$

where C contains all parameters and functions in the integrand. This integral, via coordinate transformations $\vec{k}_1 + \vec{k}_2 = \vec{k}_R$ and $\vec{k}_1 - \vec{k}_2 = \vec{k}_r$, can be re-written as:

$$\mathcal{I}_{2,4} = \frac{1}{8}\int_{\vec{x}_{12},\vec{k}_R,\vec{k}_r} e^{i(\vec{k}_R-\vec{k})\cdot\vec{x}_{12}}\, C(\vec{k}_R,\vec{k}_r,\vec{x}_1,\vec{x}_2)\,. \tag{2.88}$$

Inside C, there are combinations of products such as $\hat{k}_R\cdot\hat{k}_r$, $\hat{k}_R\cdot\hat{x}_1$, $\hat{k}_r\cdot\hat{x}_1$, etc. We first take the integral over $\vec{k}_r$. For this purpose, we choose the coordinate system whose "z" direction is defined by $\hat{k}_R$, i.e. $\hat{z}' \equiv \hat{k}_R$ and $\hat{x}'$, $\hat{y}'$ are defined accordingly on its normal plane. As an example, let us consider the following integral, which we call it $\tilde{\mathcal{I}}_{2,4}$, as one of the most general form of the terms

that appear in Eq. (2.88):

$$\tilde{\mathcal{I}}_{2,4} = \int_{\vec{x}_{12},\vec{k}_R,\vec{k}_r} e^{i(\vec{k}_R-\vec{k})\cdot\vec{x}_{12}}(\hat{k}_r\cdot\hat{x}_1)^2(\hat{k}_r\cdot\hat{x}_2)^2\,\mathcal{F}(\vec{k}_R\cdot\hat{x}_1,\vec{k}_R\cdot\hat{x}_2,\hat{k}_r\cdot\hat{k}_R,k_r,k_R) \tag{2.89}$$

with $\mathcal{F}$ being a function. The first expression can be decomposed in the above-mentioned coordinate system as: $(\hat{k}_r\cdot\hat{x}_1)^2(\hat{k}_r\cdot\hat{x}_2)^2 = (\hat{k}_{ri'}\hat{x}_{1i'})^2(\hat{k}_{rj'}\hat{x}_{2j'})^2$ with repeated indices being summed over and i', j' denoting (x', y', z') each. Now we can write the components in terms of the corresponding spherical coordinates: $\hat{k}_{rx'} = \sin(\theta_r)\cos(\phi_r)$, $\hat{k}_{ry'} = \sin(\theta_r)\sin(\phi_r)$, $\hat{k}_{rz'} = \cos(\theta_r)$ and similarly, $\hat{x}_{1x'} = \sin(\theta_1)\cos(\phi_1)$, $\hat{x}_{1y'} = \sin(\theta_1)\sin(\phi_1)$, $\hat{x}_{1z'} = \cos(\theta_1)$, etc. Also let's define $\hat{k}_r\cdot\hat{k}_R = \cos(\theta_r) \equiv \mu_r$. Plugging all these into Eq. (2.89), we first take the integral over ϕ_r (note that arguments of $\mathcal{F}$ are all independent of ϕ_r). The result, after some algebra, is:

$$\begin{aligned}\tilde{\mathcal{I}}_{2,4} = \int_{\vec{x}_{12},\vec{k}_R} e^{i(\vec{k}_R-\vec{k})\cdot\vec{x}_{12}}\int dk_r d\mu_r k_r^2\left(\frac{\pi}{4}\right)\Big[&\left(1+2(\hat{x}_1\cdot\hat{x}_2)^2\right)(\mu_r^2-1)^2 \\ -4\left(1-6\mu_r^2+5\mu_r^4\right)&(\hat{x}_1\cdot\hat{x}_2)(\hat{k}_R\cdot\hat{x}_1)(\hat{k}_R\cdot\hat{x}_2) + \left(-1+6\mu_r^2-5\mu_r^4\right)\left((\hat{k}_R\cdot\hat{x}_1)^2+(\hat{k}_R\cdot\hat{x}_2)^2\right) \\ +(3-30\mu_r^2+35\mu_r^4)&(\hat{k}_R\cdot\hat{x}_1)^2(\hat{k}_R\cdot\hat{x}_2)^2\Big]\mathcal{F}(\vec{k}_R\cdot\hat{x}_1,\vec{k}_R.\hat{x}_2,\mu_r,k_r,k_R)\end{aligned} \tag{2.90}$$

Now, considering the 2D integral inside, we are left with two remaining integrals (over $\vec{k}_R$ and $\vec{x}_{12}$) and a dependence on $\hat{x}_1.\hat{x}_2$ that can be added to the $\mathcal{F}$ function. The same is true for the first and third integrals of Eq. (2.77) and they are even simpler because there is no $\hat{x}_1.\hat{x}_2$ term produced in the calculations. For the first one the analogue of the 2D integral is the loop integral inside power spectra. For the third one, $\vec{k}_2$ plays the role of $\vec{k}_r$ and the steps are the same.

The two-dimensional loop integrals are the only objects that need to be evaluated numerically which is not difficult given their simple structure. The rest of the calculations are analytic. Therefore, the most general outcome for each of the four integrals of the local power spectrum

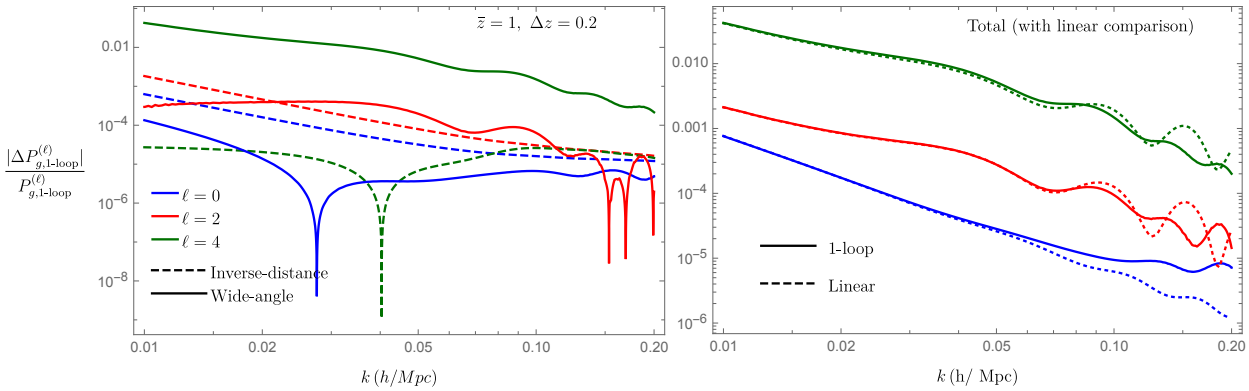

Figure 2.5: Non-linear beyond plane-parallel corrections to multipoles of 1-loop galaxy power spectrum, for a Euclid-like galaxy sample. The left figure separates wide-angle and inverse-distance corrections, both relative to nonlinear plane-parallel multipoles. The bias parameters are $b_1 = 1.46$ and b_2, γ_2 and γ_{21} which are obtained from Eqs. (2.93-2.95). The figure on the right combines both corrections and shows the total result. Also on that panel, the total nonlinear corrections are compared with the corresponding linear ratio.

Eq. (2.77) takes the form:

$$\mathcal{I}_\alpha(\vec{k},\vec{x}_c) = \int_{\vec{x}_{12},\vec{k}'} e^{i(\vec{k}'-\vec{k})\cdot\vec{x}_{12}}\, C_\alpha(\hat{k}'\cdot\hat{x}_1,\ \hat{k}'\cdot\hat{x}_2,\ \hat{x}_1\cdot\hat{x}_2,\ k',\ \frac{1}{x_1},\ \frac{1}{x_2}) \tag{2.91}$$

with $\alpha = 1, 2, 3, 4$. This is where we can employ the perturbative expansions to find wide-angle corrections to any desired order. Replacing the unit vectors and $1/x$ factors with the expansions in Eq. (2.58), we can follow the same steps as in linear case (Eqs 2.59 – 2.61) and find all leading order wide-angle contributions. Although the procedure is straightforward, the number of terms involved is quite large and therefore we do not write them down explicitly here.

The final result for the one-loop local galaxy power spectrum beyond the plane-parallel limit takes the following form:

$$\begin{aligned} P^{\text{loc}}_{g,s}(\vec{k},\vec{x}_c) &= P^{pp}_{\text{g,1-loop}}(k,\eta) + \frac{1}{(kx_c)^2} P^{\text{id}}_{\text{g,1-loop}}(k,\eta) \\ &+ \frac{1}{(kx_c)^2} P^{\text{wa}}_{\text{g,1-loop}}(k,\eta) + O(\frac{1}{(kx_c)^4}) \end{aligned} \tag{2.92}$$

where as before $\eta \equiv \hat{k} \cdot \hat{x}_c$. $P^{pp}_{\text{g,1-loop}}(k, \eta)$ represents the plane-parallel result of Eq. (2.77) which is obtained by neglecting all inverse-distance terms in the D-functions (see Eq. 2.76) and also setting $\hat{x}_1 = \hat{x}_2 = \hat{x}_c$. The following two terms are inverse-distance and wide-angle corrections respectively, which are obtained following the steps explained previously. For bias parameters we use local-Lagrangian values for γ_2, γ_{21} and peak-background split fit for quadratic bias [30, 5, 71, 49, 48]:

$$b_2 = 0.412 - 2.143 b_1 + 0.929 b_1^2 + 0.008 b_1^3 + \frac{4}{3}\gamma_2\,, \tag{2.93}$$

$$\gamma_2 = -\frac{2}{7}(b_1 - 1)\,, \tag{2.94}$$

$$\gamma_{21} = \frac{2}{21}(b_1 - 1) + \frac{6}{7}\gamma_2\,. \tag{2.95}$$

The last two equations above are based on extrapolations to the initial conditions where non-local bias terms vanish. This causes the biases not to depend on tidal fields and only depend on the linear density perturbations (hence the dependence on b_1 only). The first equation above is based on measurements in simulations of dark matter halos where a long-wavelength mode is added to calculate the bias of tracers (peak-background split fit). The dependence on the sample in all the relations above comes through the value of b_1.

Inserting Eq. (2.92) into Eq. (2.7), one can find the local multipoles and then, by plugging the result into Eq. (2.8), find the final multipoles. For the plane-parallel one-loop case, this yields even parity multipoles up to $\ell = 8$ and wide-angle corrections increase it to $\ell = 10$. However, given the difficulty in detecting high multipoles, we only plot the first three, using Eq. (2.57) for a Euclid like survey bin [52] with $\bar{z} = 1$, $\Delta z = 0.2$ and $b_1 = 1.46$. It is worth reminding that for loop calculations, we didn't include magnification bias.

Figure 2.5 shows relative plots of such corrections for this survey bin. The figure on the right shows the total corrections which are also compared with their linear counterparts. Although loop effects start becoming important after $k \gtrsim 0.1\ h$/Mpc, they do not make any enhancement

in the magnitudes of corrections beyond the plane-parallel approximation that could be important in practice. The most significant enhancement is seen in the monopole, but this happens when the corrections are already well below detectable levels for the foreseeable future. In any case, the perturbative procedure developed here can be a fast and easy way for assessing the importance of such effects for different galaxy samples, if desired.

2.5.3 Velocity dispersion and cosmological distortions

Velocities of galaxies within virialized halos can be significantly larger than peculiar velocities predicted from linear theory. This causes apparent elongation of galaxy clusters along the line-of-sight known as the Fingers of God (FoG) effect. To see how this changes in the presence of corrections to the plane-parallel approximation, it is enough to consider a simple approach to velocity dispersion effects, where the pairwise velocity distribution is Gaussian and scale-independent characterized by variance σ_p. In this case, the linear redshift space power spectrum gets modulated by a damping factor [86, 33, 87]. Neglecting wide-angle and relativistic effects for now, this reads

$$P^{\rm loc}_{g,L}(\vec{k},\vec{x}_c) = (b_1 + f\,(\hat{k}\cdot\hat{x}_c)^2)^2 \exp\left[-\frac{(k\sigma_p(\hat{k}\cdot\hat{x}_c))^2}{2}\right] P_L(k) \tag{2.96}$$

Similar to previous cases, the final multipoles for this modulated local power spectrum can be found. Figure 2.6 shows a comparison between FoG corrections to the monopole and quadrupole power against the corrections from linear wide-angle and local (non-integrated) relativistic terms we found earlier. We have used $\sigma_p \approx 4.5$ Mpc/h for $\bar{z}$ =1 from [121], $b_e = 0$, $s = 1$ and other parameters are as presented in the 1-loop case. This figure implies that one can ignore the mixing between wide-angle/relativistic corrections with FoG corrections at large scales shown as these are all sub-leading. In fact, wide-angle and relativistic corrections are suppressed by $1/(kx_c)^2$ and $(\mathcal{H}/k)^2$ while leading FoG corrections are suppressed by $\sim (k\sigma_p)^2$. Therefore, the mixing

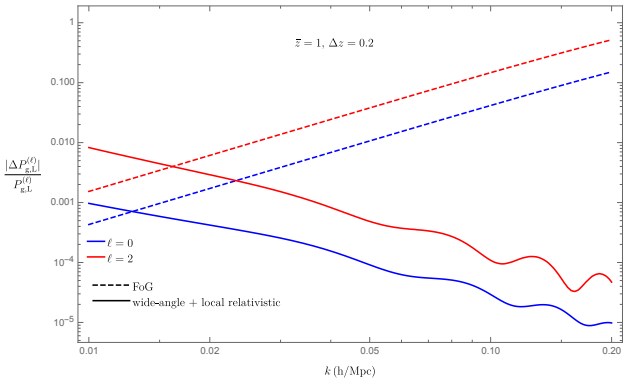

Figure 2.6: Comparison between corrections to plane-parallel monopole and quadrupole power and the corresponding corrections due to velocity dispersion effects (FoG). Here we have included local (non-integrated) relativistic corrections only, for the sake of illustration.

are suppressed by $\sim \sigma_p/x_c$ and $\sim \mathcal{H}\sigma_p$ which are subleading to wide-angle/relativistic terms at these scales. Therefore, one can separately modulate the plane-parallel power spectrum as in Eq. (2.96) and then add wide-angle and relativistic contributions. In other words:

$$P_{g,L}^{\rm loc}(\vec{k},\vec{x}_c) = P_{g,L}^{\rm PP,\,FoG}(\vec{k},\vec{x}_c) + \text{wide-angle} + \text{relativistic}\,. \tag{2.97}$$

Therefore, in practice, one can compute the nonlinear redshift-space power spectrum (including loop and FoG effects) in the plane-parallel approximation and then simply add linear wide-angle and relativistic corrections on top.

Finally, let us briefly comment on the impact of going beyond the plane-parallel approximation in cosmological distortions. The Alcock-Paczynski (AP) parameters ($\alpha_\perp$, $\alpha_\parallel$) [2] scale the actual modes in perpendicular and parallel directions to account for the anisotropic distortion caused by the assumption of the wrong cosmology when mapping angles and redshifts to comoving positions or wavevectors. In other words, one replaces $k_\parallel \to k_\parallel/\alpha_\parallel$ (or $x_\parallel \to x_\parallel\alpha_\parallel$) and $k_\perp \to k_\perp/\alpha_\perp$ (or $x_\perp \to x_\perp\alpha_\perp$) and constrains α's from data (using the true cosmological model leads to both parameters being measured to be 1). This parametrization can be easily applied to the previous calculations of wide-angle effects based on local power spectrum definitions. For

example, at the linear level, one can start from Eq. (2.65) and rescale k, x_c and $\eta \equiv \hat{k} \cdot \hat{x}_c$ as:

$$
\begin{aligned}
& k \longrightarrow k \left(\frac{\eta^2}{\alpha_{\parallel}^2} + \frac{(1-\eta^2)}{\alpha_{\perp}^2} \right)^{1/2} , \\
& x_c \longrightarrow \alpha_{\parallel}\, x_c \,, \\
& \eta \longrightarrow \frac{\eta}{\alpha_{\parallel}} \left(\frac{\eta^2}{\alpha_{\parallel}^2} + \frac{(1-\eta^2)}{\alpha_{\perp}^2} \right)^{-1/2} .
\end{aligned}
\tag{2.98}
$$

In this way, AP effects can be included in k-space in the presence of wide-angle corrections at both linear and nonlinear regimes. Such effects have been investigated for wide-angle two-point correlation functions of galaxies at the linear level in [107].

2.5.4 Wide-angle and relativistic corrections in the presence of nonilinearities

We now summarize the results of previous parts and make a general conclusion. Figures 2.5 and 2.6 imply that at large scales the presence of nonlinear effects will not change the relative size of the wide-angle corrections. The same thing can be said about relativistic effects. This means that in practice we can separately calculate corrections from non-linear terms and wide-angle and relativistic contributions and calculate the latter in linear theory. In other words we have:

$$
\begin{aligned}
& P_{g,L}^{\rm loc}(\vec{k}, \vec{x}_c) = \\
& P_{g,L}^{\rm PP}(\vec{k}, \hat{x}_c) + \text{non-linear corrections} + \\
& \text{linear wide-angle} + \text{linear relativistic} + \\
& \text{subleading cross-terms} \,.
\end{aligned}
\tag{2.99}
$$

which significantly simplifies the calculations.

2.6 Inclusion of window effects

We finish the power spectrum section by discussing how the results of previous parts can be generalized to situations where window effects become important. Here by window function we also mean the function that determines the shape of the survey volume. Beginning from Eq. (2.4), one can write the product of window functions as

$$W(\vec{x}_1)W(\vec{x}_2) = \int_{\vec{x}'_{12}} \delta_D(\vec{x}'_{12} - \vec{x}_{12}) W(\vec{x}_c + \frac{\vec{x}'_{12}}{2}) W(\vec{x}_c - \frac{\vec{x}'_{12}}{2}) \tag{2.100}$$

which leads to the convolution:

$$\begin{aligned} P_g^\ell(k) &= \frac{(2\pi)^3}{V_s}(2\ell+1) \int \frac{d\Omega_k}{4\pi} \int_{\vec{x}_c} \mathcal{L}_\ell(\hat{k}\cdot\hat{x}_c) \int \frac{d^3q}{(2\pi)^3} \int_{\vec{x}_{12}} e^{-i(\vec{k}-\vec{q})\cdot\vec{x}_{12}} \left\langle \delta_g(\vec{x}_1)\, \delta_g(\vec{x}_2) \right\rangle \times \\ &\int_{\vec{x}'_{12}} e^{-i\vec{q}\cdot\vec{x}'_{12}} W(\vec{x}_c + \frac{\vec{x}'_{12}}{2}) W(\vec{x}_c - \frac{\vec{x}'_{12}}{2}) \end{aligned} \tag{2.101}$$

where the integration over d^3q comes from the definition of delta function for $\delta_D(\vec{x}'_{12} - \vec{x}_{12})$. The integral in front of d^3q is the local power spectrum according to Eq. (2.5) which is exactly what we calculated in previous parts. One can use those results and replace $\vec{k}$ with $\vec{k} - \vec{q}$. More straightforwardly, one can make a change of variables: $\vec{k} - \vec{q} \equiv \vec{p}$ to write:

$$\begin{aligned} P_g^\ell(k) &= \frac{(2\pi)^3}{V_s}(2\ell+1) \int \frac{d\Omega_k}{4\pi} \int_{\vec{x}_c} \mathcal{L}_\ell(\hat{k}\cdot\hat{x}_c) \int \frac{d^3p}{(2\pi)^3} P_g^{\rm loc}(\vec{p},\vec{x}_c) \times \\ &\int_{\vec{x}'_{12}} e^{-i(\vec{k}-\vec{p})\cdot\vec{x}'_{12}} W(\vec{x}_c + \frac{\vec{x}'_{12}}{2}) W(\vec{x}_c - \frac{\vec{x}'_{12}}{2})\,. \end{aligned} \tag{2.102}$$

This result implies that in order to incorporate window effects which also include the effects of non-trivial geometry all one needs to do is to find the convolution between the results of previous parts (for $P_g^{\rm loc}(\vec{p},\vec{x}_c)$) and window products. It is clear from this integral that for modes that are well below the survey size (i.e. k^{-1} much smaller than survey size), the integral over window functions can be approximated with a delta function that reproduces the previous results (the window function always enforces the integral over x_c to be limited to the survey volume).

2.7 Summary

In this chapter we first found a relation for the evolution of the linear galaxy density contrast in a relativistic context. We then calculated wide-angle and relativistic corrections to multipoles of the linear galaxy power spectrum. We estimated that not including these effects can lead to a measurement of a "fake" local primordial non-Gaussianity parameter, $f_{\rm NL}$, that is of order a few. We then showed that non-linear and FoG corrections to galaxy power spectrum in redshift space have negligible mixing with linear wide-angle/relativistic corrections and, therefore, can be calculated separately.

3 | Wide-angle and relativistic effects on galaxy bispectrum

3.1 Introduction

In this chapter, we investigate wide-angle and relativistic corrections to multipoles of galaxy bispectrum in redshift space. Regarding statistics beyond two point function or power spectrum, three-point correlation functions (3PCFs) in redshift space have been largely studied in the plane-parallel approximation in both Fourier (bispectra) and configuration spaces [106, 116, 109, 62, 41, 121, 18, 77]. Extensions to this include full sky analysis of bispectrum/3PCF in angular space and/with inclusion of relativistic corrections [13, 43, 32, 64, 75, 46, 66, 53]. However, to the best of our knowledge, a full calculation of wide-angle contributions to bispectra and higher order correlations in Cartesian Fourier space have not been carried out yet. The perturbative procedure followed in this work can be easily extended to facilitate such computations. We make use of that to calculate leading order wide-angle effects on galaxy bispectrum multipoles and compare them with inverse-distance/relativistic contributions. See also a recent work, [85], where authors find wide-angle effects in the galaxy bispectrum using a formulation based on an expansion in spherical tensors.

It has been realized that relativistic effects in the plane-parallel approximation can result in non-zero odd-parity multipoles such as a dipole for bispectrum [32, 64, 75, 66] which are also

detectable in upcoming surveys. In this chapter we show that wide-angle effects alone, with symmetric LOS definitions, also lead to such multipoles and that these are as important as (and in many cases more important than) relativistic contributions and should not be neglected for constraining relativistic parameters from data. Our perturbative procedure helps us separate different contributions in an efficient way. We also provide an estimator for the measurement of leading order dipole signal from data which is based on a symmetric LOS definition.

Finally, similar to the previous chapter, we estimate the contamination that wide-angle and inverse-distance effects can have on local primordial non-Gaussianity parameter, $f_{\rm NL}$ measurements by estimating the "fake" $f_{\rm Nl}$ induced by these effects due to similar scaling with the terms that are proportional to $f_{\rm NL}$ from primordial non-Gaussian contributions.

Again we use the following conventions for integrals in configuration and Fourier spaces throughout this chapter:

$$\int_{\vec{x}} \equiv \int \frac{d^3x}{(2\pi)^3}, \qquad \int_{\vec{k}} \equiv \int d^3k \tag{3.1}$$

3.2 Basic Definitions

Similar to the power spectrum case, we first start with the definition of the local bispectrum [104]:

$$\begin{aligned} B^{loc}_{g,s}(\vec{k}_1,\vec{k}_2,\vec{x}_c) &= \int \frac{d^3\vec{x}_{13}}{(2\pi)^3}\frac{d^3\vec{x}_{23}}{(2\pi)^3}\, e^{-i\vec{k}_1\cdot\vec{x}_{13}} e^{-i\vec{k}_2\cdot\vec{x}_{23}} \times \\ &\quad \left\langle \delta_{g,s}\left(\vec{x}_1\right)\delta_{g,s}\left(\vec{x}_2\right)\delta_{g,s}\left(\vec{x}_3\right)\right\rangle \end{aligned} \tag{3.2}$$

for which we are considering triangle configurations in k-space satisfying $\vec{k}_3+\vec{k}_1+\vec{k}_2=0$. For the local bispectrum, $\vec{x}_c=(\vec{x}_1+\vec{x}_2+\vec{x}_3)/3$ is the centroid of the corresponding real-space triangles made by the points at which vectors $\vec{x}_1$, $\vec{x}_2$ and $\vec{x}_3$ end. The geometry of the problem is drawn in Figure 3.1. We choose $\vec{x}_c$ to define our LOS for the local bispectrum. This has the ad-

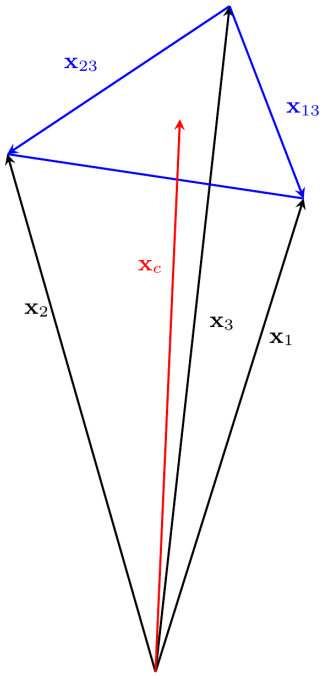

Figure 3.1: Relevant geometry for local bispectrum calculations. Here $\vec{x}_c$ is the centroid of the triangle which we take to be te line-of-sight. Also, $\vec{x}_{nm} = \vec{x}_n - \vec{x}_m$.

vantage of being fully symmetric with respect to point exchanges. To describe k-space triangle configurations one needs five parameters. Using the parametrization in [106], three of these can be k_1, k_2 and the cosine of angle between their vectors ($\hat{k}_1 \cdot \hat{k}_2 \equiv \cos\theta \equiv \mu$). The other two determine the orientation of the triangle with respect to the observer. One of them can be defined, without loss of generality, as the angle between the centroid (LOS) vector and the k_1 side ($\cos\theta_1 \equiv \hat{k}_1 \cdot \hat{x}_c$). The other one, ϕ_{12}, can be defined in the following way: in the plane whose normal is determined by $\vec{k}_1$, ϕ_{12} is the angle between projections of $\vec{k}_2$ and $\vec{x}_c$ onto that plane. This implies $\hat{k}_2 \cdot \hat{x}_c = \mu \cos\theta_1 + \sqrt{1-\mu^2}\ \sin\theta_1\ \cos\phi_{12}$.

The local bispectrum can then be expanded in terms of spherical harmonics defined by orientation angles:

$$B^{loc}_{g,s}(\vec{k}_1, \vec{k}_2, \vec{x}_c) = \sum_{\ell,m} \mathcal{B}^{(\ell,m)}_{g,s}(k_1, k_2, \mu, x_c)\ Y_{\ell m}(\theta_1, \phi_{12})\,,$$

and, similar to the power spectrum, “local multipoles" of the bispectrum can be obtained from:

$$\mathcal{B}_{g,s}^{(\ell,m)}(k_1,k_2,\mu,x_c)=\frac{(2\ell+1)}{4\pi}\int d\Omega_T\, B_{g,s}^{loc}(\vec{k}_1,\vec{k}_2,\vec{x}_c)\; Y_{\ell m}^{*}(\theta_1,\phi_{12})\,. \tag{3.3}$$

where $d\Omega_T \equiv d\cos\theta_1\, d\phi_{12}$. Ultimately, the “final" multipoles can be calculated by integrating over LOS vectors within the survey volume:

$$B_{g,s}^{(\ell,m)}(k_1,k_2,\mu)=\int_{V_s}\frac{d^3\vec{x}_c}{V_s}\;\mathcal{B}_{g,s}^{(\ell,m)}(k_1,k_2,\mu,x_c)\,. \tag{3.4}$$

The plane-parallel multipoles of the bispectrum can be obtained taking the limit $\vec{x}_1=\vec{x}_2=\vec{x}_c$ and $\vec{x}_c\longrightarrow\infty$. In the following subsections we go beyond this limit and investigate contributions from relativistic and wide-angle terms.

3.3 Odd-Parity (Imaginary) Multipoles from Relativistic and Wide-angle contributions

Inclusion of relativistic corrections to the galaxy number density contrast can lead to imaginary odd-parity multipoles [32, 64, 75]. In this section we show that, in addition to relativistic terms, wide-angle corrections alone produce odd-parity multipoles too. We calculate these imaginary terms from different physical origins and compare them.

For the tree-level galaxy bispectrum, only terms up to second order in δ or $\vec{u}$ are needed. Also for relativistic contributions, we only need to keep terms that produce odd-parity multipoles in which we are interested in this part. We use the results in [44] (see also [127, 11, 42]) for relevant second-order relativistic terms. Combining Eq. (2.12) with these terms leads to:

$$\delta_{g,s}(\vec{x}_1) = \delta_g(\vec{x}_1) + \left[f\,\hat{x}_{1j}\,\partial_{x_{1j}}\left[(\vec{u}_g(\vec{x}_1)\cdot\hat{x}_1)(1+\delta_g(\vec{x}_1))\right] + \frac{f^2}{2}\,\hat{x}_{1k}\,\hat{x}_{1j}\,\partial_{x_{1j}}\partial_{x_{1k}}\left[(\vec{u}_g(\vec{x}_1)\cdot\hat{x}_1)^2\right]\right]$$
$$+\frac{1}{x_1}\left[f\,(2-5s)(\vec{u}_g(\vec{x}_1)\cdot\hat{x}_1)\left[1+\delta_g(\vec{x}_1)\right] + (2-\frac{5}{2}s)f^2\,\hat{x}_{1j}\,\partial_{x_{1j}}\left[(\vec{u}_g(\vec{x}_1)\cdot\hat{x}_1)^2\right]\right] \tag{3.5}$$
$$+\mathcal{H}\left[\mathcal{A}_1\,f\,\vec{u}_g(\vec{x}_1)\cdot\hat{x} + \mathcal{A}_2\,f^2\,\hat{x}_{1j}\,\partial_{x_{1j}}\left[(\vec{u}_g(\vec{x}_1)\cdot\hat{x}_1)^2\right] + \mathcal{A}_1\,f\,\vec{u}_g(\vec{x}_1)\cdot\hat{x}_1\,\delta_g(\vec{x}_1)\right.$$
$$-\frac{f}{\mathcal{H}}\vec{u}_g(\vec{x}_1)\cdot\hat{x}_1\dot{\delta}_g(\vec{x}_1) - 2\,f^2\,\vec{u}_{gj}\partial_{x_{1j}}(\vec{u}_g(\vec{x}_1)\cdot\hat{x}_1) + \frac{f}{\mathcal{H}^2}\,\phi\;\hat{x}_{1j}\hat{x}_{1k}\,\partial_{x_{1j}}\partial_{x_{1k}}\,(\vec{u}_g(\vec{x}_1)\cdot\hat{x}_1)$$
$$\left.+\frac{1}{\mathcal{H}^2}\,\phi\;\hat{x}_{1j}\partial_{x_{1j}}\delta_g(\vec{x}_1) - \frac{f}{\mathcal{H}^2}(\vec{u}_g(\vec{x}_1)\cdot\hat{x}_1)\,\hat{x}_{1j}\hat{x}_{1k}\,\partial_{x_{1j}}\partial_{x_{1k}}\phi\right].$$

Here δ_g's are in SCG (as the difference with the CNG parameter is subleading for odd-parity multipoles) but we have dropped the "tilde" for simplicity. Also here $\mathcal{A}_1 \equiv (5s + 1 - \frac{3}{2}\Omega_M - b_e)$ and $\mathcal{A}_2 \equiv (3 - \frac{9}{4}\Omega_M + \frac{5}{2}s - b_e)$. Also we have used $\dot{\mathcal{H}}/\mathcal{H}^2 = 1 - (3/2)\,\Omega_M$.

There are three brackets after $\delta_g(\vec{x}_1)$ in this equation. The first one is the RSD contribution. The second one is inverse-distance term which is part of Eq. (2.12) but its coefficient has been modified to include magnification bias [44]. Since the leading suppression factor in the imaginary bispectrum will be $1/(kx_c)$, we neglect $1/x_n^2$ terms in Eq. (2.12). They will be relevant for real (even parity) multipoles which we consider later. The last bracket is the "pure" relativistic contribution which leads to a $\mathcal{H}/k_n$ suppression in the bispectrum. Again, usually the last two brackets combined are called relativistic terms.

Similar to the power spectrum case, we assume here that the velocity field is unbiased, i.e. $\vec{u}_g = \vec{u}$ and for density field biasing we use Eq. (2.80) up to quadratic order needed for the tree-level bispectrum, i.e. we omit the γ_{21} contribution. This leads to the following Fourier space relation:

$$\delta_g(\vec{k}) = b_1\,\delta(\vec{k}) + \frac{b_2}{2}\int_{\vec{x},\vec{q}_1,\vec{q}_2} e^{i(\vec{q}_1+\vec{q}_2-\vec{k})\cdot\vec{x}}\,\delta(\vec{q}_1)\delta(\vec{q}_2) \quad + \gamma_2 \int_{\vec{x},\vec{q}_1,\vec{q}_2} e^{i(\vec{q}_1+\vec{q}_2-\vec{k})\cdot\vec{x}}\,K(\vec{q}_1,\vec{q}_2)\,\delta(\vec{q}_1)\delta(\vec{q}_2) \tag{3.6}$$

where K is given in Eq. (2.85). Since we keep terms up to second order in δ or Θ, most of the Fourier fields from δ_g's and $\vec{u}_g$'s in Eq. (3.5) can be treated as linear. For a few other terms which appear at first order we can write:

$$\delta(\vec{k}) = \delta_L(\vec{k}) + \int_{\vec{q}_1,\vec{q}_2} \delta_D(\vec{k}-\vec{q}_1-\vec{q}_2)\,F_2(\vec{q}_1,\vec{q}_2)\delta_L(\vec{q}_1)\delta_L(\vec{q}_2) \tag{3.7}$$

and

$$\Theta(\vec{k}) = \delta_L(\vec{k}) + \int_{\vec{q}_1,\vec{q}_2} \delta_D(\vec{k}-\vec{q}_1-\vec{q}_2)\,G_2(\vec{q}_1,\vec{q}_2)\delta_L(\vec{q}_1)\delta_L(\vec{q}_2)\,. \tag{3.8}$$

where the second-order SPT kernels F_2, G_2 are given in Eq. (2.85). Note that in Eq. (3.5) we also use $\dot{\delta} = f\mathcal{H}\delta$ and $\phi(\vec{k}) = -(3/2)\Omega_M(\mathcal{H}^2/k^2)\delta(\vec{k})$ from Eq. (2.45) (again, tilde sign for SCG parameter is dropped for simplicity). Taking all these into account and sorting terms out, the final result for galaxy number density contrast up to second order in δ_L becomes:

$$\delta_{g,s}(\vec{x}_1) = \int_{\vec{q}_1} e^{i\vec{q}_1\cdot\vec{x}_1} R_1^{\rm total}(\vec{q}_1,\vec{x}_1)\,\delta_L(\vec{q}_1) + \int_{\vec{q}_1,\vec{q}_2} e^{i\vec{q}_{12}\cdot\vec{x}_1} R_2^{\rm total}(\vec{q}_1,\vec{q}_2,\vec{x}_1)\,\delta_L(\vec{q}_1)\,\delta_L(\vec{q}_2) \tag{3.9}$$

where $\vec{q}_{12} = \vec{q}_1 + \vec{q}_2$. We have $R_1^{\rm total}(\vec{q}_1,\vec{x}_n) \equiv R_1^{\rm RSD}(\vec{q}_1,\vec{x}_n) + R_1^{\rm ID}(\vec{q}_1,\vec{x}_n) + R_1^{\rm rel}(\vec{q}_1,\vec{x}_n)$ with $n = 1, 2$ and similarly for $R_2^{\rm total}(\vec{q}_1,\vec{q}_2,\vec{x}_n)$. Here we have separated inverse-distance (denoted 'ID') terms from "pure" relativistic ones (denoted 'rel') just to keep track of different suppression factors. For these functions we have:

$$R_1^{\rm RSD}(\vec{q}_1,\vec{x}_1) = b_1 + f\frac{(\vec{q}_1\cdot\hat{x}_1)^2}{q_1^2}\,, \tag{3.10}$$

$$\begin{aligned} R_2^{\rm RSD}(\vec{q}_1,\vec{q}_2,\vec{x}_1) = {} & b_1\,F_2(\vec{q}_1,\vec{q}_2) + \frac{b_2}{2} + \gamma_2\,K(\vec{q}_1,\vec{q}_2) + f\,\frac{(\vec{q}_{12}\cdot\hat{x}_1)^2}{q_{12}^2}G_2(\vec{q}_1,\vec{q}_2) \\ & + f\,b_1\frac{(\vec{q}_{12}\cdot\hat{x}_1)(\vec{q}_1\cdot\hat{x}_1)}{q_1^2} + f^2\,\frac{(\vec{q}_1\cdot\hat{x}_1)(\vec{q}_2\cdot\hat{x}_1)}{2q_1^2q_2^2}(\vec{q}_{12}\cdot\hat{x}_1)^2\,, \end{aligned} \tag{3.11}$$

$$R_1^{\rm ID}(\vec{q}_1,\vec{x}_1) = -f(2-5s)\frac{i}{x_1}\,\frac{\vec{q}_1\cdot\hat{x}_1}{q_1^2}\,, \tag{3.12}$$

$$R_2^{\rm ID}(\vec{q}_1,\vec{q}_2,\vec{x}_1) = -\frac{i}{x_1}\left[f(2-5s)\frac{\vec{q}_{12}\cdot\hat{x}_1}{q_{12}^2}G_2(\vec{q}_1,\vec{q}_2) + f(2-5s)\,b_1\,\frac{\vec{q}_1\cdot\hat{x}_1}{q_1^2}\right. \tag{3.13}$$

$$\left. + f^2(2-\frac{5}{2}s)\frac{(\vec{q}_1\cdot\hat{x}_1)(\vec{q}_2\cdot\hat{x}_1)}{q_1^2q_2^2}(\vec{q}_{12}\cdot\hat{x}_1)\right] \tag{3.14}$$

$$R_1^{\rm rel}(\vec{q}_1,\hat{x}_1) = -\frac{\mathcal{H}}{q_1}\, i f\, \mathcal{A}_1 \frac{\vec{q}_1\cdot\hat{x}_1}{q_1}\,, \tag{3.15}$$

$$\begin{aligned} R_2^{\rm rel}(\vec{q}_1,\vec{q}_2,\hat{x}_1) = \mathcal{H}\Bigg[& -if\mathcal{A}_1 \frac{\vec{q}_{12}\cdot\hat{x}_1}{q_{12}^2}\, G_2(\vec{q}_1,\vec{q}_2) - i\mathcal{A}_2 f^2 \frac{(\vec{q}_1\cdot\hat{x}_1)\,(\vec{q}_2\cdot\hat{x}_1)(\vec{q}_{12}\cdot\hat{x}_1)}{q_1^2\, q_2^2} \\ & -ib_1 f\,(\mathcal{A}_1 - f)\frac{\vec{q}_1\cdot\hat{x}_1}{q_1^2} + 2\,if^2\frac{\hat{q}_1\cdot\hat{q}_2}{q_1 q_2}(\vec{q}_1\cdot\hat{x}_1) \;-\frac{3}{2} i\, f\,\Omega_m \frac{(\vec{q}_1\cdot\hat{x}_1)^3}{q_1^2\, q_2^2} \\ & -\frac{3}{2} i\, b_1\,\Omega_m \frac{\vec{q}_2\cdot\hat{x}_1}{q_1^2} + \frac{3}{2} i\, f\,\Omega_m \frac{(\vec{q}_1\cdot\hat{x}_1)^2 \vec{q}_2\cdot\hat{x}_1}{q_1^2 q_1^2}\Bigg] \end{aligned} \tag{3.16}$$

Now we can calculate the local bispectrum by plugging Eq. (3.9) into Eq. (3.2). The result is:

$$\begin{aligned} B_{g,s}^{\rm loc}(\vec{k}_1,\vec{k}_2,\vec{x}_c) = & \int_{\vec{q}_1,\vec{q}_2,\vec{x}_{13},\vec{x}_{23}} e^{i(\vec{q}_1-\vec{k}_1)\cdot\vec{x}_{13}} e^{i(\vec{q}_2-\vec{k}_2)\cdot\vec{x}_{23}} R_1^{\rm total}(\vec{q}_1,\vec{x}_1)\, R_1^{\rm total}(\vec{q}_2,\vec{x}_2)\Big[R_2^{\rm total}(-\vec{q}_1,-\vec{q}_2,\vec{x}_3) \\ & + R_2^{\rm total}(-\vec{q}_2,-\vec{q}_1,\vec{x}_3)\Big] P_L(q_1)P_L(q_2) \;+ \begin{pmatrix} \vec{k}_1 \\ \vec{k}_2 \to \vec{k}_3 \end{pmatrix} + \begin{pmatrix} \vec{k}_1 \to \vec{k}_2 \\ \vec{k}_3 \end{pmatrix}, \end{aligned} \tag{3.17}$$

which assumes closed triangle configurations, i.e. $\vec{k}_3 = -\vec{k}_1 - \vec{k}_2$.

Our goal is to find odd-parity "local" multipoles (all imaginary) by inserting this equation into Eq. (3.3). In fact, there is no plane-parallel contributions (which come from $R^{\rm RSD}$ terms only) for these multipoles. The leading order imaginary terms are produced by inverse-distance, pure relativistic and wide-angle contributions. Before calculating them we find the plane-parallel local bispectrum, which is all real, by inserting $R_{1,2}^{\rm RSD}$ into the equation above and taking the limit $\hat{x}_1 = \hat{x}_2 = \hat{x}_c$. It can be easily seen that the result is:

$$\begin{aligned} B_g^{\rm local,pp}(\vec{k}_1,\vec{k}_2,\vec{x}_c) \;=\; & R_1^{\rm RSD}(\vec{k}_1,\vec{x}_c)\, R_1^{\rm RSD}(\vec{k}_2,\vec{x}_c)\Big[R_2^{\rm RSD}(-\vec{k}_1,-\vec{k}_2,\vec{x}_c) \;+\; R_2^{\rm RSD}(-\vec{k}_2,-\vec{k}_1,\vec{x}_c)\Big]\times \\ & P_L(k_1)P_L(k_2) + \begin{pmatrix} \vec{k}_1 \\ \vec{k}_2 \to \vec{k}_3 \end{pmatrix} \;+\; \begin{pmatrix} \vec{k}_1 \to \vec{k}_2 \\ \vec{k}_3 \end{pmatrix} \end{aligned} \tag{3.18}$$

which can then be used in Eq. (3.3) to yield the local plane-parallel multipoles:

$$\mathcal{B}^{(\ell,m)}_{g,\rm pp}(k_1,k_2,\mu,x_c)=\frac{(2\ell+1)}{4\pi}\int d\Omega_T\, B^{\rm local,pp}_g(\vec{k}_1,\vec{k}_2,\vec{x}_c)\, Y^*_{\ell m}(\theta_1,\phi_{12}) \tag{3.19}$$

and the final multipoles are found by integrating this over LOS vectors within the survey volume via Eq. (3.4). The only non-zero multipoles for the plane-parallel case are those of even ℓ.

Let us now explain how each of the aforementioned odd-parity contributions are obtained.

3.4 Odd-parity Multipoles from Inverse-distance and Relativistic Terms

For inverse-distance terms we mix RSD functions, $R^{\rm RSD}_{1,2}$ from Eqs. (3.10-3.11), with $R^{\rm ID}_{1,2}$ from Eqs. (3.12-3.13) in Eq. (3.17) and separate the imaginary part. For relativistic terms we do the same but with $R^{\rm rel}_{1,2}$ from Eqs. (3.15-3.16). Also, since these contributions are separate from wide-angle ones (the leading order suppression factors of all three contributions are of the same order, i.e. it is $1/(kx_c)$ for ID and wide-angle terms and $\mathcal{H}/k$ for relativistic terms), they do not mix with each other and we can simply set $\hat{x}_n=\hat{x}_c$ and $1/x_n=1/x_c$ for inverse-distance and relativistic contributions. Therefore we have:

$$\begin{aligned}
&B^{\rm local,ID/rel}_g(\vec{k}_1,\vec{k}_2,\vec{x}_c)\;=\\
&\Big\{R^{\rm RSD}_1(\vec{k}_1,\vec{x}_c)\,R^{\rm RSD}_1(\vec{k}_2,\vec{x}_c)\Big[R^{\rm ID/rel}_2(-\vec{k}_1,-\vec{k}_2,\vec{x}_c)\;+\;R^{\rm ID/rel}_2(-\vec{k}_2,-\vec{k}_1,\vec{x}_c)\Big]+\\
&+\Big(R^{\rm ID/rel}_1(\vec{k}_1,\vec{x}_c)\,R^{\rm RSD}_1(\vec{k}_2,\vec{x}_c)+R^{\rm RSD}_1(\vec{k}_1,\vec{x}_c)\,R^{\rm ID/rel}_1(\vec{k}_2,\vec{x}_c)\Big)\Big[R^{\rm RSD}_2(-\vec{k}_1,-\vec{k}_2,\vec{x}_c)+\\
&+\;R^{\rm RSD}_2(-\vec{k}_2,-\vec{k}_1,\vec{x}_c)\Big]\Big\}P_L(k_1)P_L(k_2)\;+\;\begin{pmatrix}\vec{k}_1\\ \vec{k}_2\to\vec{k}_3\end{pmatrix}\;+\;\begin{pmatrix}\vec{k}_1\to\vec{k}_2\\ \vec{k}_3\end{pmatrix}
\end{aligned} \tag{3.20}$$

and use this into Eq. (3.4) to integrate over x_c to find the final multipoles. We will later plot them together and call this combination "relativistic terms" to be consistent with the literature.

3.5 Odd-parity Wide-angle Multipoles

Leading order wide-angle terms that produce imaginary odd-parity multipoles are also suppressed by $1/(kx)$ factors and, as mentioned above, there is no mixing between these and inverse-distance/relativistic terms at leading order. Therefore, to find the leading wide-angle contributions we only need to put the $R_{1,2}^{\rm RSD}$ functions into Eq. (3.17) and take the imaginary part (as real parts are all even-parity). We have,

$$
\begin{aligned}
&B_g^{\rm local,wa}(\vec{k}_1,\vec{k}_2,\vec{x}_c) = \\
&\Im\Bigg\{\int_{\vec{q}_1,\vec{q}_2,\vec{x}_{13},\vec{x}_{23}} e^{i(\vec{q}_1-\vec{k}_1)\cdot\vec{x}_{13}} e^{i(\vec{q}_2-\vec{k}_2)\cdot\vec{x}_{23}} R_1^{\rm RSD}(\vec{q}_1,\vec{x}_1)\, R_1^{\rm RSD}(\vec{q}_2,\vec{x}_2)\Big[R_2^{\rm RSD}(-\vec{q}_1,-\vec{q}_2,\vec{x}_3) \;+ \\
&+ R_2^{\rm RSD}(-\vec{q}_2,-\vec{q}_1,\vec{x}_3)\Big] P_L(q_1)P_L(q_2)\Bigg\} \;+\; \begin{pmatrix} \vec{k}_1 \\ \vec{k}_2 \longrightarrow \vec{k}_3 \end{pmatrix} \;+\; \begin{pmatrix} \vec{k}_1 \longrightarrow \vec{k}_2 \\ \vec{k}_3 \end{pmatrix},
\end{aligned}
\tag{3.21}
$$

Now, to extract wide-angle terms we use a method inspired by the geometry of the problem in Fig. 3.1, which is the natural extension of what we did in the power spectrum case. Let's define the perturbation vectors as:

$$
\boldsymbol{\epsilon}_1 \equiv \frac{\vec{x}_{13}}{x_c}\,, \qquad \boldsymbol{\epsilon}_2 \equiv \frac{\vec{x}_{23}}{x_c}\,. \tag{3.22}
$$

There can be pairs for which these quantities are larger than one. However, their corresponding separations are most of the time much larger than k_1^{-1} and k_2^{-1} for the scales we are interested in. Therefore, these have negligible contributions and one can still use the entire survey volume.

Now, using $\vec{x}_1 = \vec{x}_c + 2\,\vec{x}_{13}/3 - \vec{x}_{23}/3$, $\vec{x}_2 = \vec{x}_c + 2\,\vec{x}_{23}/3 - \vec{x}_{13}/3$ and $\vec{x}_3 = \vec{x}_c - \vec{x}_{13}/3 - \vec{x}_{23}/3$, we

can expand $\hat{x}_n$'s up to any desired order in ϵ's. For example we have:

$$\hat{x}_1 = \frac{\vec{x}_c + 2\,\vec{x}_{13}/3 - \vec{x}_{23}/3}{|\vec{x}_c + 2\,\vec{x}_{13}/3 - \vec{x}_{23}/3|} = \hat{x}_c + \frac{2}{3}\vec{\epsilon}_1 \; + \ldots, \tag{3.23}$$

$$\frac{1}{x_1} = \frac{1}{|\vec{x}_c + 2\,\vec{x}_{13}/3 - \vec{x}_{23}/3|} = \frac{1}{x_c}(1 - \frac{2}{3}\boldsymbol{\epsilon}_1.\hat{x}_c + \frac{1}{3}\boldsymbol{\epsilon}_2.\hat{x}_c + \ldots) \tag{3.24}$$

and similar expansions for $\hat{x}_2$, $\hat{x}_3$, $1/x_2$ and $1/x_3$. For the odd-parity case, we neglect $O(\epsilon_{1,2}^2)$ terms and higher. Again, plane-parallel contributions, Eq. (3.18), are reproduced in the limit $\epsilon_{1,2} \longrightarrow 0$ or $\hat{x}_1 \simeq \hat{x}_2 \simeq \hat{x}_3 \simeq \hat{x}_c$ and $1/x_c \longrightarrow \infty$.

By applying these expansions to unit vectors in the $R_{1,2}^{\rm RSD}$ functions, defined in Eqs. (3.10-3.11) we can separate all terms of order ϵ_1 and ϵ_2 in Eq. (3.21) and find the leading order wide-angle contributions. Such terms have the following general form:

$$\begin{aligned} &\mathcal{I}^{wa}_{(a_1,\ldots,a_6)}(\vec{k}_1,\vec{k}_2,\vec{x}_c) = \\ &\int_{\vec{q}_1,\vec{q}_2,\vec{x}_{13},\vec{x}_{23}} e^{i(\vec{q}_1-\vec{k}_1)\cdot\vec{x}_{13}} e^{i(\vec{q}_2-\vec{k}_2)\cdot\vec{x}_{23}} C_{a_1,\ldots,a_6}(\vec{q}_1,\vec{q}_2,\hat{x}_c) \times \\ &\times(\boldsymbol{\epsilon}_{1x})^{a_1}(\boldsymbol{\epsilon}_{1y})^{a_2}(\boldsymbol{\epsilon}_{1z})^{a_3}(\boldsymbol{\epsilon}_{2x})^{a_4}(\boldsymbol{\epsilon}_{2y})^{a_5}(\boldsymbol{\epsilon}_{2z})^{a_6} + \text{cyclic} \end{aligned} \tag{3.25}$$

where"cyclic" refers to cyclic permutations of $\vec{k}$'s (like in Eq. (3.21)) and C contains all objects except perturbation parameters and $a_1 \ldots a_6$ can be 0 or 1 with $\sum_{j=1}^{6} a_j = 1$.

Now, from Eq. (3.22), we can pull ϵ_{1j} and ϵ_{2j} factors out of integral by replacing $\vec{x}_{13j}$ and $\vec{x}_{23j}$ with derivatives $i\,\partial/\partial k_{1j}$ and $i\,\partial/\partial k_{2j}$ which act on the entire integral. Doing so, the integrals over $\vec{x}_{13}$ and $\vec{x}_{23}$ turn into delta functions and that simply replaces $\vec{q}$'s with $\vec{k}$'s. In this way the above expression becomes:

$$\begin{aligned} \mathcal{I}^{wa}_{(a_1,\ldots,a_6)}(\vec{k}_1,\vec{k}_2,\vec{x}_c) = \left(\frac{i^{(a_1+\ldots+a_6)}}{x_c^{a_1}\ldots x_c^{a_6}}\right)\left(\frac{\partial^{a_1}}{\partial k_{1x}^{a_1}}\ldots\frac{\partial^{a_6}}{\partial k_{2z}^{a_6}}\right)\; C_{a_1,\ldots,a_6}(\vec{k}_1,\vec{k}_2,\hat{x}_c) \\ +\;\text{cyclic} \end{aligned}$$

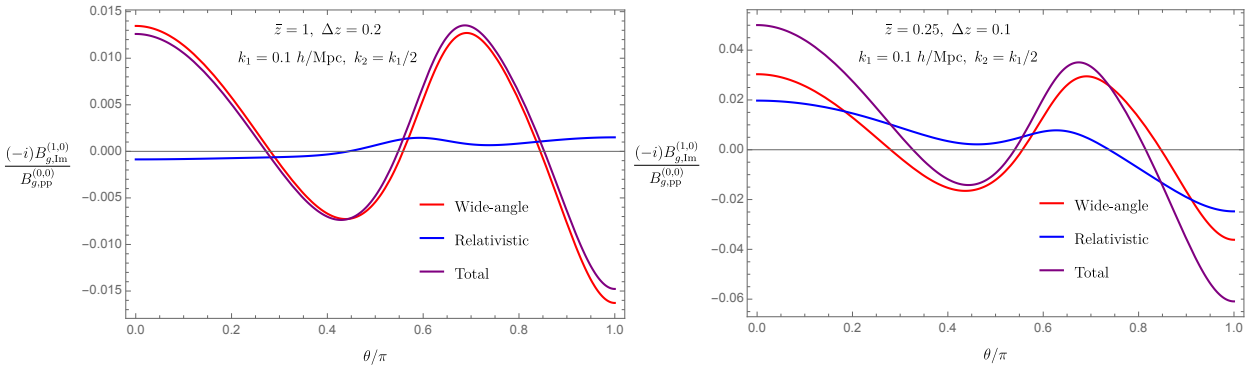

Figure 3.2: Examples for imaginary dipole moments of galaxy bispectrum from different origins. Relativistic terms also include inverse-distance contributions. These are plotted for different triangle configurations as function of the angle between $\vec{k}_1$ and $\vec{k}_2$ ($\theta \equiv \cos^{-1}\mu$). Bias parameters are $b_1 = 1.46$ for $\bar{z} = 1$ bin and $b_1 = 1.5$ for the other one with b_2, γ_2 calculated from Eqs. (2.93) and (2.94) for each bin. Also for relativistic coefficients, we set $b_e = 0$ and $s = 1$.

where we use $\vec{k}_3 = -\vec{k}_1 - \vec{k}_2$ for cyclic permutations. Given the condition on a_j's, this result produces imaginary terms that are suppressed by factors of $1/(k_1 x_c)$, $1/(k_2 x_c)$ and $1/(k_{12} x_c)$. The final wide-angle local bispectrum is the sum of all such terms:

$$B^{\mathrm{loc,wa}}_{g,\mathrm{Im}}(\vec{k}_1, \vec{k}_2, \vec{x}_c) = \sum_{\{a_1,\ldots,a_6\}} \mathcal{I}^{wa}_{(a_1,\ldots,a_6)}(\vec{k}_1, \vec{k}_2, \vec{x}_c) \tag{3.26}$$

Again, this expression depends on k_1, k_2, μ, $\hat{k}_1 \cdot \hat{x}_c = \cos\theta_1$ and $\hat{k}_2 \cdot \hat{x}_c = \mu\cos\theta_1 + \sqrt{1-\mu^2}\,\sin\theta_1\,\cos\phi_{12}$. Finally, to get odd-parity multipoles, we repeat the same steps of using this result in Eq. (3.3) (which integrates over $\cos\theta_1$ and ϕ_{12}) to find the corresponding local multipoles $\mathcal{B}^{(\ell,m)}_{\mathrm{Im,\,wa}}(k_1, k_2, \mu, x_c)$, and then insert these into Eq. (3.4) to find the final multipoles.

3.6 Dipole Moment, Signal-to-Noise and Measurements

From the previous two subsections we get the final local odd-parity multipoles as:

$$\mathcal{B}^{(\ell,m)}_{g,\mathrm{Im}}(k_1,k_2,\mu,x_c) = \mathcal{B}^{(\ell,m)}_{\mathrm{Im,\,ID}}(k_1,k_2,\mu,x_c) + \mathcal{B}^{(\ell,m)}_{\mathrm{Im,\,rel}}(k_1,k_2,\mu) + \mathcal{B}^{(\ell,m)}_{\mathrm{Im,\,wa}}(k_1,k_2,\mu,x_c). \quad (3.27)$$

with different contributions separated as labeled. We can then find the final multipoles using

$$B^{(\ell,m)}_{g,\mathrm{Im}}(k_1,k_2,\mu) = \int_{V_{\mathrm{bin}}} \frac{d^3\vec{x}_c}{V_{\mathrm{bin}}}\, \mathcal{B}^{(\ell,m)}_{g,\mathrm{Im}}(k_1,k_2,\mu,x_c) \quad (3.28)$$

and separate each contribution.

Figure 3.2 shows examples for the relative size of the dipole moment ($\ell = 1$) from wide-angle contributions ($B^{(\ell,0)}_{\mathrm{Im,\,wa}}$) and inverse-distance + pure relativistic (or relativistic in general) terms ($B^{(\ell,0)}_{\mathrm{Im,\,ID}} + B^{(\ell,0)}_{\mathrm{Im,\,rel}}$) with respect to the plane-parallel monopole moment ($B^{(0,0)}_{g,\mathrm{pp}}$). These quantities are plotted against θ/π which is the angle between two sides of the triangle, k_1 and k_2. The plots in Fig. 3.2 correspond to two redshift bins, one being a Euclid-like sample bin with $\bar{z} = 1$, $\Delta z = 0.2$ and $V_s = 7.94\,\mathrm{Gpc}^3h^{-3}$ [52] and the other one being a DESI BGS (Bright Galaxy Survey)-like sample bin with $\bar{z} = 0.25$, $\Delta z = 0.1$ and $V_s = 0.58\,\mathrm{Gpc}^3h^{-3}$ [38].

From these plots we clearly see that that wide-angle contributions have important effects on odd-parity signals and should not be neglected if one intends to constrain relativistic effects from imaginary signals.

Let us now estimate signal-to-nose ratio for the bispectrum dipole as a function of relativistic parameters b_e and s. For noise we use the Gaussian cosmic variance of the bispectrum dipole, assuming $m = 0$ for simplicity. This can be a reasonable approximation for the scales we are considering. We have

$$(\sigma^{(1,0)}_B)^2 = \langle \widehat{B}^{(1,0)}_g(k_1,k_2,\mu)^2\rangle - \langle \widehat{B}^{(1,0)}_g(k_1,k_2,\mu)\rangle^2 \quad (3.29)$$

and we can use the following estimator (we only need leading contributions to dipole variance so we can neglect relativistic and wide-angle corrections here):

$$\widehat{B}_g^{(1,0)}(k_1,k_2,\mu)=\frac{3}{V_{123}}\prod_{i=1}^{3}\int_{k_i}d^3q_i\delta_D(\vec{q}_{123})\mathcal{L}_1(\hat{q}_1.\hat{x}_c)\delta_{g,s}\left(\vec{q}_1\right)\delta_{g,s}\left(\vec{q}_2\right)\delta_{g,s}\left(\vec{q}_3\right) \tag{3.30}$$

where we have set: $\int(d\Omega_T/4\pi)F(\vec{q}_n)=(1/V_{123})\prod_{i=1}^{3}\int_{k_n}d^3\vec{q}_n\delta_D(\vec{q}_{123})F(\vec{q}_i)$ with $V_{123}=\int_{k_n}d^3\vec{q}_n\delta_D(\vec{q}_{123})\simeq 8\pi^2k_1k_2k_3\Delta k^3$. Again, since we are only interested in leading contributions to the variance, we can put $\delta_{g,s}(\vec{q})=\left(b_1+f(\hat{q}\cdot\hat{x}_c)^2\right)\delta_{\rm L}(q)$. Using Eq. (3.30) in Eq. (3.29), after some straightforward calculations and taking shot noise into account, one can write:

$$(\sigma_B^{(1,0)})^2=-s_{123}\frac{V_f}{V_{123}}\frac{9}{4\pi}\int_{-1}^{1}d\eta_1\int_0^{2\pi}d\phi_{12}\,\mathcal{L}_1(\eta_1)^2\prod_{a=1}^{3}\left[P_{g,pp}(k_a,\eta_a)+\frac{1}{(2\pi)^3\bar{n}_g}\right] \tag{3.31}$$

which leads to an imaginary error for dipole, as expected. Here $s_{123}=6,2,1$ for equilateral, isosceles and other triangles respectively, V_f is the volume of the fundamental cell in Fourier space, i.e. $V_f\equiv(2\pi)^3/V_s$ and $P_{g,pp}(k,\eta)=(b_1+f\eta^2)^2P_L(k)$. Here $\eta_1=\hat{k}_1\cdot\hat{x}_c=\cos\theta_1$, $\eta_2=\hat{k}_2\cdot\hat{x}_c=\eta_1\mu+\sqrt{1-\eta_1^2}\sqrt{1-\mu^2}\cos\phi_{12}$ and $\eta_3=\hat{k}_3\cdot\hat{x}_c$ which can be expressed in terms of the previous two expressions using $\vec{k}_3=-\vec{k}_1-\vec{k}_2$.

We calculate signal-to-noise S/N for a given redshift bin using:

$$(S/N)^2=\sum_{\{k_1,k_2,k_3\}}\frac{B_{g,\rm Im}^{(\ell,m)}(k_1,k_2,\mu)B_{g,\rm Im}^{*(\ell,m)}(k_1,k_2,\mu)}{(\sigma_B^{(1,0)})^2} \tag{3.32}$$

where we sum over all triangles assuming $k_1\leq k_2\leq k_3$, from a minimum wavenumber $k_{\rm min}=0.007\,h$/Mpc in steps of $\Delta k=k_f=(2\pi)/V_s^{1/3}$. Figure 3.3 shows S/N for different surveys as a function of evolution bias, b_e, (with $s=1$) and magnification bias, s, with ($b_e=0$). For Euclid results we used forecast parameters from [52] (Table 3) and considered the whole range ($0.9<z<1.8$) as one bin centered at $\bar{z}=1.35$. For DESI we have used forecast data in [38] (Tables 2.3 and

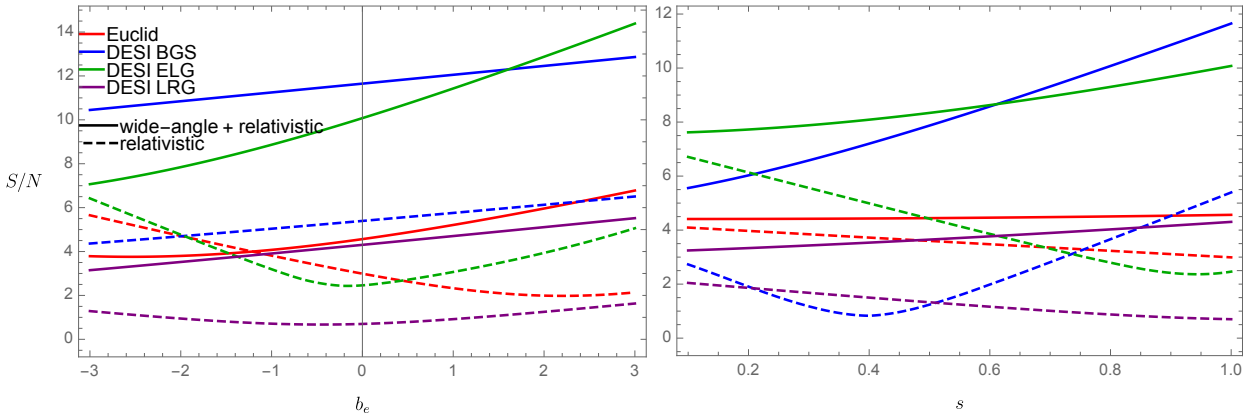

Figure 3.3: Estimates of signal-to-noise ratio for bispectrum dipole moments in different surveys as a function of evolution bias (b_e) and magnification bias (s). For the former (left plots) we set $s = 1$ and for the latter (right) we used $b_e = 0$. All forecast parameters are taken from [52, 38] for DESI and Euclid surveys respectively. Solid lines show results when all contributions to dipole are included. Dashed lines show results when wide-angle terms are neglected.

2.5). We take $0 < z < 0.5$ for BGS (Bright Galaxy survey) and $0.6 < z < 1.2$ for LRG (Luminous Red Galaxies) as single bins. For ELG (Emission Line Galaxies), we break the redshift range into two bins: $0.6 < z < 1.2$, $1.2 < z < 1.7$ and add up their corresponding S/N. The signal-to-noise for relativistic-only dipole (dashed line) is quite consistent with the results in [75], re-emphasizing its detectability in upcoming surveys. However, we are also showing here that wide-angle effects are even more important in many cases (as can be seen from the solid lines) and should be taken into account for any likelihood analysis of relativistic parameters from bispectrum dipole data.

Let us finish this section commenting on the measurement of odd-parity signals accounting for wide-angle effects that we just calculated. Using Eqs. (3.2-3.4), and changing variables ($\vec{x}_{13}$, $\vec{x}_{23}$, $\vec{x}_c$) back to ($\vec{x}_1$,$\vec{x}_2$,$\vec{x}_3$) we can rewrite the multipole formula as (we take $m = 0$ for simplicity):

$$B_{g,s}^{(\ell,0)}(k_1,k_2,\mu) = \tag{3.33}$$
$$\frac{(2\ell+1)}{V_{123}}\prod_{i=1}^{3}\int_{k_i} d^3q_i\,\delta_D(\vec{q}_{123})\int_{V_s}\frac{d^3\vec{x}_1}{(2\pi)^3}\frac{d^3\vec{x}_2}{(2\pi)^3}\frac{d^3\vec{x}_3}{(2\pi)^3}\,e^{-i\vec{q}_1\cdot\vec{x}_1}e^{-i\vec{q}_2\cdot\vec{x}_2}e^{i\vec{q}_3\cdot\vec{x}_3}\mathcal{L}_\ell(\hat{q}_1\cdot\hat{x}_c)$$
$$\left\langle\delta_{g,s}\left(\vec{x}_1\right)\delta_{g,s}\left(\vec{x}_2\right)\delta_{g,s}\left(\vec{x}_3\right)\right\rangle$$

where the integration is over positions of tracers inside the survey volume V_s. One way to evaluate this integral using Fast Fourier Transforms is to replace x_c with $\hat{x}_1$ [104]. However, for odd-parity signals the leading suppression factor is $(k_n x_c)^{-1}$, and to this order one can factorize the integral without such replacement, therefore being more accurate. Indeed, from the expansion in Eq. (3.23) we can see that:

$$\hat{x}_1 + \hat{x}_2 + \hat{x}_3 = 3\,\hat{x}_c + O(\epsilon_{1,2}^2), \tag{3.34}$$

which means the leading order correction to this sum is subleading for odd-party multipoles whose corrections were $O(\epsilon_{1,2})$. Therefore, we can simply replace $\hat{x}_c$ with $1/3\ (\hat{x}_1 + \hat{x}_2 + \hat{x}_3)$ and factorize the integrals. As an example, for dipole we can write: $\mathcal{L}_1(\hat{k}_1 \cdot \hat{x}_c) = 1/3\,(\mathcal{L}_1(\hat{k}_1 \cdot \hat{x}_1) + \mathcal{L}_1(\hat{k}_1 \cdot \hat{x}_2) + \mathcal{L}_1(\hat{k}_1 \cdot \hat{x}_3))$ which simplifies Eq. (3.33) for numerical integrations with subleading errors compared to relativistic and wide-angle effects. This can be used for calculation of imaginary multipoles from data.

3.7 Beyond Plane-Parallel Corrections to Even-Parity (Real) Multipoles

We now compute corrections beyond the plane-parallel approximation in Eq. (2.12), keeping terms up to second order in $\vec{u}$ and δ for the tree-level bispectrum. We also keep $1/x^2$ corrections because, as we will see, the leading order suppression factor for real multipoles is $1/(kx)^2$. We have:

$$\begin{aligned}\delta_{g,s}(\vec{x}) \;=\; & \delta_g(\vec{x}) + f\,\hat{x}_j\,\partial_{x_j}\left[(\vec{u}_g(\vec{x})\cdot\hat{x})(1+\delta_g(\vec{x}))\right] + f\,\frac{2}{x}(\vec{u}_g(\vec{x})\cdot\hat{x})\left[1+\delta_g(\vec{x})\right] + \\ & \frac{f^2}{2}\,\hat{x}_k\,\hat{x}_j\,\partial_{x_j}\partial_{x_k}\left[(\vec{u}_g(\vec{x})\cdot\hat{x})^2\right] + f^2\frac{2}{x}\,\hat{x}_j\,\partial_{x_j}\left[(\vec{u}_g(\vec{x})\cdot\hat{x})^2\right] + \frac{f^2}{x^2}\left[(\vec{u}_g(\vec{x})\cdot\hat{x})^2\right].\end{aligned} \tag{3.35}$$

Here we do not include relativistic corrections, which are suppressed by powers of $\mathcal{H}/k$ in Fourier space, but we keep inverse-distance terms. This is adequate for our purpose of comparing wide-angle corrections with other contributions because, again, inverse-distance and relativistic corrections are of the same order. In addition to that, wide-angle and inverse-distance terms combined comprise the leading corrections to multipoles of the plane-parallel bispectrum.

Similar to the odd-parity case, we use Eqs. (3.6-3.8) to re-write Eq. (3.35) in the following form:

$$\delta_{g,s}(\vec{x}) = \int_{\vec{q}_1} e^{i\vec{q}_1\cdot\vec{x}}\, R_1^{\rm total}(\vec{q}_1,\vec{x})\,\delta_L(\vec{q}_1) + \int_{\vec{q}_1,\vec{q}_2} e^{i\vec{q}_{12}\cdot\vec{x}}\, R_{2'}^{\rm total}(\vec{q}_1,\vec{q}_2,\vec{x})\,\delta_L(\vec{q}_1)\,\delta_L(\vec{q}_2) \tag{3.36}$$

where $R_1^{\rm total} \equiv R_1^{\rm RSD} + R_1^{\rm ID}$ and $R_{2'}^{\rm total} \equiv R_2^{\rm RSD} + R_{2'}^{\rm ID}$. $R_{1,2}^{\rm RSD}$ and $R_1^{\rm ID}$ are the same as Eqs. (3.10), (3.11) and (3.12). For $R_{2'}^{\rm ID}$, the following term should be added to Eq. (3.13) that was subleading in previous case,

$$R_{2'}^{\rm ID}(\vec{q}_1,\vec{q}_2,\vec{x}) = R_2^{\rm ID}(\vec{q}_1,\vec{q}_2,\vec{x}) - \frac{f^2}{x^2}\frac{(\vec{q}_1\cdot\hat{x})(\vec{q}_2\cdot\hat{x})}{q_1^2 q_2^2} \tag{3.37}$$

The relation for the local bispectrum is Eq. (3.17) with $R_2^{\rm total}$ replaced with $R_{2'}^{\rm total}$. Also, we remind the reader that the plane-parallel parallel multipoles are obtained from Eq. (3.18).

3.7.1 Inverse-distance Corrections

Similar to the previous cases, since we are separating inverse-distance corrections from wide-angle ones, we can set $\hat{x}_1 = \hat{x}_2 = \hat{x}_c$ for these contributions. Contrary to the imaginary case, there is mixing between wide-angle and inverse-distance corrections here. We will include these mixing terms later when we calculate wide-angle corrections so here we focus on inverse-distance terms alone. Therefore, since there is no $\vec{x}_1$ and $\vec{x}_2$ dependence in this case, the integrations over $\vec{x}_{13}$, $\vec{x}_{23}$ in Eq. (3.17) turns into delta functions replacing $\vec{q}$'s with $\vec{k}$'s. This leads to the following

expression for leading order real inverse-distance corrections:

$$
\begin{aligned}
B^{\rm local,ID}_{g,\mathcal{R}}(\vec{k}_1,\vec{k}_2,\vec{x}_c) = \Bigg\{ & R_1^{\rm RSD}(\vec{k}_1,\vec{x}_c)\, R_1^{\rm RSD}(\vec{k}_2,\vec{x}_c)\left[-\frac{2f^2}{x_c^2}\frac{(\vec{k}_1\cdot\hat{x}_c)(\vec{k}_2\cdot\hat{x}_c)}{k_1^2k_2^2}\right]+ \\
& + R_1^{\rm ID}(\vec{k}_1,\vec{x}_c)\, R_1^{\rm ID}(\vec{k}_2,\vec{x}_c)\left[R_2^{\rm RSD}(-\vec{k}_1,-\vec{k}_2,\vec{x}_c) + \; R_2^{\rm RSD}(-\vec{k}_2,-\vec{k}_1,\vec{x}_c)\right]+ \\
& + \left(R_1^{\rm RSD}(\vec{k}_1,\vec{x}_c)R_1^{\rm ID}(\vec{k}_2,\vec{x}_c) + R_1^{\rm ID}(\vec{k}_1,\vec{x}_c)R_1^{\rm RSD}(\vec{k}_2,\vec{x}_c)\right)\times \\
& \times\left[R_2^{\rm ID}(-\vec{k}_1,-\vec{k}_2,\vec{x}_c) + R_2^{\rm ID}(-\vec{k}_2,-\vec{k}_1,\vec{x}_c)\right]\Bigg\} P_L(k_1)P_L(k_2) \quad + \\
& + \begin{pmatrix} \vec{k}_1 \\ \vec{k}_2 \to \vec{k}_3 \end{pmatrix} \quad + \quad \begin{pmatrix} \vec{k}_1 \to \vec{k}_2 \\ \vec{k}_3 \end{pmatrix},
\end{aligned}
\tag{3.38}
$$

where $R_2^{\rm RSD}$'s in this equation are given in Eq. (3.11). From this expression, it is straightforward to calculate the real local multipoles from Eq. (3.3):

$$
\mathcal{B}^{(\ell,m)}_{\mathcal{R},\rm ID}(k_1,k_2,\mu,x_c) = \frac{(2\ell+1)}{4\pi}\int d\Omega_k\, B^{\rm local,ID}_{g,\mathcal{R}}(\vec{k}_1,\vec{k}_2,\vec{x}_c)\, Y^*_{\ell m}(\theta,\phi)\,. \tag{3.39}
$$

3.7.2 Wide-angle Corrections

The last step is to find the real (even-parity) wide-angle corrections to the plane-parallel multipoles. Similar to the inverse-distance terms these are suppressed by $1/(kx_c)^2$. Therefore, from Eq. (3.17), we start from the following local bispectrum which includes RSD terms plus $R^{\rm ID}_{1,2}$ contributions that come with an imaginary i/x factor. The latter, when mixed with wide-angle corrections, become real and get an extra $1/x$ factor like other leading order real corrections. These

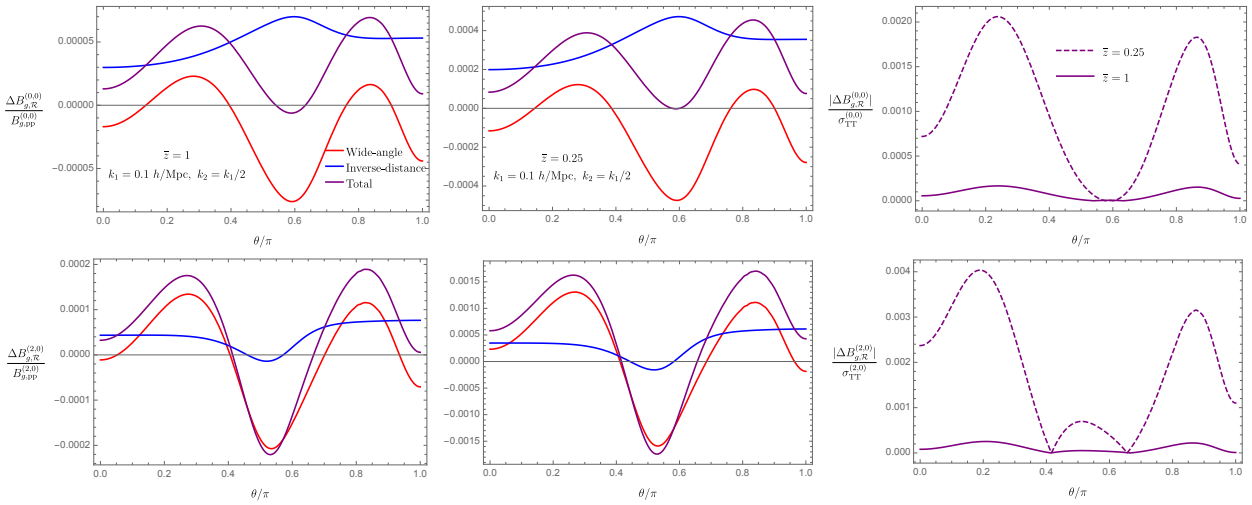

Figure 3.4: Corrections to plane-parallel multipoles of the bispectrum for different triangle shapes for monopole (top) and quadrupole (bottom) with $m = 0$ in all cases. Again, θ is the angle between $\vec{k}_1$ and $\vec{k}_2$. We assumed the same redshift bins as in the dipole case. The rightmost plots are ratios of total corrections to the corresponding sample variances calculated from Eq. (3.46). We set $\Delta k = k_f$ for each bin.

are the mixing terms. We have:

$$
\begin{aligned}
B_{g,\mathcal{R}}^{\text{local, (pp+wa)}}(\vec{k}_1,\vec{k}_2,\vec{x}_c) = \mathfrak{R}\Bigg\{ \int_{\vec{q}_1,\vec{q}_2,\vec{x}_{13},\vec{x}_{23}} e^{i(\vec{q}_1-\vec{k}_1)\cdot\vec{x}_{13}} e^{i(\vec{q}_2-\vec{k}_2)\cdot\vec{x}_{23}} \Bigg(\Big(R_1^{\text{RSD}}(\vec{q}_1,\vec{x}_1)\, R_1^{\text{RSD}}(\vec{q}_2,\vec{x}_2) \\
+ R_1^{\text{RSD}}(\vec{q}_1,\vec{x}_1)\, R_1^{\text{ID}}(\vec{q}_2,\vec{x}_2) + R_1^{\text{ID}}(\vec{q}_1,\vec{x}_1)\, R_1^{\text{RSD}}(\vec{q}_2,\vec{x}_2) \Big) \Big[R_2^{\text{RSD}}(-\vec{q}_1,-\vec{q}_2,\vec{x}_3) \\
+ R_2^{\text{RSD}}(-\vec{q}_2,-\vec{q}_1,\vec{x}_3) \Big] + R_1^{\text{RSD}}(\vec{q}_1,\vec{x}_1)\, R_1^{\text{RSD}}(\vec{q}_2,\vec{x}_2) \Big[R_2^{\text{ID}}(-\vec{q}_1,-\vec{q}_2,\vec{x}_3) \\
+ R_2^{\text{ID}}(-\vec{q}_2,-\vec{q}_1,\vec{x}_3) \Big] \Bigg) P_L(q_1) P_L(q_2) \Bigg\} + \begin{pmatrix} \vec{k}_1 \\ \vec{k}_2 \to \vec{k}_3 \end{pmatrix} + \begin{pmatrix} \vec{k}_1 \to \vec{k}_2 \\ \vec{k}_3 \end{pmatrix} .
\end{aligned}
\tag{3.40}
$$

where "pp" refers to plane-parallel contribution which is the special limit of the expression above. Similar to the imaginary case, to extract wide-angle corrections we consider the geometry of Fig. 3.1 and make use of expansions as in Eq. (3.23) and Eq. (3.24) for unit vectors and $1/x_n$ terms in these expressions. In this case we keep terms up to second order in ϵ_1 and ϵ_2 and their mixing.

Then, Eq. (3.40) can be written as sum of terms that take the following general form:

$$\mathcal{I}^{\mathcal{R}}_{b_1,\ldots,b_6}(\vec{k}_1,\vec{k}_2,\vec{x}_c) = \int_{\{\vec{q}_1,\vec{q}_2,\vec{x}_{13},\vec{x}_{23}\}} e^{i(\vec{q}_1-\vec{k}_1)\cdot\vec{x}_{13}} e^{i(\vec{q}_2-\vec{k}_2)\cdot\vec{x}_{23}} \mathcal{C}_{b_1,\ldots,b_6}(\vec{q}_1,\vec{q}_2,\vec{x}_c) \times (\boldsymbol{\epsilon}_{1x})^{b_1}(\boldsymbol{\epsilon}_{1y})^{b_2}(\boldsymbol{\epsilon}_{1z})^{b_3}(\boldsymbol{\epsilon}_{2x})^{b_4}(\boldsymbol{\epsilon}_{2y})^{b_5}(\boldsymbol{\epsilon}_{2z})^{b_6} + \text{c.p}\,. \tag{3.41}$$

where $b_1 \ldots b_6$ can be 0, 1 or 2 with the condition: $\sum_{j=1}^{6} b_j \leq 2$ for leading order contributions. Again, we can pull $\epsilon_{1j,2k}$ factors out of the integral to obtain:

$$\mathcal{I}^{\mathcal{R}}_{b_1,\ldots,b_6}(\vec{k}_1,\vec{k}_2,\vec{x}_c) = \left(\frac{i^{(b_1+\ldots+b_6)}}{x_c^{b_1}\ldots x_c^{b_6}}\right)\left(\frac{\partial^{b_1}}{\partial k_{1x}^{b_1}}\ldots\frac{\partial^{b_6}}{\partial k_{2z}^{b_6}}\right)\mathcal{C}_{b_1,\ldots,b_6}(\vec{k}_1,\vec{k}_2,\vec{x}_c) + \text{c.p}\,. \tag{3.42}$$

The plane-parallel contributions, Eq. (3.18), are reproduced in the limit $\vec{\epsilon}_{1,2} \longrightarrow 0$ or $\hat{x}_1 \simeq \hat{x}_2 \simeq \hat{x}_3 \simeq \hat{x}_c$ and $1/x_c \longrightarrow \infty$. For such terms $b_m = 0$. These are followed by leading order wide-angle corrections which build up the corresponding local bispectrum:

$$B^{\text{loc,wa}}_{g,\mathcal{R}}(\vec{k}_1,\vec{k}_2,\vec{x}_c) = \sum_{\{b_1,b_2,\ldots,b_6\}} \mathcal{I}^{\mathcal{R}}_{b_1,\ldots,b_6}(\vec{k}_1,\vec{k}_2,\vec{x}_c) \tag{3.43}$$

with $\sum_{j=1}^{6} b_j$ =1 or 2 (in the case of 1 in Eq. (3.41) there is an extra $1/kx_c$ factor which comes from ID terms). Finally, it is straightforward to calculate wide-angle multipoles using Eq. (3.3) and Eq. (3.42):

$$\mathcal{B}^{(\ell,m)}_{\mathcal{R},\text{wa}}(k_1,k_2,\mu,x_c) = \frac{(2\ell+1)}{4\pi}\int d\Omega_k\, B^{\text{loc,wa}}_{g,\mathcal{R}}(\vec{k}_1,\vec{k}_2,\vec{x}_c)\, Y^*_{\ell m}(\theta,\phi)\,. \tag{3.44}$$

Again, we do not write down the expressions explicitly because of the large number of terms involved in the expansion.

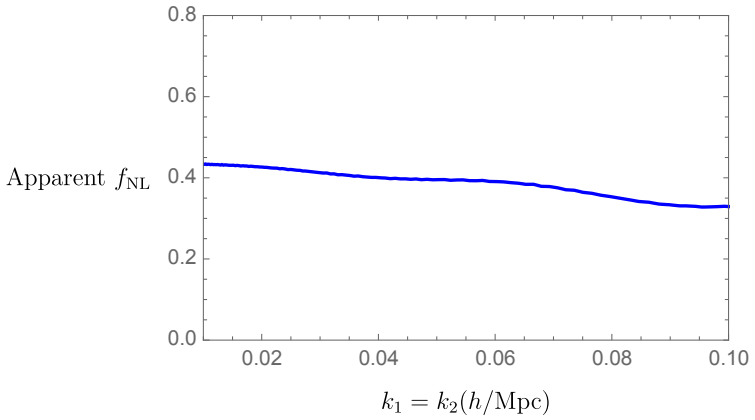

Figure 3.5: An estimate of the apparent primordial local non-Gaussianity parameter $f_{\rm NL}$ when ignoring wide-angle and inverse-distance effects. For simplicity, we have ignored stochasticity, $b_1 = 1.5$ and $z = 1$.

3.8 Full Results

Using the local multipoles from previous results into Eq. (3.4), we get the following contributions for the final multipoles:

$$\begin{aligned} B^{(\ell,m)}_{g,\mathcal{R}}(k_1,k_2,\mu) &= B^{(\ell,m)}_{g,\rm pp}(k_1,k_2,\mu) + B^{(\ell,m)}_{\mathcal{R},\rm wa}(k_1,k_2,\mu) \\ &\quad + B^{(\ell,m)}_{\mathcal{R},\rm ID}(k_1,k_2,\mu)\,. \end{aligned} \tag{3.45}$$

In this section we plot the relative magnitude of corrections to plane-parallel multipoles for $\ell = 0$, 2 ($m = 0$) and compare them to cosmic variance. Figure 3.4 shows examples of such quantities where $\Delta B^{(\ell,0)}_{g,\mathcal{R}} = B^{(\ell,m)}_{\mathcal{R},\rm wa/ID}(k_1,k_2,\mu)$ and their sum. Plots are generated for the same two redshift bins used in odd-parity cases. Variances are calculated by following the same procedure that resulted in Eq. (3.31). For even values of ℓ (m = 0) one finds:

$$(\sigma^{(\ell,0)}_B)^2 = s_{123}\frac{V_f}{V_{123}}\frac{(2\ell+1)}{4\pi}\int_{-1}^{1}d\eta_1\int_0^{2\pi}d\phi_{12}\,\mathcal{L}_\ell(\eta_1)^2\prod_{a=1}^{3}\left[P_{g,pp}(k_a,\eta_a)+\frac{1}{(2\pi)^3\bar{n}_g}\right] \tag{3.46}$$

The relative sizes of these corrections are sub-percent and smaller compared to the imaginary

case. This is expected because of the additional suppression factor in this case. The ratio to cosmic variance also suggests that although these corrections become more important at lower redshifts, they can be safely neglected given the current and near future precision.

3.9 Impact of wide-angle effects on primordial non-Gaussianity parameter measurements

Finally, we comment on how big a contamination wide-angle effects are to local $f_{\rm NL}$ constraints from galaxy bispectrum measurements. At leading order primordial non-gaussianity leaves its footprints in galaxy bispectrum with corrections linear in $f_{\rm NL}$. Similar to what was done in power spectrum case, to have an idea about how important these contaminations are, we can find the "apparent" $f_{\rm NL}$ by comparing the linear (in $f_{\rm NL}$) non-gaussian contribution to the bispectrum for isosceles triangles in the squeezed limit with the local monopole of the wide-angle and inverse-distance corrections. From the general relation for the primordial non-gaussianity term in bispectrum [40], we take the special case $k_1 = k_2 \gg k_3$ which results in:

$$B_g^f(k_1,k_2,k_3,z) \approx \frac{3f_{\rm NL}\delta_{cr}(b_1-1)\Omega_{M0}H_0^2}{D(z)T(k_3)}\frac{P_m(k_1)P_m(k_3)}{k_3^2}\left[\frac{2b_1^3}{\delta_{cr}(b_1-1)}\right.$$
$$\left.+2\,b_1^2\left(\frac{(2\delta_{cr}-1)(b_1-1)+\delta_{cr}b_2^L}{2\delta_{cr}(b_1-1)}\right)+2b_1\left(\frac{10}{7}b_1+b_2-\frac{2}{3}b_{K^2}\right)\right] \tag{3.47}$$

where we have ignored stochasticity, $b_{\rm K^2} = \gamma_2$, $b_2^L = b_2 - 8/21(b_1-1)$ is the Lagrangian quadratic bias. Figure 3.5 shows plot of the apparant PNG parameter such a plot as a function of the isosceles triangle scale with $\theta = 0.95\pi$. Other parameters are similar to previous plots. This result implies that wide-angle and inverse-distance corrections should not be a significant problem for $f_{\rm NL}$ measurements from the galaxy bispectrum when using the plane-parallel assumption until precision of $\Delta f_{\rm NL} \sim 1$ is reached.

3.10 Summary

In this chapter, we investigated the effects of wide-angle and inverse-distance corrects on multipoles of galaxy bispectrum in redshift space. We showed that wide-angle effects alone can induce observable imaginary odd-parity signals that are comparable and, in many cases, even large than similar signals produced by relativistic effetcts. We also showed that wide-angle and inverse-distance corrections are negligible when it comes to real even parity bispectrum multipoles like monopole, quadrupole, etc. Finally, we showed that wide-angle and inverse-distance corrections can be mistaken with a local primordial non-Gaussianity signal with $f_{\rm NL}$ of order unity.

4 PAIRWISE VELOCITIES AND THE REDSHIFT SPACE GALAXY BISPECTRUM

4.1 Introduction

The distribution of dark matter density fluctuations, and consequently that of tracers, in the universe is not Gaussian. Even with fully Gaussian initial conditions, the nonlinear evolution of dark matter density contrast leads to non-Gaussianity of its distribution. Therefore, we need statistics beyond the two-point correlation function or its Fourier space counterpart, the power spectrum, to extract more information from the observations. In Fourier space, the Bispectrum is the simplest statistic beyond power spectrum for this purpose. To mention some examples, it has been shown that the bispectrum can be used to obtain better constraints on galaxy biases and cosmological parameters [83, 50, 82], neutrino masses [96, 60, 59] and primordial non-Gaussianity parameters [68, 80, 36] from clustering data.

Significant amount of work has been done towards modeling the redshift space bispectrum from leading order (tree level) in Standard Perturbation Theory (SPT) [106] to one-loop order in Effective Field Theory of Large Scale Structure (EFTofLSS) (see e.g. [90]). However, the most recent models include a large number of free parameters in the modeling to capture various physical impacts on the redshift space bispectrum. Among the most important ones are "Fingers-of-God" (FoG) contributions that lead to a weakening of the bispectrum signal due to velocity

dispersion effects. The inclusion of several free parameters along with various nonlinear (one-loop order) contributions makes the models complicated and, possibly, computationally costly for cosmological inferences. In this chapter we provide a model for FoG contributions to the galaxy bispectrum that is based on closed form "dispersion factors" that only depend on one free parameter that can be fitted to the power spectrum data. We also show that including non-linear terms by simple modifications in the tree-level FoG-corrected bispectrum can lead to significant improvement at quasi-linear scales.

Similar to previous chapters, we use the following conventions for integrals in configuration and Fourier spaces:

$$\int_{\vec{x}} \equiv \int \frac{d^3x}{(2\pi)^3}, \qquad \int_{\vec{k}} \equiv \int d^3k \tag{4.1}$$

4.2 Basic Definitions

The redshift space bispectrum, defined as $\langle \delta_s(\vec{k}_1)\delta_s(\vec{k}_2)\delta_s(\vec{k}_3)\rangle \equiv B_s(\vec{k}_1,\vec{k}_2)\,\delta_D(\vec{k}_1+\vec{k}_2+\vec{k}_3)$, can be extracted from expansion of the following combination: $\langle(\delta_D(\vec{k}_1)+\delta_s(\vec{k}_1))(\delta_D(\vec{k}_2)+\delta_s(\vec{k}_2))(\delta_D(\vec{k}_3)+\delta_s(\vec{k}_3)\rangle$. The unexpanded expectation value itself can be evaluated using the equation [103]:

$$\delta_D(\vec{k})+\delta_s(\vec{k}) = \int_{\vec{x}} e^{-i\vec{k}\cdot\vec{x}} e^{ifk_z u_z(\vec{x})}\,[1+\delta(\vec{x})]\,, \tag{4.2}$$

where δ is the density perturbation in real space and $u_z = -(\vec{v}\cdot\hat{z})/(\mathcal{H}f)$ is the line-of-sight (LOS) projected peculiar velocity field (subscript z denotes projection along LOS). Here we start with dark matter density fluctuation and will extend the results to galaxies later by appropriately including bias coefficients. Similar to previous chapters, we ignore velocity bias and assume that galaxy and dark matter peculiar velocities are the same.

It is worth noting that this equation implies that the mapping between real and redshift spaces introduces a new type of nonlinearity to the redshift space density fluctuation due to the exponential factor, $\exp(ifk_z u_z)$. This is different from nonlinearities that originate from dynamical evolution of $\delta(\vec{x})$ (like loop terms in SPT). It has been shown [103, 105] and will also be shown here that even if one expands u_z in perturbation theory, the nonlinear mapping between real and redshift spaces leaves its footprint in terms of nonlinear suppression factors that can be expressed in terms of velocity zero lag terms (i.e. terms like the average of the square of the linear velocities at the same position).

The expansion mentioned above produces the bispectrum in addition to seven other terms but three of them are zero by the assumption: $\langle \delta_s(\vec{k}) \rangle = 0$, another three can be written in terms of the redshift space power spectrum, $\langle \delta_s(\vec{k}_1)\delta_s(\vec{k}_2)\rangle \equiv P_s(\vec{k}_1)\delta_D(\vec{k}_1+\vec{k}_2)$, and a last term which is a product of delta functions. It should be emphasized that we always consider triangle configurations satisfying $\vec{k}_1+\vec{k}_2+\vec{k}_3=0$. Defining: $\vec{k}_{123\ldots} \equiv \vec{k}_1+\vec{k}_2+\vec{k}_3+\ldots$, we utilize the equations $\delta_D(\vec{k}_1)\delta_D(\vec{k}_{12}) = \delta_D(\vec{k}_1)\delta_D(\vec{k}_{123})$ and $\delta_D(\vec{k}_1)\delta_D(\vec{k}_2)\delta_D(\vec{k}_3) = \delta_D(\vec{k}_{123})\delta_D(\vec{k}_1)\delta_D(\vec{k}_2)$ to obtain, after some algebra and manipulation of integrals, the following relation for the bispectrum in redshift space:

$$B_s(\vec{k}_1,\vec{k}_2) = \int_{\vec{x}_{13},\vec{x}_{23}} e^{-i\vec{k}_1.\vec{x}_{13}} e^{-i\vec{k}_2.\vec{x}_{23}} \Big[\mathcal{Z}_{123}(\lambda_1,\lambda_2,\vec{x}_{13},\vec{x}_{23}) - \mathcal{Z}_{13}(\lambda_1,\vec{x}_{13}) - \mathcal{Z}_{23}(\lambda_2,\vec{x}_{23}) - \mathcal{Z}_{12}(\lambda_1,\vec{x}_{13},\vec{x}_{23}) + 2 \Big] \tag{4.3}$$

where $\vec{x}_{nm} \equiv \vec{x}_n - \vec{x}_m$ and $\lambda_n \equiv ifk_{nz}$. The $\mathcal{Z}$ functions in this equation are:

$$\mathcal{Z}_{123}(\lambda_1, \lambda_2, \vec{x}_{13}, \vec{x}_{23}) = \left\langle e^{\lambda_1 \Delta u_{13}} e^{\lambda_2 \Delta u_{23}} (1 + \delta(\vec{x}_1))(1 + \delta(\vec{x}_2))(1 + \delta(\vec{x}_3)) \right\rangle \tag{4.4}$$

$$\mathcal{Z}_{13}(\lambda_1, \vec{x}_{13}) = \left\langle e^{\lambda_1 \Delta u_{13}} (1 + \delta(\vec{x}_1))(1 + \delta(\vec{x}_3)) \right\rangle \tag{4.5}$$

$$\mathcal{Z}_{23}(\lambda_2, \vec{x}_{23}) = \left\langle e^{\lambda_2 \Delta u_{23}} (1 + \delta(\vec{x}_2))(1 + \delta(\vec{x}_3)) \right\rangle \tag{4.6}$$

$$\mathcal{Z}_{12}(\lambda_1, \vec{x}_{13}, \vec{x}_{23}) = \left\langle e^{\lambda_1 \Delta u_{12}} (1 + \delta(\vec{x}_1))(1 + \delta(\vec{x}_2)) \right\rangle . \tag{4.7}$$

with $\Delta u_{mn} \equiv u_z(\vec{x}_m) - u_z(\vec{x}_n)$. For the last equation, it is worth noting that since $(\vec{x}_1, \vec{x}_2, \vec{x}_3)$ can be expressed in terms of $(\vec{x}_{13}, \vec{x}_{23}, \vec{x}_c)$ with $\vec{x}_c \equiv (\vec{x}_1 + \vec{x}_2 + \vec{x}_3)/3$, the combination inside the expectation value is a function of the latter triad. Furthermore, since we are working in the plane-parallel approximation, ultimately there will be no $\vec{x}_c$ dependence. This justifies the way the dependence of the $\mathcal{Z}_{12}$ function on position is written. Similar arguments can be made for the other functions.

4.3 Velocity difference generating function

Following ideas in [105], to calculate the aforementioned $\mathcal{Z}$-functions, one can first find a closed relation for the velocity difference generating function, that is the expectation value of the exponential terms alone, and then include the contribution of density fluctuations perturbatively. The velocity difference generating functions corresponding to Eqs (4.4)-(4.7) are then defined as:

$$W_{123}(\lambda_1, \lambda_2, \vec{x}_{13}, \vec{x}_{23}) = \left\langle e^{\lambda_1 \Delta u_{13}} e^{\lambda_2 \Delta u_{23}} \right\rangle \tag{4.8}$$

$$W_{13}(\lambda_1, \vec{x}_{13}) = \left\langle e^{\lambda_1 \Delta u_{13}} \right\rangle \tag{4.9}$$

$$W_{23}(\lambda_2, \vec{x}_{23}) = \left\langle e^{\lambda_2 \Delta u_{23}} \right\rangle \tag{4.10}$$

$$W_{12}(\lambda_1, \vec{x}_{13}, \vec{x}_{23}) = \left\langle e^{\lambda_1 \Delta u_{12}} \right\rangle . \tag{4.11}$$

In [105], the generating function corresponding to one velocity difference, like in Eqs. (4.9) and (4.10), is first calculated by expanding the velocity difference to quadratic order in Gaussian fluctuations in perturbation theory. The expressions are then discretized in terms of plane waves living in a cubic box of length L. Following a similar procedure here, we get:

$$\Delta u_{mn} = \Delta u^{(1)}_{mn} + \Delta u^{(2)}_{mn} = \sum_{k} w_{\vec{k}}(\vec{x}_{mn})\theta_{\vec{k}} + \sum_{\vec{k}_1,\vec{k}_2} g_{\vec{k}_1\vec{k}_2}(\vec{x}_{mn})\theta_{\vec{k}_1}\theta_{\vec{k}_2} \tag{4.12}$$

where $\theta_{\vec{k}} = k_F^3\theta(\vec{k})$ is the discretized version of the the divergence of the linear velocity field with $k_F = 2\pi/L$ (fundamental mode) and

$$w_{\vec{k}}(\vec{x}_{mn}) = \frac{i\hat{k}\cdot\hat{z}}{k}(1 - e^{i\vec{k}\cdot\vec{x}_{mn}}); \qquad g_{\vec{k}_1\vec{k}_2}(\vec{x}_{mn}) = w_{\vec{k}_{12}}(\vec{x}_{mn})\; G_2(\vec{k}_1,\vec{k}_2)\,. \tag{4.13}$$

where we have chosen the origin of coordinates to be at $\vec{x}_n$ as we are considering plane-parallel approximation. Also here: $\vec{k}_{12} = \vec{k}_1 + \vec{k}_2$. Again, this is the discretized standard perturbation theory expansion for the divergence of the linear velocity field with G_2 being the second order SPT velocity kernel.

These expressions can be substituted for velocity differences in Eqs.(4.8)-(4.11) and the corresponding expectation values can be calculated given the Gaussianity of θ_k's. As an example, for Eq.(4.9), one has [105]:

$$\begin{aligned} W_{13}(\lambda_1,\vec{x}_{13}) &= \int_{\theta_{\vec{k}_1}}\cdots\int_{\theta_{\vec{k}_N}} \frac{e^{-\frac{1}{2}\sum_{\vec{k}_i,\vec{k}_j}\delta^K_{\vec{k}_i\vec{k}_j}\theta_{\vec{k}_i}\theta_{\vec{k}_j}/\widehat{P}_{\theta\theta}(k_i)}\, e^{\lambda_1\sum_{\vec{k}_i,\vec{k}_j} g_{\vec{k}_i\vec{k}_j}(\vec{x}_{13})\theta_{\vec{k}_i}\theta_{\vec{k}_j}}}{\sqrt{\mathrm{Det}\,2\pi\mathcal{P}}} e^{\lambda_1\sum_{\vec{k}_i} w_{\vec{k}_i}(\vec{x}_{13})\theta_{\vec{k}_i}} \\ &= \frac{\left\langle e^{\lambda_1\sum_{\vec{k}_i} w_{\vec{k}_i}(\vec{x}_{13})\theta_{\vec{k}_i}}\right\rangle_{\mathrm{M}}}{\sqrt{\mathrm{Det}\,(\mathcal{M}^{-1}\mathcal{P})}} \end{aligned} \tag{4.14}$$

where N is the number of modes, $\widehat{P}_{\theta\theta}(k_i)$ is the power spectrum of discretized modes, $\mathcal{P}_{\theta_{\vec{k}_i}\theta_{\vec{k}_j}} \equiv \delta^K_{\vec{k}_i\vec{k}_j}\widehat{P}_{\theta\theta}(k_i)$ is the diagonal covariance matrix of the $\theta_{\vec{k}}$'s and $\delta^K_{\vec{k}_i\vec{k}_j}$ is one when $\vec{k}_i+\vec{k}_j = 0$ (opposite

vectors) and zero otherwise. This enforces translational invariance. The quadratic contribution in the Gaussian integral above "renormalizes" the covariance matrix, making it non-diagonal:

$$\mathcal{M}^{-1}_{\vec{k}_1\vec{k}_2}(\lambda_1,\vec{x}_{13}) = \frac{\delta^K_{\vec{k}_1\vec{k}_2}}{\widehat{P}_{\theta\theta}(k_1)} - 2\lambda_1 g_{\vec{k}_1\vec{k}_2}(\vec{x}_{13}) \tag{4.15}$$

Therefore, $\langle\rangle_M$ in (4.14) means expectation value with respect to this normalized covariance matrix. In other words:

$$W_{13}(\lambda_1,\vec{x}_{13}) = \frac{e^{\lambda_1^2 \sum_{\vec{k}_1,\vec{k}_2} w_{\vec{k}_1}(\vec{x}_{13})\mathcal{M}_{\vec{k}_1\vec{k}_2}(\lambda_1,\vec{x}_{13})w_{\vec{k}_2}(\vec{x}_{13})/2}}{\sqrt{\mathrm{Det}\,(\mathcal{M}^{-1}\mathcal{P})}} \tag{4.16}$$

The final step is to calculate $\mathcal{M}_{\vec{k}_1\vec{k}_2}(\lambda_1,\vec{x}_{13})$ from (4.15) and use that to find $\sqrt{\mathrm{Det}\,(\mathcal{M}^{-1}\mathcal{P})}$. Keeping terms up to one-loop, the final result for (4.9) and similarly for (4.10) and (4.11) becomes [105]:

$$W_{13}(\lambda_1,\vec{x}_{13}) = \frac{1}{\sqrt{1-\lambda_1^2\langle[\Delta u^{(2)}_{13}]^2\rangle}} \exp\left(\frac{\lambda_1^2\langle[\Delta u^{(1)}_{13}]^2\rangle + \frac{\lambda_1^3}{3}\langle[\Delta u_{13}]^3\rangle_c}{2(1-\lambda_1^2\langle[\Delta u^{(2)}_{13}]^2\rangle)}\right), \tag{4.17}$$

$$W_{23}(\lambda_2,\vec{x}_{23}) = \frac{1}{\sqrt{1-\lambda_2^2\langle[\Delta u^{(2)}_{23}]^2\rangle}} \exp\left(\frac{\lambda_2^2\langle[\Delta u^{(1)}_{23}]^2\rangle + \frac{\lambda_2^3}{3}\langle[\Delta u_{23}]^3\rangle_c}{2(1-\lambda_2^2\langle[\Delta u^{(2)}_{23}]^2\rangle)}\right), \tag{4.18}$$

$$W_{12}(\lambda_1,\vec{x}_{13},\vec{x}_{23}) = \frac{1}{\sqrt{1-\lambda_1^2\langle[\Delta u^{(2)}_{12}]^2\rangle}} \exp\left(\frac{\lambda_1^2\langle[\Delta u^{(1)}_{12}]^2\rangle + \frac{\lambda_1^3}{3}\langle[\Delta u_{12}]^3\rangle_c}{2(1-\lambda_1^2\langle[\Delta u^{(2)}_{12}]^2\rangle)}\right). \tag{4.19}$$

In these equations, $\langle[\Delta u_{mn}]^3\rangle_c = \langle[\Delta u_{mn}]^3\rangle_{\text{tree}}$ which can be proved from the relation between cumulant and moment generating functions: $\langle e^{\lambda\Delta u}\rangle_c = \ln\left(\langle e^{\lambda\Delta u}\rangle\right)$.

So far, since the expansion in Eq. (4.12) was up to second order in $\theta_{\vec{k}}$, the one-loop contribution that appears in equations above is in the form of $\langle[\Delta u^{(2)}_{mn}]^2\rangle$. However, the one-loop term should have another piece, namely $2\langle\Delta u^{(1)}_{mn}\Delta u^{(3)}_{mn}\rangle$, which contains cubic contributions that were not include in the expansion of (4.12). To amend this, one can simply add this term to the quadratic

piece and promote it to the full one-loop term [105]:

$$\langle [\Delta u^{(2)}_{mn}]^2 \rangle \longrightarrow \langle [\Delta u^{(2)}_{mn}]^2 \rangle + 2\langle \Delta u^{(1)}_{mn} \Delta u^{(3)}_{mn} \rangle \equiv \langle [\Delta u_{mn}]^2 \rangle_{\rm 1L}. \tag{4.20}$$

One motivation behind this is that at the very end, when the power spectrum is calculated, this replacement reproduces the already-known form of the one-loop power spectrum in redshift space without FoG. There is one more step that can be taken to further improve the velocity generating function. Until now, we have worked in perturbation theory and Eqs (4.17)- (4.19) capture the velocity dispersion effects from large scale fluctuations in the standard perturbation theory up to one loop. However, another important source of velocity dispersion emanate from small scale, "virial" velocities from virial equilibrium in gravitational bound structures, like clusters within dark matter halos. To include this contribution, we assume that we can treat this source of dispersion as independent from the one originating from the perturbation theory and add it to the one-loop component as [105]:

$$\langle [\Delta u_{mn}]^2 \rangle_{\rm 1L} \longrightarrow \langle [\Delta u_{mn}]^2 \rangle_{\rm 1L} + \langle [\Delta u_{mn}]^2 \rangle_{\rm vir}. \tag{4.21}$$

This is a phenomenological approach and the leading contribution of the virial part will be parameterized in terms of a constant whose value should be obtained by direct fitting to the data.

It is straightforward to generalize these results to calculate the generating function in Eq (4.8) (which then can be used for Eq. (4.4)). Using the expressions in (4.12), we can write:

$$\begin{aligned} &\lambda_1 \Delta u_{13} + \lambda_2 \Delta u_{23} = \sum_k \left(\lambda_1 w_{\vec{k}}(\vec{x}_{13}) + \lambda_2 w_{\vec{k}}(\vec{x}_{23}) \right) \theta_{\vec{k}} \\ &+ \sum_{\vec{k}_1, \vec{k}_2} \left(\lambda_1 g_{\vec{k}_1 \vec{k}_2}(\vec{x}_{13}) + \lambda_2 g_{\vec{k}_1 \vec{k}_2}(\vec{x}_{23}) \right) \theta_{\vec{k}_1} \theta_{\vec{k}_2} \equiv \sum_k \tilde{\lambda}\ \tilde{w}_{\vec{k}}(\vec{x}_{13}, \vec{x}_{23})\ \theta_{\vec{k}} + \\ &\sum_{\vec{k}_1, \vec{k}_2} \bar{\lambda}\ \bar{g}_{\vec{k}_1 \vec{k}_2}(\vec{x}_{13}, \vec{x}_{23})\ \theta_{\vec{k}_1} \theta_{\vec{k}_2}\ . \end{aligned} \tag{4.22}$$

Following steps similar to what was shown before, results in:

$$W_{123}(\lambda_1,\lambda_2,\vec{x}_{13},\vec{x}_{23}) = \frac{1}{\sqrt{1-\langle[\lambda_1\Delta u_{13}^{(2)}+\lambda_2\Delta u_{23}^{(2)}]^2\rangle}}\times \exp\left(\frac{\langle[\lambda_1\Delta u_{13}^{(1)}+\lambda_2\Delta u_{23}^{(1)}]^2\rangle+\frac{1}{3}\langle[\lambda_1\Delta u_{13}+\lambda_2\Delta u_{23}]^3\rangle_c}{2(1-\langle[\lambda_1\Delta u_{13}^{(2)}+\lambda_2\Delta u_{23}^{(2)}]^2\rangle)}\right). \quad (4.23)$$

Now, the $\mathcal{Z}$-functions defined in Eqs (4.4) - (4.7), can be re-written in the following forms:

$$\mathcal{Z}_{123}(\lambda_1,\lambda_2,\vec{x}_{13},\vec{x}_{23}) = \frac{1}{\sqrt{1-[\lambda_{123}\,\sigma_{123}]^2}}\exp\left(\frac{[\lambda_{123}\,\bar{\sigma}_{123}]^2+\frac{1}{3}\langle[\lambda_{123}\,\Delta u_{123}]^3\rangle_{\rm tree}}{2(1-[\lambda_{123}\,\sigma_{123}]^2)}\right)\times \left(1+\delta\mathcal{Z}_{123}(\lambda_1,\lambda_2,\vec{x}_{13},\vec{x}_{23})\right) \quad (4.24)$$

$$\mathcal{Z}_{13}(\lambda_1,\vec{x}_{13}) = \frac{1}{\sqrt{1-\lambda_1^2\sigma_{13}^2}}\exp\left(\frac{\lambda_1^2\bar{\sigma}_{13}^2+\frac{1}{3}\lambda_1^3\langle(\Delta u_{13})^3\rangle_{\rm tree}}{2(1-\lambda_1^2{\sigma_{13}}^2)}\right)\left(1+\delta\mathcal{Z}_{13}(\lambda_1,\vec{x}_{13})\right), \quad (4.25)$$

$$\mathcal{Z}_{23}(\lambda_2,\vec{x}_{23}) = \frac{1}{\sqrt{1-\lambda_2^2\sigma_{23}^2}}\exp\left(\frac{\lambda_2^2\bar{\sigma}_{23}^2+\frac{1}{3}\lambda_2^3\langle(\Delta u_{23})^3\rangle_{\rm tree}}{2(1-\lambda_2^2{\sigma_{23}}^2)}\right)\left(1+\delta\mathcal{Z}_{23}(\lambda_2,\vec{x}_{23})\right), \quad (4.26)$$

$$\mathcal{Z}_{12}(\lambda_1,\vec{x}_{13},\vec{x}_{23}) = \frac{1}{\sqrt{1-\lambda_1^2\sigma_{12}^2}}\exp\left(\frac{\lambda_1^2\bar{\sigma}_{12}^2+\frac{1}{3}\lambda_1^3\langle(\Delta u_{12})^3\rangle_{\rm tree}}{2(1-\lambda_1^2{\sigma_{12}}^2)}\right)\times \left(1+\delta\mathcal{Z}_{12}(\lambda_1,\vec{x}_{13},\vec{x}_{23})\right). \quad (4.27)$$

where for Eqs. (4.25)-(4.27) we have defined:

$$\sigma_{13}^2 \equiv \langle[\Delta u_{13}]^2\rangle_{\rm 1L}+\langle[\Delta u_{13}]^2\rangle_{\rm vir}, \qquad \bar{\sigma}_{13}^2 \equiv \langle[\Delta u_{13}]^2\rangle_{\rm lin} \quad (4.28)$$

$$\sigma_{23}^2 \equiv \langle[\Delta u_{23}]^2\rangle_{\rm 1L}+\langle[\Delta u_{23}]^2\rangle_{\rm vir}, \qquad \bar{\sigma}_{23}^2 \equiv \langle[\Delta u_{23}]^2\rangle_{\rm lin} \quad (4.29)$$

$$\sigma_{12}^2 \equiv \langle[\Delta u_{12}]^2\rangle_{\rm 1L}+\langle[\Delta u_{12}]^2\rangle_{\rm vir}, \qquad \bar{\sigma}_{12}^2 \equiv \langle[\Delta u_{12}]^2\rangle_{\rm lin}\,. \quad (4.30)$$

Regarding Eq. (4.24), we first note that by squaring the equation $\Delta u_{12} = \Delta u_{13} - \Delta u_{23}$ one obtains:

$2\Delta u_{13}\Delta u_{23} = (\Delta u_{13})^2 + (\Delta u_{23})^2 - (\Delta u_{12})^2$ which implies:

$$(\lambda_1\Delta u_{13} + \lambda_2\Delta u_{23})^2 = (\lambda_1^2 + \lambda_1\lambda_2)(\Delta u_{13})^2 + (\lambda_2^2 + \lambda_1\lambda_2)(\Delta u_{23})^2 - \lambda_1\lambda_2(\Delta u_{12})^2\,. \tag{4.31}$$

This equation applies to both quadratic and linear velocity combinations in Eq. (4.23). Also, similar to what was done before, a similar shift can be performed for quadratic loop terms to promote them to the full 1-loop plus virial contributions. Taking all these into account, for Eq. (4.24) we have defined:

$$[\lambda_{123}\Delta u_{123}] \equiv \lambda_1\Delta u_{13} + \lambda_2\Delta u_{23} \tag{4.32}$$

$$[\lambda_{123}\ \sigma_{123}]^2 \equiv (\lambda_1^2 + \lambda_1\lambda_2)\sigma_{13}^2 + (\lambda_2^2 + \lambda_1\lambda_2)\sigma_{23}^2 - \lambda_1\lambda_2\sigma_{12}^2 \tag{4.33}$$

$$[\lambda_{123}\ \bar{\sigma}_{123}]^2 \equiv (\lambda_1^2 + \lambda_1\lambda_2)\bar{\sigma}_{13}^2 + (\lambda_2^2 + \lambda_1\lambda_2)\bar{\sigma}_{23}^2 - \lambda_1\lambda_2\bar{\sigma}_{12}^2\,. \tag{4.34}$$

where all σ_{mn}^2's and $\bar{\sigma}_{mn}^2$'s were defined in Eqs (4.28)-(4.30)

4.4 $\mathcal{Z}$-FUNCTIONS

Considering Eqs. (4.24)-(4.27), the contribution of $\delta(\vec{x})$'s to $\mathcal{Z}$-functions (initially defined in Eqs (4.4)-(4.7)) is packed up in the $\delta\mathcal{Z}$-functions. We aim to calculate these expressions up to 1-loop order. To show how calculations can be done, we can focus on one of the terms that appear in the expansion of Eq.(4.4), namely:

$$\mathcal{Z}_{123}^{(123)}(\lambda_1, \lambda_2, \vec{x}_{13}, \vec{x}_{23}) = \left\langle e^{\lambda_1\Delta u_{13}} e^{\lambda_2\Delta u_{23}} \delta(\vec{x}_1)\delta(\vec{x}_2)\delta(\vec{x}_3)\right\rangle. \tag{4.35}$$

We can re-write this expression as:

$$\mathcal{Z}_{123}^{(123)}(\lambda_1, \lambda_2, \vec{x}_{13}, \vec{x}_{23}) = \left[\frac{\partial}{\partial J_1}\frac{\partial}{\partial J_2}\frac{\partial}{\partial J_3}\left\langle e^{\lambda_1\Delta u_{13}} e^{\lambda_2\Delta u_{23}} e^{J_1\delta(\vec{x}_1)+J_2\delta(\vec{x}_2)+J_3\delta(\vec{x}_3)}\right\rangle\right]_{(J1\to 0,\ J2\to 0,\ J3\to 0)} \tag{4.36}$$

where we have introduced the J_i constants to move the δ's to the exponent. These will be set to zero at the end, reproducing the exact form of Eq. (4.35). Now we can follow, exactly, the same steps explained above for the calculations involving Δu's. In fact, δ's also have a perturbation theory expansion similar to (4.12). The only difference is that we should use slightly different expressions instead of w_k and $g_{\vec{k}_1,\vec{k}_2}$ to reflect their corresponding second order expansion in SPT. Also note that in the expansion of (4.12), $\theta_{\vec{k}} = \delta_{\vec{k}}$ as these are linear Gaussian fluctuations in SPT. Therefore, δ's are expanded in terms of the same Gaussian fields and all previous steps can be repeated with inclusion of δ's to obtain the expectation value in Eq. (4.36). Finally, we take derivatives with respect to J_i's and set the J_i's to zero at the end.

Below are the final results for $\delta\mathcal{Z}_{12}$, $\delta\mathcal{Z}_{13}$ and $\delta\mathcal{Z}_{23}$ ($\delta_a \equiv \delta(\vec{x}_a)$) [105]:

$$\begin{aligned}\delta\mathcal{Z}_{mn} \;=\; & \frac{\langle\delta_m\delta_n\rangle_{\rm lin} + L_{mn}(\lambda_m)\langle\delta_m\delta_n\rangle_{\rm 1L}}{1-\lambda_m^2\sigma_{mn}^2} \\ & +\lambda_m\frac{\langle\Delta u_{mn}(\delta_m+\delta_n)\rangle_{\rm lin} + L_{mn}(\lambda_m)\langle\Delta u_{mn}(\delta_m+\delta_n)\rangle_{\rm 1L} + \langle\Delta u_{mn}\delta_m\delta_n\rangle_{\rm tree}}{1-\lambda_m^2\sigma_{mn}^2} \\ & +\lambda_m^2\left[\frac{1}{2}\frac{\langle(\Delta u_{mn})^2(\delta_m+\delta_n)\rangle_{\rm tree}}{1-\lambda_m^2\sigma_{mn}^2} + \frac{\langle\Delta u_{mn}\delta_m\rangle_{\rm lin}\langle\Delta u_{mn}\delta_n\rangle_{\rm lin}}{(1-\lambda_m^2\sigma_{mn}^2)^2}\right]\end{aligned} \tag{4.37}$$

and for $\delta\mathcal{Z}_{123}$ we obtain:

$$\begin{aligned}
\delta\mathcal{Z}_{123} = &\left\{\frac{\langle(\lambda_{123}\Delta u_{123})(\delta_1+\delta_2+\delta_3)\rangle_{\rm lin} + L_{123}(\lambda_1,\lambda_2)\langle(\lambda_{123}\Delta u_{123})(\delta_1+\delta_2+\delta_3)\rangle_{\rm 1L}}{1-\left[\lambda_{123}\,\sigma_{123}\right]^2} + \right.\\
&\left.+\frac{1}{2}\frac{\langle(\lambda_{123}\Delta u_{123})^2(\delta_1+\delta_2+\delta_3)\rangle_{\rm tree}}{1-\left[\lambda_{123}\,\sigma_{123}\right]^2}\right\}+\left\{\frac{(\langle\delta_1\delta_2\rangle_{\rm lin}+{\rm cyc}) + L_{123}(\lambda_1,\lambda_2)(\langle\delta_1\delta_2\rangle_{\rm 1L}+{\rm cyc})}{1-\left[\lambda_{123}\,\sigma_{123}\right]^2} + \right.\\
&\left.+\frac{\langle(\lambda_{123}\Delta u_{123})\delta_1\delta_2\rangle_{\rm tree}+{\rm cyc}}{1-\left[\lambda_{123}\,\sigma_{123}\right]^2} + \frac{\langle(\lambda_{123}\Delta u_{123})\delta_1\rangle_{\rm lin}\langle(\lambda_{123}\Delta u_{123})\delta_2\rangle_{\rm lin}+{\rm cyc}}{(1-\left[\lambda_{123}\,\sigma_{123}\right]^2)^2}\right\}+\\
&+\left\{\frac{\langle\delta_1\delta_2\delta_3\rangle_{\rm tree}}{1-\left[\lambda_{123}\,\sigma_{123}\right]^2} + \frac{\langle(\lambda_{123}\Delta u_{123})\delta_1\rangle_{\rm lin}\langle\delta_2\delta_3\rangle_{\rm lin}+{\rm cyc}}{(1-\left[\lambda_{123}\,\sigma_{123}\right]^2)^2}\right.\\
&+\frac{(L_{123}(\lambda_1,\lambda_2)+2)(\langle\delta_1\delta_2\rangle_{\rm lin}\langle(\lambda_{123}\Delta u_{123})\delta_3\rangle_{\rm 1L}+{\rm cyc})}{(1-\left[\lambda_{123}\,\sigma_{123}\right]^2)^2} +\\
&+\frac{(L_{123}(\lambda_1,\lambda_2)+2)(\langle(\lambda_{123}\Delta u_{123})\delta_1\rangle_{\rm lin}\langle\delta_2\delta_3\rangle_{\rm 1L}+{\rm cyc})}{(1-\left[\lambda_{123}\,\sigma_{123}\right]^2)^2} +\\
&\frac{\langle(\lambda_{123}\Delta u_{123})\delta_1\rangle_{\rm lin}\langle\lambda_{123}\Delta u_{123}\delta_2\delta_3\rangle_{\rm tree}+{\rm cyc}}{(1-\left[\lambda_{123}\,\sigma_{123}\right]^2)^2}\\
&\left.+\frac{\langle\delta_1\delta_2\rangle_{\rm lin}\langle(\lambda_{123}\Delta u_{123})^2\delta_3\rangle_{\rm tree}+{\rm cyc}}{2(1-\left[\lambda_{123}\,\sigma_{123}\right]^2)^2} + \frac{\langle(\lambda_{123}\Delta u_{123})\delta_1\rangle_{\rm lin}\langle(\lambda_{123}\Delta u_{123})\delta_2\rangle_{\rm lin}\langle(\lambda_{123}\Delta u_{123})\delta_3\rangle_{\rm lin}}{(1-\left[\lambda_{123}\,\sigma_{123}\right]^2)^3}\right\},
\end{aligned} \tag{4.38}$$

where each "cyc" corresponds to cyclic permutations on δ_i's which adds two more terms to its preceding expression. Finally, the "loop factors" in the expressions above (Eqs. (4.37), (4.38)) are defined as:

$$L_{mn}(\lambda_m) \equiv 1 + \frac{\lambda_m^2\bar{\sigma}_{mn}^2}{1-\lambda_m^2\sigma_{mn}^2} + \frac{\lambda_m^3}{3}\frac{\langle(\Delta u_{mn})^3\rangle_{\rm tree}}{1-\lambda_m^2\sigma_{mn}^2}\,, \tag{4.39}$$

$$L_{123}(\lambda_1,\lambda_2) \equiv 1 + \frac{\left[\lambda_{123}\,\bar{\sigma}_{123}\right]^2}{1-\left[\lambda_{123}\,\sigma_{123}\right]^2} + \frac{\langle(\lambda_{123}\Delta u_{123})^3\rangle_{\rm tree}}{3(1-\left[\lambda_{123}\,\sigma_{123}\right]^2)}\,. \tag{4.40}$$

4.5 Tree level bispectrum at large separations

Starting from Eq. (4.3) and making use of definitions (4.24)-(4.27) with $\delta\mathcal{Z}$'s defined in Eqs (4.37) and (4.38), one can obtain an analytic relation for the bispectrum at large scales by calculating

most of the expectation values in standard perturbation theory. Exceptions are virial contributions and those terms in $\delta\mathcal{Z}$'s that are evaluated at the same position, e.g. $\langle\, \delta_m\, {u_m}^2 \rangle$. Regarding the virial velocity difference expectation values, like $\langle [\Delta u_{mn}]^2 \rangle_{\rm vir} = 2\langle u_m^2 \rangle_{\rm vir} + 2\langle u_m u_n \rangle_{\rm vir}$, one can ignore the cross term at large scales and only keep the constant contribution, i.e. $\langle u_m^2 \rangle_{\rm vir} = \langle u_n^2 \rangle_{\rm vir}$ which are expectation values at the same position [105]. Returning to Eq. (4.3), all terms except the first one give delta functions. Assuming $\vec{k}_1 \neq 0$ and $\vec{k}_2 \neq 0$, these terms vanish. Therefore, we only need to consider Eq. (4.24) with $\delta\mathcal{Z}_{123}$ defined in Eq. (4.38). First, using the definitions (4.28)-(4.30) and (4.32)-(4.34), the velocity difference generating function can be expanded as:

$$W_{123}(\lambda_1,\lambda_2,\vec{x}_{13},\vec{x}_{23}) = \frac{1}{\sqrt{1-[\lambda_{123}\,\sigma_{123}]^2}} \exp\left(\frac{[\lambda_{123}\,\bar{\sigma}_{123}]^2 + \frac{1}{3}\langle[\lambda_{123}\,\Delta u_{123}]^3\rangle_{\rm tree}}{2(1-[\lambda_{123}\,\sigma_{123}]^2)}\right) = \tag{4.41}$$
$$\frac{\exp\left(\frac{(\lambda_1^2+\lambda_2^2+\lambda_1\lambda_2)\sigma_v^2}{1-(\lambda_1^2+\lambda_2^2+\lambda_1\lambda_2)a_{\rm vir}^2}\right)}{\sqrt{1-(\lambda_1^2+\lambda_2^2+\lambda_1\lambda_2)a_{\rm vir}^2}}\Bigg[1 - \frac{(\lambda_1^2+\lambda_1\lambda_2)\langle u_1u_3\rangle_{\rm lin} + (\lambda_2^2+\lambda_1\lambda_2)\langle u_2u_3\rangle_{\rm lin} - \lambda_1\lambda_2\langle u_1u_2\rangle_{\rm lin}}{1-(\lambda_1^2+\lambda_2^2+\lambda_1\lambda_2)a_{\rm vir}^2}\Bigg(1 +$$
$$\frac{1}{6}\frac{\langle(\lambda_1\Delta u_{13}+\lambda_2\Delta u_{23})^3\rangle_{\rm tree}}{1-(\lambda_1^2+\lambda_2^2+\lambda_1\lambda_2)a_{\rm vir}^2}\Bigg) + \frac{\left((\lambda_1^2+\lambda_1\lambda_2)\langle u_1u_3\rangle_{\rm lin} + (\lambda_2^2+\lambda_1\lambda_2)\langle u_2u_3\rangle_{\rm lin} - \lambda_1\lambda_2\langle u_1u_2\rangle_{\rm lin}\right)^2}{2\left(1-(\lambda_1^2+\lambda_2^2+\lambda_1\lambda_2)a_{\rm vir}^2\right)^2} -$$
$$\frac{(\lambda_1^2+\lambda_1\lambda_2)\langle u_1u_3\rangle_{\rm 1L} + (\lambda_2^2+\lambda_1\lambda_2)\langle u_2u_3\rangle_{\rm 1L} - \lambda_1\lambda_2\langle u_1u_2\rangle_{\rm 1L}}{1-(\lambda_1^2+\lambda_2^2+\lambda_1\lambda_2)a_{\rm vir}^2}\Bigg(1 + \frac{2(\lambda_1^2+\lambda_2^2+\lambda_1\lambda_2)\sigma_v^2}{1-(\lambda_1^2+\lambda_2^2+\lambda_1\lambda_2)a_{\rm vir}^2} +$$
$$\frac{1}{2}\frac{\langle(\lambda_1\Delta u_{13}+\lambda_2\Delta u_{23})^3\rangle_{\rm tree}}{1-(\lambda_1^2+\lambda_2^2+\lambda_1\lambda_2)a_{\rm vir}^2}\Bigg) + \frac{1}{6}\frac{\langle(\lambda_1\Delta u_{13}+\lambda_2\Delta u_{23})^3\rangle_{\rm tree}}{1-(\lambda_1^2+\lambda_2^2+\lambda_1\lambda_2)a_{\rm vir}^2} + \ldots\Bigg]$$

where $\ldots$ corresponds to expressions that next-to-leading order and lead to $P_{\rm L}^3$ terms (cubic in linear power spectrum) in Fourier space which can be ignored for the tree-level bispectrum which is proportional to P_L^2 as is shown below. We also have defined:

$$a_{\rm vir}^2 \equiv 2\langle\, u^2\rangle_{\rm 1L} + 2\langle\, u^2\rangle_{\rm vir}, \qquad \sigma_v^2 \equiv \langle\, u^2\rangle_{\rm lin}\,. \tag{4.42}$$

Now, to find the corresponding $\mathcal{Z}_{123}$, one can insert this expansion into Eq. (4.24) and keep only the relevant terms for the tree-level bispectrum after multiplying by $\delta\mathcal{Z}$ from Eq. (4.38).

The final outcome *that leads to non-zero bispectrum* (after performing the integral of (4.3)) is:

$$\begin{aligned}
\mathcal{Z}_{123} = & \frac{\exp\left(\frac{(\lambda_1^2+\lambda_2^2+\lambda_1\lambda_2)\sigma_v^2}{1-(\lambda_1^2+\lambda_2^2+\lambda_1\lambda_2)a_{\rm vir}^2}\right)}{\left(1-(\lambda_1^2+\lambda_2^2+\lambda_1\lambda_2)a_{\rm vir}^2\right)^{3/2}}\Bigg[\langle\delta_1\delta_2\delta_3\rangle_{\rm tree}+\frac{1}{2}\langle(\lambda_{123}\Delta u_{123})^2(\delta_1+\delta_2+\delta_3)\rangle_{\rm tree}+\\
&(\langle(\lambda_{123}\Delta u_{123})\delta_1\delta_2\rangle_{\rm tree}+{\rm cyc})+\frac{1}{6}\langle(\lambda_1\Delta u_{13}+\lambda_2\Delta u_{23})^3\rangle_{\rm tree}+\\
&+\frac{\langle(\lambda_{123}\Delta u_{123})\delta_1\rangle_{\rm lin}\langle(\lambda_{123}\Delta u_{123})\delta_2\rangle_{\rm lin}+{\rm cyc}}{1-(\lambda_1^2+\lambda_2^2+\lambda_1\lambda_2)a_{\rm vir}^2}\\
&-\frac{(\lambda_1^2+\lambda_1\lambda_2)\langle u_1u_3\rangle_{\rm lin}+(\lambda_2^2+\lambda_1\lambda_2)\langle u_2u_3\rangle_{\rm lin}-\lambda_1\lambda_2\langle u_1u_2\rangle_{\rm lin}}{1-(\lambda_1^2+\lambda_2^2+\lambda_1\lambda_2)a_{\rm vir}^2}\times\\
&\Big(\langle(\lambda_{123}\Delta u_{123})(\delta_1+\delta_2+\delta_3)\rangle_{\rm lin}+(\langle\delta_1\delta_2\rangle_{\rm lin}+{\rm cyc})\Big)+\\
&\frac{\langle(\lambda_{123}\Delta u_{123})\delta_1\rangle_{\rm lin}\langle\delta_2\delta_3\rangle_{\rm lin}+{\rm cyc}}{1-(\lambda_1^2+\lambda_2^2+\lambda_1\lambda_2)a_{\rm vir}^2}+\\
&+\frac{\left((\lambda_1^2+\lambda_1\lambda_2)\langle u_1u_3\rangle_{\rm lin}+(\lambda_2^2+\lambda_1\lambda_2)\langle u_2u_3\rangle_{\rm lin}-\lambda_1\lambda_2\langle u_1u_2\rangle_{\rm lin}\right)^2}{2\left(1-(\lambda_1^2+\lambda_2^2+\lambda_1\lambda_2)a_{\rm vir}^2\right)}\Bigg]+C_{123}
\end{aligned}\tag{4.43}$$

with:

$$\begin{aligned}
C_{123} = & \frac{\exp\left(\frac{(\lambda_1^2+\lambda_2^2+\lambda_1\lambda_2)\sigma_v^2}{1-(\lambda_1^2+\lambda_2^2+\lambda_1\lambda_2)a_{\rm vir}^2}\right)}{\left(1-(\lambda_1^2+\lambda_2^2+\lambda_1\lambda_2)a_{\rm vir}^2\right)^{5/2}}(\langle u_z^2\delta\rangle)\Bigg[\frac{1}{6}\langle(\lambda_1\Delta u_{13}+\lambda_2\Delta u_{23})^3\rangle_{\rm tree}(\lambda_1^2+\lambda_2^2+\lambda_1\lambda_2)+\\
&\frac{\left((\lambda_1^2+\lambda_1\lambda_2)\langle u_1u_3\rangle_{\rm lin}+(\lambda_2^2+\lambda_1\lambda_2)\langle u_2u_3\rangle_{\rm lin}-\lambda_1\lambda_2\langle u_1u_2\rangle_{\rm lin}\right)^2}{2\left(1-(\lambda_1^2+\lambda_2^2+\lambda_1\lambda_2)a_{\rm vir}^2\right)}(\lambda_1^2+\lambda_2^2+\lambda_1\lambda_2)-\\
&\frac{(\lambda_1^2+\lambda_1\lambda_2)\langle u_1u_3\rangle_{\rm lin}+(\lambda_2^2+\lambda_1\lambda_2)\langle u_2u_3\rangle_{\rm lin}-\lambda_1\lambda_2\langle u_1u_2\rangle_{\rm lin}}{2\left(1-(\lambda_1^2+\lambda_2^2+\lambda_1\lambda_2)a_{\rm vir}^2\right)}\times\\
&\left((\lambda_1+\lambda_2)^2\langle\delta_1\delta_2\rangle_{\rm lin}+\lambda_2^2\langle\delta_1\delta_3\rangle_{\rm lin}+\lambda_1^2\langle\delta_2\delta_3\rangle_{\rm lin}\right)\Bigg]
\end{aligned}\tag{4.44}$$

which is the contribution to the tree level bispectrum that is generated by the constant expectation value $\langle u_z^2\delta\rangle$, the value of which is not necessarily well estimated in perturbation theory because it involves field products at the same location. Therefore, one can calculate its perturbation theory (PT) value and modulate it with a constant γ that encapsulates the deviations from that. One can also make judicious estimates of γ to appraise the upper bounds of this contribution.

The last step is to plug this result into Eq. (4.3) and take the Fourier integrals to obtain the bispectrum. For this stage, one can use the equations in Appendix B. The final result takes the relatively simple form:

$$
\begin{aligned}
B_s(\vec{k}_1,\vec{k}_2) &= \exp\left(\frac{-(k_1^2\mu_1^2+k_2^2\mu_2^2+k_1k_2\mu_1\mu_2)f^2\sigma_v^2}{1+(k_1^2\mu_1^2+k_2^2\mu_2^2+k_1k_2\mu_1\mu_2)f^2a_{\rm vir}^2}\right)\times \\
&\left\{\frac{2(1+f\mu_1^2)(1+f\mu_2^2)\left[F_2(\vec{k}_1,\vec{k}_2)+f\mu_{12}^2G_2(\vec{k}_1,\vec{k}_2)\right]P(k_1)P(k_2)+\text{cyc}}{\left(1+(k_1^2\mu_1^2+k_2^2\mu_2^2+k_1k_2\mu_1\mu_2)f^2a_{\rm vir}^2\right)^{3/2}}+\right. \\
&\left.\frac{(1+f\mu_1^2)(1+f\mu_2^2)f\left(k_1\mu_1+k_2\mu_2\right)\left[\frac{\mu_2}{k_2}(1+f\mu_1^2)+\frac{\mu_1}{k_1}(1+f\mu_2^2)\right]P(k_1)P(k_2)+\text{cyc}}{\left(1+(k_1^2\mu_1^2+k_2^2\mu_2^2+k_1k_2\mu_1\mu_2)f^2a_{\rm vir}^2\right)^{5/2}}\right\} \\
&+C(\vec{k}_1,\vec{k}_2)
\end{aligned}
\tag{4.45}
$$

with

$$
\begin{aligned}
C(\vec{k}_1,\vec{k}_2) &= \exp\left(\frac{-(k_1^2\mu_1^2+k_2^2\mu_2^2+k_1k_2\mu_1\mu_2)f^2\sigma_v^2}{1+(k_1^2\mu_1^2+k_2^2\mu_2^2+k_1k_2\mu_1\mu_2)f^2a_{\rm vir}^2}\right)(\langle u_z^2\delta\rangle)\times \\
&\left\{-\frac{2f^5G_2(\vec{k}_1,\vec{k}_2)\mu_{12}^2\mu_1^2\mu_2^2\left(k_1^2\mu_1^2+k_2^2\mu_2^2+k_1k_2\mu_1\mu_2\right)P(k_1)P(k_2)+\text{cyc}}{\left(1+(k_1^2\mu_1^2+k_2^2\mu_2^2+k_1k_2\mu_1\mu_2)f^2a_{\rm vir}^2\right)^{5/2}}\right. \\
&-\frac{\left(f^6\mu_1^3\mu_2^3\left(k_1\mu_1+k_2\mu_2\right)^2\left(\frac{k_1}{k_2}\mu_1^2+\frac{k_2}{k_1}\mu_2^2+\mu_1\mu_2\right)\right)P(k_1)P(k_2)+\text{cyc}}{\left(1+(k_1^2\mu_1^2+k_2^2\mu_2^2+k_1k_2\mu_1\mu_2)f^2a_{\rm vir}^2\right)^{7/2}} \\
&\left.-\frac{\left(\frac{1}{2}f^4\left(k_1\mu_1+k_2\mu_2\right)\left(k_1\mu_1^5+k_2\mu_2^5\right)\right)P(k_1)P(k_2)+\text{cyc}}{\left(1+(k_1^2\mu_1^2+k_2^2\mu_2^2+k_1k_2\mu_1\mu_2)f^2a_{\rm vir}^2\right)^{7/2}}\right\}
\end{aligned}
\tag{4.46}
$$

where $\mu_n \equiv \hat{k}_n\cdot\hat{z}$, $\mu_{12}\equiv(\vec{k}_1\cdot\hat{z}+\vec{k}_2\cdot\hat{z})/|\vec{k}_1+\vec{k}_2|$ and:

$$
F_2(\vec{k}_1,\vec{k}_2) = \frac{5}{7}+\frac{1}{2}(\hat{k}_1.\hat{k}_2)\left(\frac{k_1}{k_2}+\frac{k_2}{k_1}\right)+\frac{2}{7}(\hat{k}_1.\hat{k}_2)^2\,, \tag{4.47}
$$

$$
G_2(\vec{k}_1,\vec{k}_2) = \frac{3}{7}+\frac{1}{2}(\hat{k}_1.\hat{k}_2)\left(\frac{k_1}{k_2}+\frac{k_2}{k_1}\right)+\frac{4}{7}(\hat{k}_1.\hat{k}_2)^2 \tag{4.48}
$$

are second order SPT kernels.

4.6 Galaxy bispectrum

It is straightforward to extend previous results to include galaxy bias parameters. Relevant to the tree-level bispectrum, we consider the following second order bias expansion [49]:

$$\delta_g(\vec{x}) = b_1\delta(\vec{x}) + \frac{b_2}{2}\left(\delta^2(\vec{x}) - \langle\delta^2(\vec{x})\rangle\right) + \gamma_2\mathcal{G}_2(\Phi_v|\vec{x})\,. \tag{4.49}$$

Here $\mathcal{G}_2(\Phi_v|\vec{x})$ is the second-order Galileon arising from tidal effects, defined as:

$$\mathcal{G}_2(\Phi_v|\vec{x}) \equiv (\partial_i\partial_j\Phi_v)^2 - (\nabla^2\Phi_v)^2 \tag{4.50}$$

where $\nabla^2\Phi_v = \Theta$ with Θ being the velocity divergence. We can drop $\langle\delta^2(\vec{x})\rangle$ term as it has no contribution to the tree-level bispectrum as long as $\vec{k}_{1,2} \neq 0$. Therefore, Eq. (4.49) can be re-written as (up to second order):

$$\delta_g(\vec{x}) = b_1\int_{\vec{q}} e^{i\vec{q}.\vec{x}}\delta_{\rm L}(\vec{q}) + \int_{\vec{q}_1,\vec{q}_2} e^{i\vec{q}_{12}.\vec{x}}\left(b_1F_2(\vec{q}_1,\vec{q}_2) + \frac{b_2}{2} + \gamma_2K(\vec{q}_1,\vec{q}_2)\right)\delta_{\rm L}(\vec{q}_1)\delta_{\rm L}(\vec{q}_2) \tag{4.51}$$

with $K(\vec{q}_1,\vec{q}_2) \equiv (\hat{q}_1\cdot\hat{q}_2)^2 - 1$. Considering this equation and the fact that one needs to replace δ with δ_g in previous calculations, to obtain the galaxy bispectum, one can shift $F_2 \longrightarrow b_1F_2 + \frac{b_2}{2} + \gamma_2K$ in the previous dark matter expressions and also modify the linear contribution (related to the first term above) by including the linear bias coefficient, b_1, when necessary. Ignoring velocity

bias, the final results for galaxy versions of Eqs. (4.45) and (4.46) read:

$$
\begin{aligned}
&B_{g,s}(\vec{k}_1,\vec{k}_2) = \exp\left(\frac{-(k_1^2\mu_1^2+k_2^2\mu_2^2+k_1k_2\mu_1\mu_2)f^2\sigma_v^2}{1+(k_1^2\mu_1^2+k_2^2\mu_2^2+k_1k_2\mu_1\mu_2)f^2a_{\rm vir}^2}\right)\times \\
&\left\{\frac{2(b_1+f\mu_1^2)(b_1+f\mu_2^2)\left[b_1F_2(\vec{k}_1,\vec{k}_2)+\frac{b_2}{2}+\gamma_2K(\vec{k}_1,\vec{k}_2)+f\mu_{12}^2G_2(\vec{k}_1,\vec{k}_2)\right]P(k_1)P(k_2)+\text{cyc}}{\left(1+(k_1^2\mu_1^2+k_2^2\mu_2^2+k_1k_2\mu_1\mu_2)f^2a_{\rm vir}^2\right)^{3/2}}+\right. \\
&\left.\frac{(b_1+f\mu_1^2)(b_1+f\mu_2^2)f\,(k_1\mu_1+k_2\mu_2)\left[\frac{\mu_2}{k_2}(b_1+f\mu_1^2)+\frac{\mu_1}{k_1}(b_1+f\mu_2^2)\right]P(k_1)P(k_2)+\text{cyc}}{\left(1+(k_1^2\mu_1^2+k_2^2\mu_2^2+k_1k_2\mu_1\mu_2)f^2a_{\rm vir}^2\right)^{5/2}}\right\} \\
&+C_g(\vec{k}_1,\vec{k}_2)
\end{aligned}
\tag{4.52}
$$

with

$$
\begin{aligned}
&C_g(\vec{k}_1,\vec{k}_2) = \exp\left(\frac{-(k_1^2\mu_1^2+k_2^2\mu_2^2+k_1k_2\mu_1\mu_2)f^2\sigma_v^2}{1+(k_1^2\mu_1^2+k_2^2\mu_2^2+k_1k_2\mu_1\mu_2)f^2a_{\rm vir}^2}\right)(\langle u_z^2\delta_g\rangle)\times \\
&\left\{-\frac{2f^5G_2(\vec{k}_1,\vec{k}_2)\mu_{12}^2\mu_1^2\mu_2^2\left(k_1^2\mu_1^2+k_2^2\mu_2^2+k_1k_2\mu_1\mu_2\right)P(k_1)P(k_2)+\text{cyc}}{\left(1+(k_1^2\mu_1^2+k_2^2\mu_2^2+k_1k_2\mu_1\mu_2)f^2a_{\rm vir}^2\right)^{5/2}}\right. \\
&-\frac{\left(f^6\mu_1^3\mu_2^3\,(k_1\mu_1+k_2\mu_2)^2\left(\frac{k_1}{k_2}\mu_1^2+\frac{k_2}{k_1}\mu_2^2+\mu_1\mu_2\right)\right)P(k_1)P(k_2)+\text{cyc}}{\left(1+(k_1^2\mu_1^2+k_2^2\mu_2^2+k_1k_2\mu_1\mu_2)f^2a_{\rm vir}^2\right)^{7/2}} \\
&\left.-\frac{\left(\frac{b_1^2}{2}f^4\,(k_1\mu_1+k_2\mu_2)\left(k_1\mu_1^5+k_2\mu_2^5\right)\right)P(k_1)P(k_2)+\text{cyc}}{\left(1+(k_1^2\mu_1^2+k_2^2\mu_2^2+k_1k_2\mu_1\mu_2)f^2a_{\rm vir}^2\right)^{7/2}}\right\}
\end{aligned}
\tag{4.53}
$$

4.7 Galaxy bispectrum multipoles

The bispectrum in redshift space can be described by five parameters [106]. Three of these are triangle sides k_1 and k_2 and the angle between them, $\mu \equiv \hat{k}_1.\hat{k}_2$, which determine the triangle shapes (all triangles satisfy $\vec{k}_1+\vec{k}_2+\vec{k}_3=0$). The remaining two determine the orientation of triangles with respect to LOS. These can be defined as the angle between k_1 and LOS unit vector, $\cos\theta_1 \equiv \hat{k}_1.\hat{z}$, and the azimuthal angle ϕ that is formed by projections of $\vec{k}_2$ and $\hat{z}$ onto the

plane whose normal is $\hat{k}_1$. The latter implies that $\hat{k}_2.\hat{z} = \mu\cos\theta_1 + \sqrt{1-\mu^2}\sin\theta_1\cos\phi$. Considering this parametrization, the bispectrum in redshift space can be expanded as $B_{g,s}(\vec{k}_1,\vec{k}_2) = \sum_{\ell=0}^{\infty}\sum_{m=-\ell}^{\ell} B_{g,s}^{(\ell,m)}(k_1,k_2,\mu)Y_{\ell m}(\theta_1,\phi)$ which implies that "bispectrum multipoles" can be calculated from:

$$B_{g,s}^{(\ell,m)}(k_1,k_2,\mu) = \frac{(2\ell+1)}{4\pi}\int d\Omega_T B_{g,s}(\vec{k}_1,\vec{k}_2)Y_{\ell m}^{*}(\theta_1,\phi) \tag{4.54}$$

where $d\Omega_T \equiv d\cos\theta_1 d\phi$. For spherical harmonics, we use the convention:
$Y_\ell^m(\theta,\phi) = \sqrt{\frac{(\ell-m)!}{(\ell+m)!}}P_\ell^m(\cos\theta)e^{im\phi}$.

Below we show some plots of galaxy bispectrum multipoles pertaining to different bias parameters and triangle shapes. For nonlinear biases, we use the following relations to relate them to the linear bias coefficient [30, 5, 71, 49, 48]:

$$b_2 = 0.412 - 2.143\,b_1 + 0.929\,b_1^2 + 0.008b_1^3 + \frac{4}{3}\gamma_2\,, \tag{4.55}$$

$$\gamma_2 = -\frac{2}{7}(b_1 - 1)\,. \tag{4.56}$$

From Fig. 4.1, we can see that FoG effects become important at higher k's, as expected. This can be seen from the visible difference between the dashed and solid lines for the blue curves and also the curves on the right panel. All these curves correspond to triangles whose sides are $k_1 = 0.1$ h/Mpc and $k_2 = 0.01$ h/Mpc. On the other hand, the dashed and solid lines for the red curves (which corresponds to triangles with the sides $k_1 = 0.02$ h/Mpc and $k_1 = 0.01$ h/Mpc) are almost coincident. Also, as expected, these plots show that the effect of FoG is to weaken the bispectrum signal. Figure 4.2 shows that at higher k's the FoG can become so important that it can change the sign of quadrupole moment.

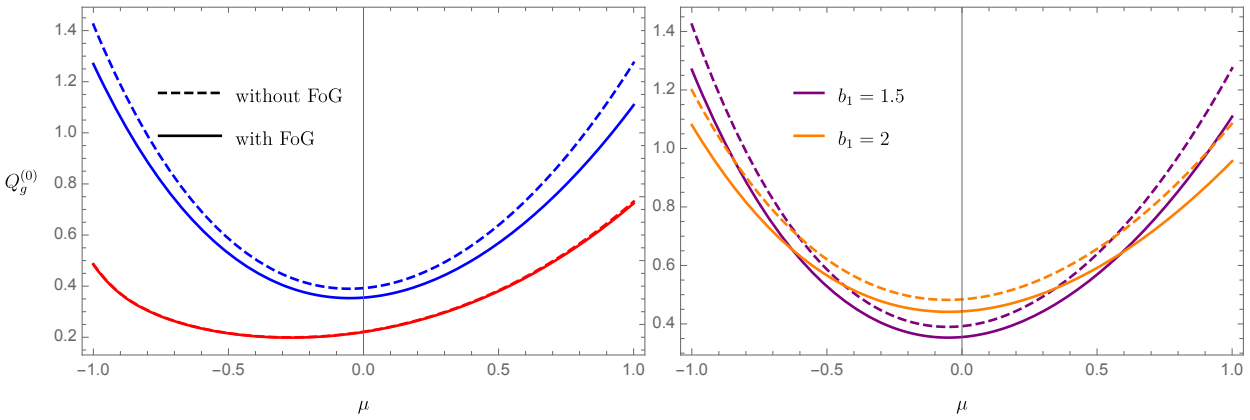

Figure 4.1: Plots of the normalized monopole of the galaxy bispectrum as a function of $\mu \equiv \hat{k}_1.\hat{k}_2$. Normalization is with respect to power spectrum monopoles, i.e $Q_g^{(0)} \equiv B_{g,s}^{(0,0)}(k_1, k_2, \mu)/(P_{g,s}^{(0)}(k_1)P_{g,s}^{(0)}(k_2) + \text{c.p.})$. On the left plot, red and blue colors correspond to triangles with $k_1 = 2k_2$ and $k_1 = 10k_2$ respectively with $k_2 = 0.01$ h/Mpc. Also $b_1 = 1.5$ for that plot. The right plot corresponds to ($k_1 = 10k_2, k_2 = 0.01$h/Mpc) triangles with different biases. For both plots b_2, γ_2 are calculated from (4.55),(4.56) and redshift is set to $z = 1$. At this redshift, we have $\sigma_v = 3.7$ Mpc/h and assume $a_{\text{vir}} = 3$ Mpc/h.

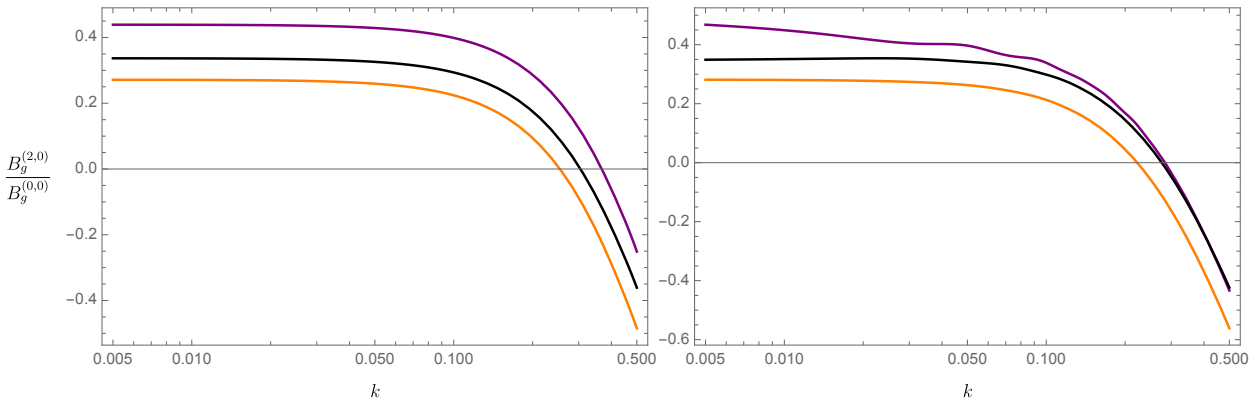

Figure 4.2: Quadrupole to monopole ratio for equilateral (left) and isosceles (right) triangles at $z = 1$. The latter corresponds to ($k_1 = k_2 \equiv k, \mu = 0$) triangles. In both panels, purple and orange curves correspond to $b_1 = 1.5$ and $b_1 = 2$ respectively. The black curve corresponds to $b_1 = 1$, $b_2 = \gamma_2 = 0$ (dark matter). Other parameters are similar to those in previous plots.

4.8 Tree-level bispectrum and comparison with N-body simulation results

To compare our tree-level galaxy bispectrum, Eq (4.52), with N-body simulation data, we use a sample of galaxies derived from Minerva N-body simulations [57], based on a halo occupation distribution model that mimics the CMASS BOSS galaxies [130]. Hereafter, we call these CMASS galaxies. These are a set of 300 realizations in a box of comoving volume $(1500\,\mathrm{Mpc/h})^3$. The CMASS galaxy biases are $b_1 = 2.022$, $b_2 = -0.2$ and $\gamma_2 = -0.46$. The redshift is $z = 0.57$. Also $\Omega_m = 0.285$ and $\Omega_\Lambda = 0.715$. Using these, we can calculate other cosmological parameters like the growth factor, f, which takes the value $f = 0.76$. Given the linear dark matter power spectrum, $P_L(k)$, used for the simulation, we can numerically calculate σ_v from (B.21):

$$\sigma_v^2 = \langle u^2 \rangle_{\rm lin} = \int_{\vec{q}} \frac{\mu_q^2}{q^2} P_{\rm L}(q) = \frac{4\pi}{3} \int_0^\infty dq P_L(q)\,. \tag{4.57}$$

To find $a_{\rm vir}$, we fit the monopole and quadrupole of the following FoG-corrected linear redshift space power spectrum (from [105]) :

$$P_{g,s}(k) = \frac{\exp\left(\frac{-f^2k^2\eta^2\sigma_v^2}{1+f^2k^2\eta^2a_{\rm vir}^2}\right)}{\left(1+f^2k^2\eta^2a_{\rm vir}^2\right)^{3/2}}(b_1^2 + 2fb_1\eta^2 + f^2\eta^4)P_L(k) \tag{4.58}$$

to their corresponding multipoles from the CMASS galaxy sample at linear scales, $k < 0.09\,\mathrm{h/Mpc}$. In this equation, $\eta \equiv \hat{k}.\hat{z}$ is the cosine of the angle between $\vec{k}$ and the line-of-sight. We obtain $\sigma_v = 4.59$ Mpc/h and find $a_{\rm vir} = 2.13$ Mpc/h from the fitting.

Figures 4.3-4.8 show comparisons between predictions for the monopole and quadrupole moments of the CMASS galaxy bispectrum for different triangle shapes obtained from our tree-level model, (4.52), with the corresponding values from the simulation. For these predictions we ig-

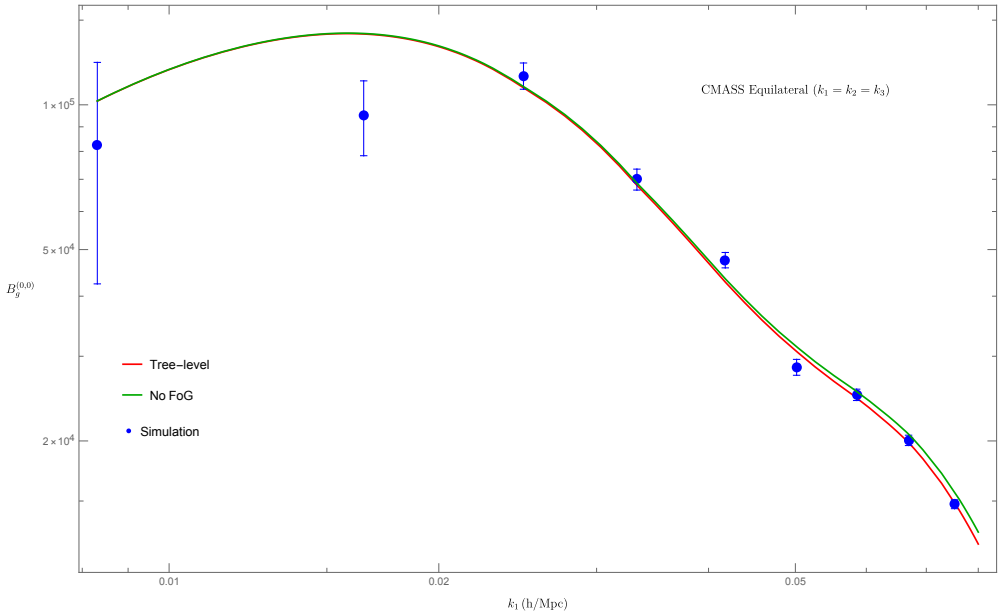

Figure 4.3: Galaxy bispectrum monopole for equilateral triangles . The red curve is the prediction of our tree-level bispectrum model and the green curve is the prediction of a tree-level bispectrum model with no FoG correction ($a_{\rm vir} = \sigma_v = 0$) . Blue points are the quadrupole values derived from the CMASS galaxy sample.

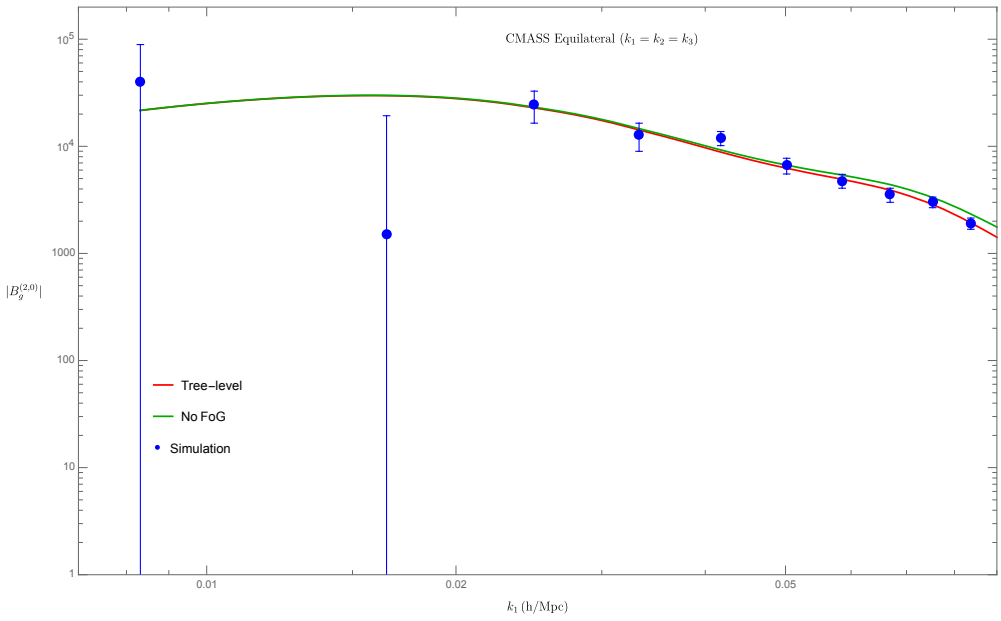

Figure 4.4: Galaxy bispectrum quadrupole for equilateral triangles . The red curve is the prediction of our tree-level bispectrum model and the green curve is the prediction of a tree-level bispectrum model with no FoG correction ($a_{\rm vir} = \sigma_v = 0$) . Blue points are the quadrupole values derived from the CMASS galaxy sample.

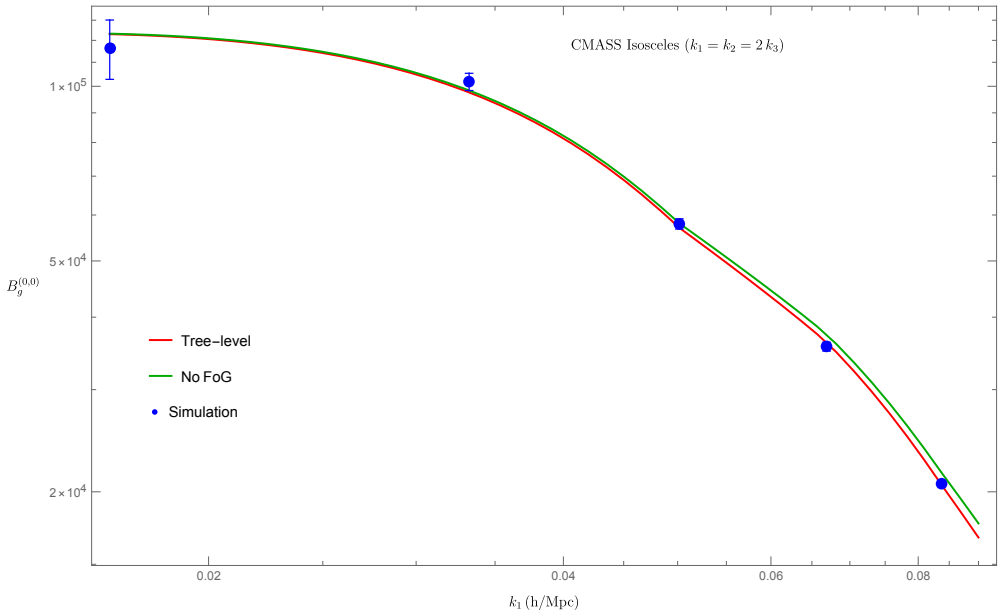

Figure 4.5: Galaxy bispectrum monopole for a set of isosceles triangles . The red curve is the prediction of our tree-level bispectrum model and the green curve is the prediction of a tree-level bispectrum model with no FoG correction ($a_{\rm vir} = \sigma_v = 0$) . Blue points are the monopole values derived from the CMASS galaxy sample.

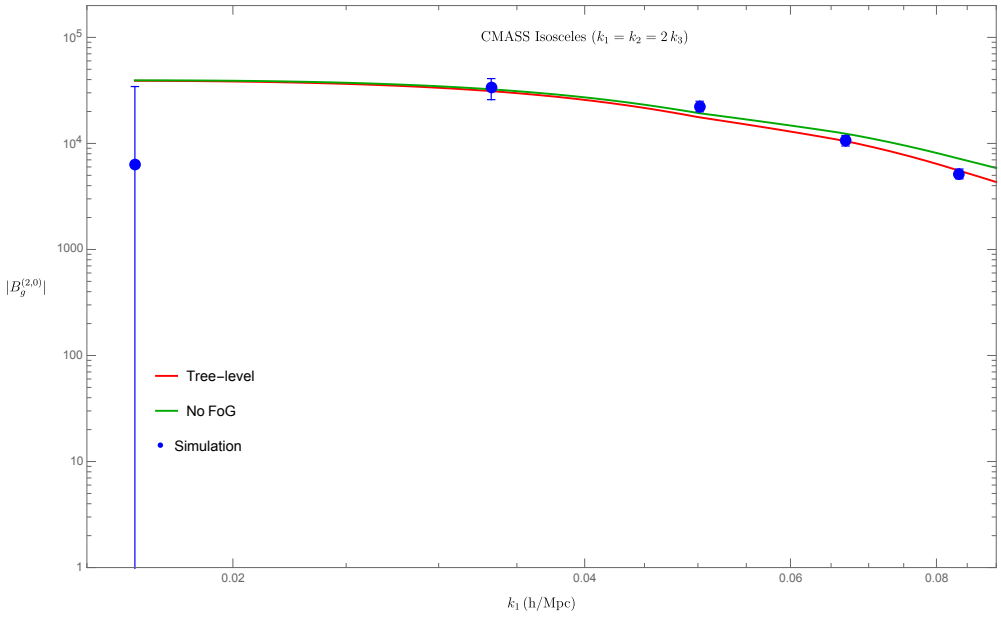

Figure 4.6: Galaxy bispectrum quadrupole for a set of isosceles triangles . The red curve is the prediction of our tree-level bispectrum model and the green curve is the prediction of a tree-level bispectrum model with no FoG correction ($a_{\rm vir} = \sigma_v = 0$) . Blue points are the quadrupole values derived from the CMASS galaxy sample.

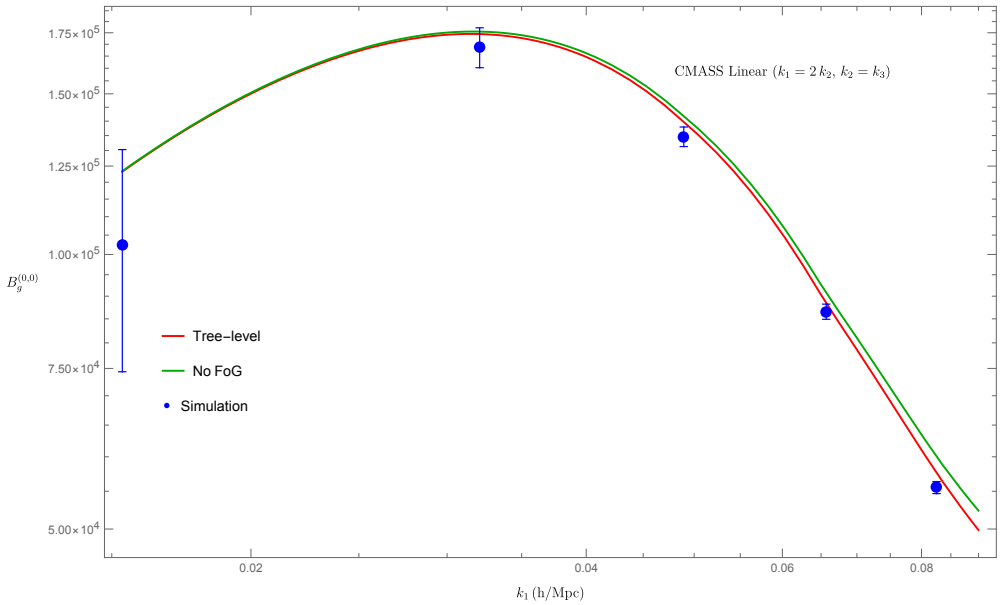

Figure 4.7: Galaxy bispectrum monopole for a set of linear triangles ($\hat{k}_1 \cdot \hat{k}_2 = \pi$). The red curve is the prediction of our tree-level bispectrum model and the green curve is the prediction of a tree-level bispectrum model with no FoG correction ($a_{\rm vir} = \sigma_v = 0$) . Blue points are the monopole values derived from the CMASS galaxy sample.

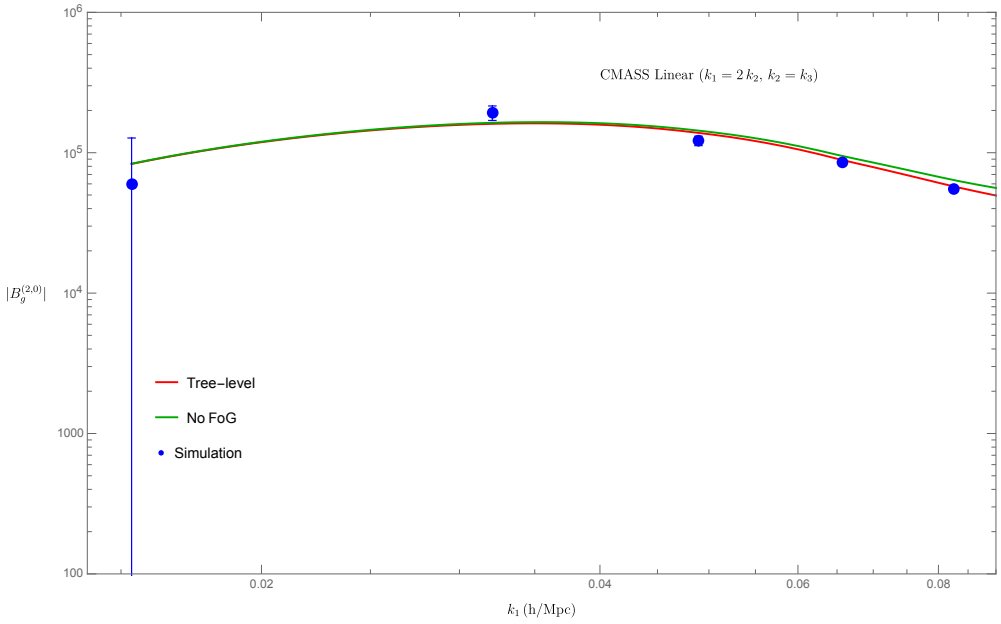

Figure 4.8: Galaxy bispectrum quadrupole for a set of linear triangles ($\hat{k}_1 \cdot \hat{k}_2 = \pi$). The red curve is the prediction of our tree-level bispectrum model and the green curve is the prediction of a tree-level bispectrum model with no FoG correction ($a_{\rm vir} = \sigma_v = 0$) . Blue points are the quadrupole values derived from the CMASS galaxy sample.

nored $C_g(\vec{k}_1, \vec{k}_2)$ in (4.52) as it had negligible contribution. We also compare similar predictions from a tree-level bispectrum model with no FoG correction, i.e. $a_{\rm vir} = \sigma_v = 0$ in (4.52), with simulation results. Here we have limited the comparisons to $k_1 < 0.09$ h/Mpc because at higher k_1's nonlinear effects become important and tree-level bispectrum alone is not suitable for those scales. We discuss this in the next section. We can see from all of the plots that as we approach higher values of k_1 (smaller scales), FoG corrections become more important and our tree-level model performs better compared to a model with no FoG.

4.9 Beyond tree-level bispectrum and comparison with N-body simulation results

To improve the result obtained in Eq (4.52), one can go beyond the tree level approximation to include some of the "1-loop" bispectrum corrections that we already neglected. These contributions can be obtained from multiplying (4.41) with (4.38), as we did before, but this time keeping higher order terms that involve more powers of density fluctuation or velocity fields. For example, two leading contributions of this kind are the following:

$$-\frac{\exp\left(\frac{(\lambda_1^2+\lambda_2^2+\lambda_1\lambda_2)\sigma_v^2}{1-(\lambda_1^2+\lambda_2^2+\lambda_1\lambda_2)a_{\rm vir}^2}\right)}{\left(1-(\lambda_1^2+\lambda_2^2+\lambda_1\lambda_2)a_{\rm vir}^2\right)^{5/2}} \left[\left((\lambda_1^2+\lambda_1\lambda_2)\langle u_1u_3\rangle_{\rm lin}+(\lambda_2^2+\lambda_1\lambda_2)\langle u_2u_3\rangle_{\rm lin}-\lambda_1\lambda_2\langle u_1u_2\rangle_{\rm lin}\right)\times \langle\delta_{g,1}\delta_{g,2}\delta_{g,3}\rangle_{\rm tree}\right], \tag{4.59}$$

$$-\frac{\exp\left(\frac{(\lambda_1^2+\lambda_2^2+\lambda_1\lambda_2)\sigma_v^2}{1-(\lambda_1^2+\lambda_2^2+\lambda_1\lambda_2)a_{\rm vir}^2}\right)}{\left(1-(\lambda_1^2+\lambda_2^2+\lambda_1\lambda_2)a_{\rm vir}^2\right)^{7/2}} \left[\left((\lambda_1^2+\lambda_1\lambda_2)\langle u_1u_3\rangle_{\rm lin}+(\lambda_2^2+\lambda_1\lambda_2)\langle u_2u_3\rangle_{\rm lin}-\lambda_1\lambda_2\langle u_1u_2\rangle_{\rm lin}\right)\times \left(\langle\lambda_{123}\Delta u_{123}\delta_{g,1}\rangle_{\rm lin}\langle\delta_{g,2}\delta_{g,3}\rangle_{\rm lin}+{\rm cyc}\right)\right]. \tag{4.60}$$

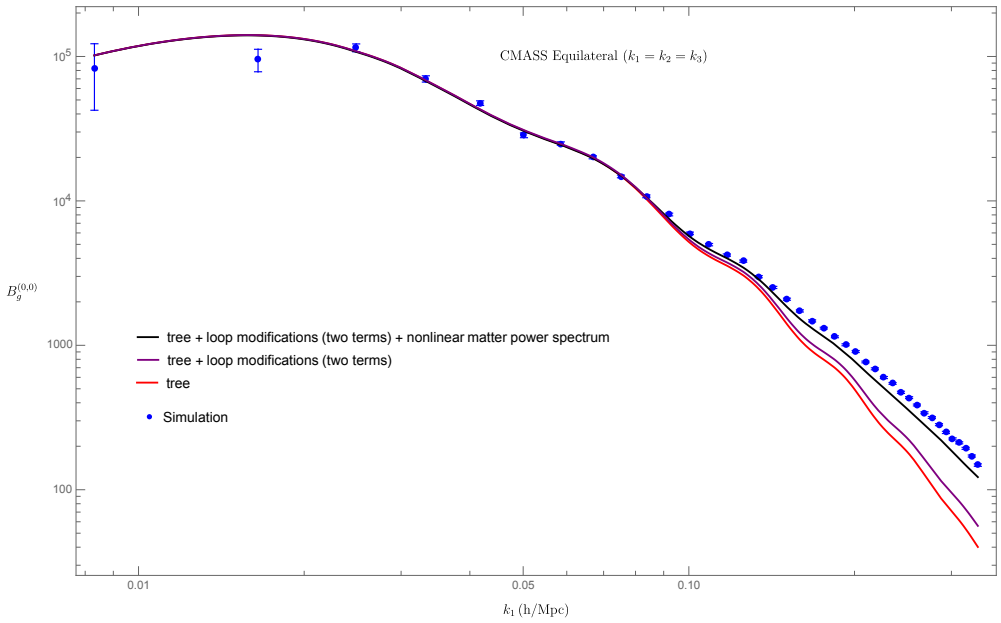

Figure 4.9: The bispectrum monopole for equilateral triangles predicted from our improved model (black curve), compared with the simulation data.

These two contributions have terms that are proportional to b_1^3 and we know that linear bias, b_1, is greater than one for many galaxy samples, including for the CMASS galaxies introduced in the previous section. We add these two expressions to the tree-level galaxy bispectrum that we already obtained and, for these two terms, we neglect b_2 and γ_2 biases as they are small compared to b_1 for CMASS galaxies. Finally, to approximately include nonlinear bispectrum contributions from merely the nonlinear evolution of the density fluctuations, we replace $P_{\rm lin}(k)$ with $P_{\text{1-loop}}(k)$ in Eq (4.52).

Figures 4.9 and 4.10 show a comparison between predictions of our improved galaxy bispectrum model with simulation results for CMASS galaxies introduced in the previous section, for two triangle configurations, equilateral ($k_1 = k_2 = k_3$) and isosceles ($k_1 = k_2 = 2k_3$). The red lines show the prediction of the tree-level bispectrum from Eq (4.52) (again neglecting $C_g(\vec{k}_1, \vec{k}_2)$). The purple lines show how the prediction alters when we add the higher order corrections (4.59) and (4.60) (for the isosceles case we only added (4.59) as the other terms had negligible contribution). Finally, the black line shows the prediction when the replacement ($P_{\rm lin}(k) \longrightarrow P_{\text{1-loop}}(k)$) is also

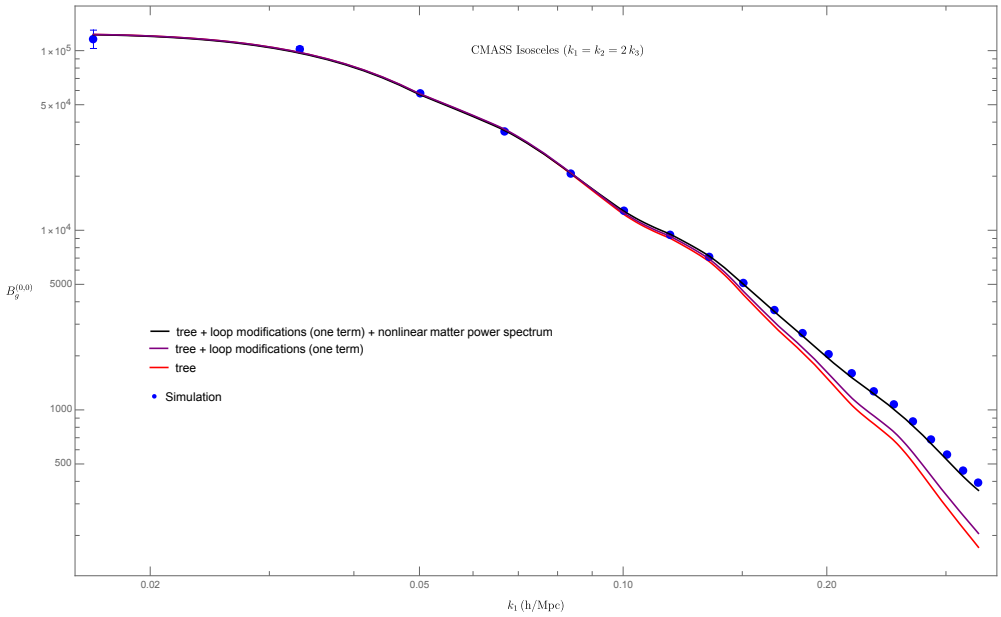

Figure 4.10: The bispectrum monopole for isosceles triangles predicted from our improved model (black curve), compared with the simulation data.

implemented in the tree level galaxy bispectrum of Eq (4.52) . It is worth noting that the small gap between the black line and simulation points in Fig. 4.9 further shrinks when we add more higher order terms.

These results show that simple improvements in our bispectrum model, to include nonlinear contributions, can lead to significantly more accurate predictions in the quasi-linear regime. It is worth reminding that our bispectrum model only depends on one free parameter, $a_{\rm vir}$, which can be constrained by fitting the redshift space power spectrum to the corresponding data, as we did here.

5 | Conclusions

In this thesis, in Chapters 2 and 3, we presented a simple analytic perturbative calculation of wide-angle and inverse-distance corrections for galaxy clustering statistics. Also, a simple procedure is provided for calculation of the evolution of fluctuations in a relativistic context. At linear level, we computed wide-angle corrections to multipoles of the galaxy power spectrum and compared these with relativistic contributions in the linear case. Figs 2.2 and 2.3 show examples of such comparisons. These show that wide-angle effects are as important as relativistic effects and their relative dominance depends on the details of the galaxy sample.

In addition, we calculated wide-angle and inverse-distance corrections (which are of the same order as local (non-integrated) relativistic corrections) to multipoles of the galaxy power spectrum in the weakly nonlinear regime (1-loop in SPT) and showed that nonlinear effects change the relative magnitude of corrections only on scales $k \gtrsim 0.1$ h/Mpc where loop effects start becoming important (see right panels in Fig. 2.5). This result implies that the mixing between nonlinear and wide-angle/relativistic effects can be ignored. Similarly, the mixing between wide-angle/relativistic corrections and FoG effects at large scales is small, as shown in Fig. 2.6.

In general, the relative sizes of all these corrections are small at $k \gtrsim 0.01h$/Mpc. Therefore, we can conclude that the plane-parallel approximation remains a valid procedure for the power spectrum at these scales as long as we are not able to resolve well-below sub-percent uncertainties. However, at large scales, wide-angle and relativistic effects can become a contaminant for local $f_{\rm NL}$ measurements because all three have similar scaling. Figure 2.4 shows an estimate of

how large this contamination can be as a function of magnification bias.

For the power spectrum case, because of parity invariance and our symmetric choice of the line of sight and the fact that we studied autocorrelations, i.e $\langle \delta_g \delta_g \rangle$, we did not find any imaginary contribution to multipoles due to parity invariance. However, this is not true in the case of cross correlations [78, 54]. In those situations, the perturbative method developed here can be used for an efficient analytic evaluation of wide-angle corrections to the power spectrum multipoles.

In Chapter 3, we extended the method to compare wide-angle effects on multipoles of the galaxy bispectrum. For the imaginary (odd-parity) case (see Fig. 3.2 for two examples), we estimated the signal-to-noise ratio based on forecast parameters of Euclid and DESI surveys (Fig. 3.3). We conclude that wide-angle effects are as important as relativistic contributions (more important in many cases) and should not be neglected if these signals are going to be used to constrain large-scale gravity. For even multipoles, Fig. 3.4, the same conclusion is true but signals are much less important because their ratio to cosmic variance is much smaller compared to similar ratios for plane parallel multipoles. Also we can conclude that assuming the plane-parallel approximation should not be a significant problem for local $f_{\rm NL}$ measurements from the galaxy bispectrum until $\Delta f_{\rm NL} \sim 1$ is reached (Fig. 3.5).

Some possible extensions of this work are worth mentioning. In this work we neglected window effects for simplicity. In general, as discussed in Section 2.6, the results obtained here can be windowed by convolution (see Eq. (2.4)). The actual mask usually has a complicated behavior depending on the geometry of the survey volume at a given redshift bin. In addition, the range of k-modes that we are interested in makes a difference in how important these effects are. For example, multipoles of the window function itself can mix up with those of power spectrum or bispectrum and cause contamination. However, for $k \geqslant 0.01$ h/Mpc, these window multipoles should not be that important (see for example [126] for a discussion on this). Nonetheless, a more realistic comparison of observationally measured and calculated multipoles requires a detailed understanding of window function for a given survey (see e.g. [14] for a detailed calculation of

window effects and their mixings with wide-angle effects in linear theory). In this work, we also assumed a uniform selection function which can be the most important source of systematic error as it limits the amount of accessible information on galaxy number density contrasts. This is, however, highly dependent on the specific survey under consideration.

Despite our simplifications, these generic conclusions are expected to apply to more realistic galaxy survey settings: 1) use of the plane-parallel galaxy power spectrum (including nonlinear corrections) is justified provided we add deviations from it in linear theory (as in Eq. (2.99)), 2) deviations from the plane-parallel approximation for the galaxy bispectrum induce imaginary contributions that are important at large scales when compared to relativistic effects. 3) wide-angle and relativistic effects can mimic "fake" local primordial non-Gaussianity parameter, $f_{\rm NL}$, with magnitudes that are of order a few for power spectrum and of order one for bispectrum.

Finally, In Chapter 4, we provided a simple model for the galaxy bispectrum at redshift space that incorporates Fingers-of-God effects and includes non-linearities in a simple manner. We showed, by comparison to the simulation results, that the model fits relatively well to the data at quasi-linear scales. The model has only one free parameter that can be obtained by fitting the redshift space power spectrum to data. This adds to the simplicity of the bispectrum model we introduced here. The results obtained here can be used for the analysis of the galaxy bispectrum in recent and upcoming surveys. There has been a previous work [101] where authors have used similar dispersion factors for FoG that depend on a single parameter ($a_{\rm vir}$) for the power spectrum analysis of the clustering data. Similar analyses can be done with the model provided here for the galaxy bispectrum.

A | Appendix I: Redshift Space Kernels

Here we derive the RSD PT kernels including wide-angle and inverse-distance corrections. The starting point is Eq. (2.10), which can be rewritten by expanding the exponential as,

$$\delta_s(\vec{k}) = \sum_{m=1}^{\infty} \frac{(f\mu_x(\vec{k})k)^{m-1}}{(m-1)!} \int_{\vec{x},\vec{p}_1\ldots\vec{p}_m} e^{i(\vec{p}_1+\ldots+\vec{p}_m-\vec{k})\cdot\vec{x}} \left[\delta(\vec{p}_1) + \frac{f\mu_x(\vec{k})k}{m}\frac{\mu_x(\vec{p}_1)}{p_1}\Theta(\vec{p}_1)\right] \times$$
$$\frac{\mu_x(\vec{p}_2)}{p_2}\Theta(\vec{p}_2)\ldots\frac{\mu_x(\vec{p}_m)}{p_m}\Theta(\vec{p}_m) \tag{A.1}$$

where $\mu_x(\vec{q}) \equiv (\hat{q}\cdot\hat{x})$ and we have assumed no velocity bias and vorticity, $\vec{u}_g(\vec{k}) = \vec{u}(\vec{k}) = -i\vec{k}\Theta(\vec{k})/k^2$. To find the RSD kernels, we must expand δ_s in terms of linear fluctuations $\delta_{\rm lin}(\vec{q})$, as usual this is done through the PT expansion for the δ and Θ fields, namely

$$\delta(\vec{k}) = \sum_{n=1}^{\infty} \int_{\vec{q}_1\ldots\vec{q}_n} \delta_D(\vec{k}-\vec{q}_1-\ldots-\vec{q}_n)\, F_n(\vec{q}_1,\ldots,\vec{q}_n)\, \delta_{\rm lin}(\vec{q}_1)\ldots\delta_{\rm lin}(\vec{q}_n) \tag{A.2}$$

$$\Theta(\vec{k}) = \sum_{n=1}^{\infty} \int_{\vec{q}_1\ldots\vec{q}_n} \delta_D(\vec{k}-\vec{q}_1-\ldots-\vec{q}_n)\, G_n(\vec{q}_1,\ldots,\vec{q}_n)\, \delta_{\rm lin}(\vec{q}_1)\ldots\delta_{\rm lin}(\vec{q}_n) \tag{A.3}$$

Using these in Eq. (A.1) and collecting terms with a given power of $\delta_{\rm lin}$ gives the RSD kernels $\widetilde{Z}_n$

$$\delta_s(\vec{k}) = \sum_{n=1}^{\infty} \int_{\vec{q}_1\ldots\vec{q}_n} \widetilde{Z}_n(\vec{k};\vec{q}_1,\ldots,\vec{q}_n)\, \delta_{\rm lin}(\vec{q}_1)\ldots\delta_{\rm lin}(\vec{q}_n) \tag{A.4}$$

where

$$\widetilde{Z}_n(\vec{k};\vec{q}_1,\ldots,\vec{q}_n) \equiv \int_{\vec{x}} \mathrm{e}^{-i(\vec{k}-\vec{q}_1-\ldots-\vec{q}_n)\cdot\vec{x}} \sum_{m=1}^{n} \frac{(f\mu_x(\vec{k})k)^{m-1}}{(m-1)!} \sum_{\substack{n_1=1 \\ n_1+\ldots+n_m=n}}^{n} \cdots \sum_{n_m=1}^{n} \Big[F_{n_1} + \frac{f\mu_x(\vec{k})k}{m} \frac{\mu_x(\vec{q}^{(n_1)})}{q^{(n_1)}} G_{n_1} \Big] \frac{\mu_x(\vec{q}^{(n_2)})}{q^{(n_2)}} G_{n_2} \cdots \frac{\mu_x(\vec{q}^{(n_m)})}{q^{(n_m)}} G_{n_m} \tag{A.5}$$

where e.g. F_{n_1} depends on the first n_1 momenta $\vec{q}_1,\ldots,\vec{q}_{n_1}$, G_{n_2} depends on the next n_2 momenta, etc, and $\vec{q}^{(n_1)}$ denotes the partial sum over the first n_1 momenta $\vec{q}^{(n_1)} \equiv \vec{q}_1 + \ldots + \vec{q}_{n_1}$, $\vec{q}^{(n_2)}$ denotes the partial sum over the next n_2 momenta, and so on. Note that if we put the observer at infinity, we recover the plane-parallel approximation recursion relations for the kernels. Indeed, then the LOS is fixed (e.g. $\mu_x(\vec{k}) \to \hat{\vec{k}} \cdot \hat{z}$) and the integral over $\vec{x}$ gives the usual momentum conserving delta function (as in Eqs. A.2-A.3) expected from the translation invariance of the plane-parallel case, thus $\widetilde{Z}_n = \delta_D(\vec{k} - \vec{q}_1 - \ldots - \vec{q}_n)\, Z_n$ with Z_n the usual RSD kernels in the plane-parallel approximation [106].

It is worth considering how this situation looks like in configuration space. Replacing the dummy integration variable $\vec{x}$ by $\vec{x}'$ in Eq. (A.5), we can write the Fourier transform of Eq. (A.4) as,

$$\delta_s(\vec{x}) = \sum_{n=1}^{\infty} \int_{\vec{x}',\vec{q}_1\ldots\vec{q}_n} \mathrm{e}^{i(\vec{q}_1+\ldots+\vec{q}_n)\cdot\vec{x}'} \Bigg\{ \sum_{m=1}^{n} \frac{(f\mu_{x'}(\vec{k})k)^{m-1}}{(m-1)!} \sum_{\substack{n_1=1 \\ n_1+\ldots+n_m=n}}^{n} \cdots \sum_{n_m=1}^{n} \Big[F_{n_1} + \frac{f\mu_{x'}(\vec{k})k}{m} \frac{\mu_{x'}(\vec{q}^{(n_1)})}{q^{(n_1)}} G_{n_1} \Big] \times \frac{\mu_{x'}(\vec{q}^{(n_2)})}{q^{(n_2)}} G_{n_2} \cdots \frac{\mu_{x'}(\vec{q}^{(n_m)})}{q^{(n_m)}} G_{n_m} \Bigg\}_{\vec{k}=-i\nabla} \times (2\pi)^3 \delta_D(\vec{x}-\vec{x}')\, \delta_{\rm lin}(\vec{q}_1)\ldots\delta_{\rm lin}(\vec{q}_n) \tag{A.6}$$

Now, the result of integrating over $\vec{x}'$ is to take derivatives of the plane wave and the object $\{\}$ with respect to $\vec{x}'$ and evaluate in $\vec{x}' = \vec{x}$. When the gradient operator acts only on the plane wave,

it just corresponds to replacing $\vec{k}$ by $\vec{q}_1 + \ldots + \vec{q}_n$ inside {}, i.e. it corresponds to the plane-parallel kernels where the LOS is set to be $\hat{x}$. If these are expanded about a fixed direction, it generates the wide-angle corrections. When at least one gradient operator acts on {}, derivatives of the unit vectors inside $\mu_{x'}$ generate inverse-distance terms (see Eq. 2.13), leading to the other set of corrections to the plane-parallel results. This means we can write,

$$\delta_s(\vec{x}) = \sum_{n=1}^{\infty} \int_{\vec{q}_1 \ldots \vec{q}_n} \mathrm{e}^{i(\vec{q}_1 + \ldots + \vec{q}_n)\cdot\vec{x}}\, Z_n^{\hat{x}}(\vec{q}_1, \ldots, \vec{q}_n)\, \delta_{\rm lin}(\vec{q}_1) \ldots \delta_{\rm lin}(\vec{q}_n)$$
$$+\text{inverse} - \text{distance corrections} \tag{A.7}$$

where $Z_n^{\hat{x}}$ denotes the plane-parallel RSD PT kernels where the fixed LOS is replaced by $\hat{x}$. This result was used in [118] to calculate the impact of the LOS variation in long-wavelength modes on the power spectrum covariance matrix.

B Appendix II: "Building Block" Correlation Functions in Perturbation Theory

Below are various two- and three-point functions (in PT), necessary for evaluation of expressions in Eqs. (4.37) and (4.38). Throughout the calculations, we use $\vec{x}_{mn} \equiv \vec{x}_m - \vec{x}_n$ (as before) and $\vec{q}_{abc\ldots} \equiv \vec{q}_a + \vec{q}_b + \vec{q}_c + \ldots$ (for momentum vectors) and, in this appendix, we have $\mu_n \equiv \hat{q}_n \cdot \hat{z}$. Also $P_{\rm L}$ is the linear matter power spectrum, $P_{\rm lin}$ and F and G functions are SPT kernels for matter and velocity divergence fluctuations respectively.

$$\langle \delta_m \delta_n \rangle_{\rm lin} = \int_{\vec{q}_1} e^{i\vec{q}_1.\vec{x}_{mn}} P_{\rm L}(q_1)\,, \tag{B.1}$$

$$\langle \delta_m \delta_n \rangle_{\rm 1L} = \int_{\vec{q}_1} e^{i\vec{q}_1.\vec{x}_{mn}} \Bigg[2 \int_{\vec{q}_2} F_2(\vec{q}_1 - \vec{q}_2, \vec{q}_2)^2 P_{\rm L}(|\vec{q}_1 - \vec{q}_2|) P_{\rm L}(q_2) \tag{B.2}$$

$$+6 P_{\rm L}(q_1) \int_{\vec{q}_2} F_3(\vec{q}_1, -\vec{q}_2, \vec{q}_2) P_{\rm L}(q_2) \Bigg]$$

$$\langle \Delta u_{mn} (\delta_m + \delta_n) \rangle_{\rm lin} = 2 \int_{\vec{q}_1} e^{i\vec{q}_1.\vec{x}_{mn}} \frac{(-i\mu_1)}{q_1} P_{\rm L}(q_1) \tag{B.3}$$

$$\langle \Delta u_{mn}(\delta_m+\delta_n)\rangle_{1\mathrm{L}} = 2\int_{\vec{q}_1} e^{i\vec{q}_1.\vec{x}_{mn}}\frac{(-i\mu_1)}{q_1}\Bigg[2\int_{\vec{q}_2} F_2(\vec{q}_1-\vec{q}_2,\vec{q}_2)G_2(\vec{q}_1-\vec{q}_2,\vec{q}_2)P_{\mathrm{L}}(|\vec{q}_1-\vec{q}_2|)P_{\mathrm{L}}(q_2)$$

$$+3P_{\mathrm{L}}(q_1)\int_{\vec{q}_2}\big(F_3(\vec{q}_1,-\vec{q}_2,\vec{q}_2)+G_3(\vec{q}_1,-\vec{q}_2,\vec{q}_2)\big)P_{\mathrm{L}}(q_2)\Bigg] \tag{B.4}$$

$$\langle \Delta u_{mn}\delta_m\delta_n\rangle_{\mathrm{tree}} = 2\int_{\vec{q}_1,\vec{q}_2} e^{i\vec{q}_1.\vec{x}_{mn}}\left[2\frac{i\mu_2}{q_2}F_2(\vec{q}_1,\vec{q}_2)-2\frac{i\mu_{12}}{q_{12}}G_2(\vec{q}_1,\vec{q}_2)\right]P_{\mathrm{L}}(q_1)P_{\mathrm{L}}(q_2)$$

$$+4\int_{\vec{q}_1,\vec{q}_2} e^{i\vec{q}_{12}.\vec{x}_{mn}}\frac{(-i\mu_1)}{q_1}F_2(\vec{q}_1,\vec{q}_2)P_{\mathrm{L}}(q_1)P_{\mathrm{L}}(q_2)\,, \tag{B.5}$$

$$\langle(\Delta u_{mn})^2(\delta_m+\delta_n)\rangle_{\mathrm{tree}} = \int_{\vec{q}_1,\vec{q}_2} e^{i\vec{q}_1.\vec{x}_{mn}}\left[\frac{8\mu_1\mu_2}{q_1q_2}F_2(\vec{q}_1,\vec{q}_2)+8(\frac{\mu_2}{q_2}-\frac{\mu_1}{q_1})\frac{\mu_{12}}{q_{12}}G_2(\vec{q}_1,\vec{q}_2)\right]\times$$

$$P_{\mathrm{L}}(q_1)P_{\mathrm{L}}(q_2)+\int_{\vec{q}_1,\vec{q}_2} e^{i\vec{q}_{12}.\vec{x}_{mn}}\left[-\frac{4\mu_1\mu_2}{q_1q_2}F_2(\vec{q}_1,\vec{q}_2)-\frac{8\mu_1\mu_{12}}{q_1q_{12}}G_2(\vec{q}_1,\vec{q}_2)\right]P_{\mathrm{L}}(q_1)P_{\mathrm{L}}(q_2) \tag{B.6}$$

$$+2\left\langle\,\delta_m u_m^2\right\rangle,$$

$$\langle\Delta u_{mn}\delta_m\rangle_{\mathrm{lin}}\langle\Delta u_{mn}\delta_n\rangle_{\mathrm{lin}} = -\int_{\vec{q}_1,\vec{q}_2} e^{i\vec{q}_{12}.\vec{x}_{mn}}\frac{\mu_1\mu_2}{q_1q_2}P_{\mathrm{L}}(q_1)P_{\mathrm{L}}(q_2)\,, \tag{B.7}$$

$$\langle\lambda_{123}\Delta u_{123}\delta_1\rangle_{\mathrm{lin}} = \lambda_2\int_{\vec{q}_1} e^{i\vec{q}_1.\vec{x}_{12}}\frac{i\mu_1}{q_1}P_{\mathrm{L}}(q_1)-(\lambda_1+\lambda_2)\int_{\vec{q}_1} e^{i\vec{q}_1.\vec{x}_{13}}\frac{i\mu_1}{q_1}P_{\mathrm{L}}(q_1)\,, \tag{B.8}$$

$$\langle\lambda_{123}\Delta u_{123}\delta_2\rangle_{\mathrm{lin}} = -\lambda_1\int_{\vec{q}_1} e^{i\vec{q}_1.\vec{x}_{12}}\frac{i\mu_1}{q_1}P_{\mathrm{L}}(q_1)-(\lambda_1+\lambda_2)\int_{\vec{q}_1} e^{i\vec{q}_1.\vec{x}_{23}}\frac{i\mu_1}{q_1}P_{\mathrm{L}}(q_1)\,, \tag{B.9}$$

$$\langle\lambda_{123}\Delta u_{123}\delta_3\rangle_{\mathrm{lin}} = -\lambda_1\int_{\vec{q}_1} e^{i\vec{q}_1.\vec{x}_{13}}\frac{i\mu_1}{q_1}P_{\mathrm{L}}(q_1)-\lambda_2\int_{\vec{q}_1} e^{i\vec{q}_1.\vec{x}_{23}}\frac{i\mu_1}{q_1}P_{\mathrm{L}}(q_1)\,, \tag{B.10}$$

$$\langle\lambda_{123}\Delta u_{123}\delta_1\rangle_{1\mathrm{L}} = \lambda_2\int_{\vec{q}_1} e^{i\vec{q}_1.\vec{x}_{12}}\frac{i\mu_1}{q_1}\Bigg[2\int_{\vec{q}_2} F_2(\vec{q}_1-\vec{q}_2,\vec{q}_2)G_2(\vec{q}_1-\vec{q}_2,\vec{q}_2)P_{\mathrm{L}}(|\vec{q}_1-\vec{q}_2|)P_{\mathrm{L}}(q_2)$$

$$+3P_{\mathrm{L}}(q_1)\int_{\vec{q}_2}\big(F_3(\vec{q}_1,-\vec{q}_2,\vec{q}_2)+G_3(\vec{q}_1,-\vec{q}_2,\vec{q}_2)\big)P_{\mathrm{L}}(q_2)\Bigg] - (\lambda_1+\lambda_2)\int_{\vec{q}_1} e^{i\vec{q}_1.\vec{x}_{13}}\frac{i\mu_1}{q_1}\times \tag{B.11}$$

$$\Bigg[2\int_{\vec{q}_2} F_2(\vec{q}_1-\vec{q}_2,\vec{q}_2)G_2(\vec{q}_1-\vec{q}_2,\vec{q}_2)P_{\mathrm{L}}(|\vec{q}_1-\vec{q}_2|)P_{\mathrm{L}}(q_2) + 3P_{\mathrm{L}}(q_1)\int_{\vec{q}_2}\big(F_3(\vec{q}_1,-\vec{q}_2,\vec{q}_2)$$

$$+G_3(\vec{q}_1,-\vec{q}_2,\vec{q}_2)\big)P_{\mathrm{L}}(q_2)\Bigg],$$

$$\langle\lambda_{123}\Delta u_{123}\delta_2\rangle_{1\mathrm{L}} = -\lambda_1\int_{\vec{q}_1} e^{i\vec{q}_1.\vec{x}_{12}}\frac{i\mu_1}{q_1}\Bigg[2\int_{\vec{q}_2} F_2(\vec{q}_1-\vec{q}_2,\vec{q}_2)G_2(\vec{q}_1-\vec{q}_2,\vec{q}_2)P_{\mathrm{L}}(|\vec{q}_1-\vec{q}_2|)P_{\mathrm{L}}(q_2)$$

$$+3P_{\mathrm{L}}(q_1)\int_{\vec{q}_2}\big(F_3(\vec{q}_1,-\vec{q}_2,\vec{q}_2)+G_3(\vec{q}_1,-\vec{q}_2,\vec{q}_2)\big)P_{\mathrm{L}}(q_2)\Bigg] - (\lambda_1+\lambda_2)\int_{\vec{q}_1} e^{i\vec{q}_1.\vec{x}_{23}}\frac{i\mu_1}{q_1}\times \tag{B.12}$$

$$\Bigg[2\int_{\vec{q}_2} F_2(\vec{q}_1-\vec{q}_2,\vec{q}_2)G_2(\vec{q}_1-\vec{q}_2,\vec{q}_2)P_{\mathrm{L}}(|\vec{q}_1-\vec{q}_2|)P_{\mathrm{L}}(q_2) + 3P_{\mathrm{L}}(q_1)\int_{\vec{q}_2}\big(F_3(\vec{q}_1,-\vec{q}_2,\vec{q}_2)$$

$$+G_3(\vec{q}_1,-\vec{q}_2,\vec{q}_2)\big)P_{\mathrm{L}}(q_2)\Bigg]$$

$$\langle\lambda_{123}\Delta u_{123}\delta_3\rangle_{1\mathrm{L}} = -\lambda_1\int_{\vec{q}_1} e^{i\vec{q}_1.\vec{x}_{13}}\frac{i\mu_1}{q_1}\Bigg[2\int_{\vec{q}_2} F_2(\vec{q}_1-\vec{q}_2,\vec{q}_2)G_2(\vec{q}_1-\vec{q}_2,\vec{q}_2)P_{\mathrm{L}}(|\vec{q}_1-\vec{q}_2|)P_{\mathrm{L}}(q_2)$$

$$+3P_{\mathrm{L}}(q_1)\int_{\vec{q}_2}\big(F_3(\vec{q}_1,-\vec{q}_2,\vec{q}_2)+G_3(\vec{q}_1,-\vec{q}_2,\vec{q}_2)\big)P_{\mathrm{L}}(q_2)\Bigg] - \lambda_2\int_{\vec{q}_1} e^{i\vec{q}_1.\vec{x}_{23}}\frac{i\mu_1}{q_1}\times \tag{B.13}$$

$$\Bigg[2\int_{\vec{q}_2} F_2(\vec{q}_1-\vec{q}_2,\vec{q}_2)G_2(\vec{q}_1-\vec{q}_2,\vec{q}_2)P_{\mathrm{L}}(|\vec{q}_1-\vec{q}_2|)P_{\mathrm{L}}(q_2) + 3P_{\mathrm{L}}(q_1)\int_{\vec{q}_2}\big(F_3(\vec{q}_1,-\vec{q}_2,\vec{q}_2)$$

$$+G_3(\vec{q}_1,-\vec{q}_2,\vec{q}_2)\big)P_{\mathrm{L}}(q_2)\Bigg]$$

$$\langle(\lambda_{123}\Delta u_{123})^2\delta_1\rangle_{\rm tree}=$$
$$\int\limits_{\vec{q}_1,\vec{q}_2} e^{i\vec{q}_1.\vec{x}_{12}}\left[4\lambda_2^2\frac{\mu_2\mu_{12}}{q_2q_{12}}G_2(\vec{q}_1,\vec{q}_2)+4\lambda_1\lambda_2\left(\frac{i\mu_2}{q_2}F_2(\vec{q}_1,\vec{q}_2)-\frac{i\mu_{12}}{q_{12}}G_2(\vec{q}_1,\vec{q}_2)\right)\right]P_{\rm L}(q_1)P_{\rm L}(q_2)$$
$$+\int\limits_{\vec{q}_1,\vec{q}_2} e^{i\vec{q}_{12}.\vec{x}_{12}}\left[-2\lambda_2^2\frac{\mu_1\mu_2}{q_1q_2}F_2(\vec{q}_1,\vec{q}_2)-4\lambda_1\lambda_2\frac{i\mu_1}{q_1}F_2(\vec{q}_1,\vec{q}_2)\right]P_{\rm L}(q_1)P_{\rm L}(q_2) \tag{B.14}$$
$$+\int\limits_{\vec{q}_1,\vec{q}_2} e^{i\vec{q}_1.\vec{x}_{13}}\left[4(\lambda_1+\lambda_2)^2\frac{\mu_2\mu_{12}}{q_2q_{12}}G_2(\vec{q}_1,\vec{q}_2)+4\lambda_1(\lambda_1+\lambda_2)\left(-\frac{i\mu_2}{q_2}F_2(\vec{q}_1,\vec{q}_2)+\frac{i\mu_{12}}{q_{12}}G_2(\vec{q}_1,\vec{q}_2)\right)\right]\times$$
$$P_{\rm L}(q_1)P_{\rm L}(q_2)+\int\limits_{\vec{q}_1,\vec{q}_2} e^{i\vec{q}_{12}.\vec{x}_{13}}\left[-2(\lambda_1+\lambda_2)^2\frac{\mu_1\mu_2}{q_1q_2}F_2(\vec{q}_1,\vec{q}_2)+4\lambda_1(\lambda_1+\lambda_2)\frac{i\mu_1}{q_1}F_2(\vec{q}_1,\vec{q}_2)\right]\times$$
$$P_{\rm L}(q_1)P_{\rm L}(q_2)-2\lambda_2(\lambda_1+\lambda_2)\int\limits_{\vec{q}_1,\vec{q}_2} e^{i\vec{q}_1.\vec{x}_{13}}e^{i\vec{q}_2.\vec{x}_{23}}\frac{\mu_2\mu_{12}}{q_2q_{12}}\Big[2G_2(\vec{q}_1,\vec{q}_2)P_{\rm L}(q_1)P_{\rm L}(q_2)$$
$$+2G_2(\vec{q}_1,-\vec{q}_{12})P_{\rm L}(q_1)P_{\rm L}(q_{12})+2F_2(\vec{q}_2,-\vec{q}_{12})P_{\rm L}(q_2)P_{\rm L}(q_{12})\Big]+\lambda_1^2\langle\,\delta_1u_1^2\rangle\,,$$
$$\langle(\lambda_{123}\Delta u_{123})^2\delta_2\rangle_{\rm tree}=$$
$$\int\limits_{\vec{q}_1,\vec{q}_2} e^{i\vec{q}_1.\vec{x}_{12}}\left[4\lambda_1^2\frac{\mu_2\mu_{12}}{q_2q_{12}}G_2(\vec{q}_1,\vec{q}_2)+4\lambda_1\lambda_2\left(-\frac{i\mu_2}{q_2}F_2(\vec{q}_1,\vec{q}_2)+\frac{i\mu_{12}}{q_{12}}G_2(\vec{q}_1,\vec{q}_2)\right)\right]P_{\rm L}(q_1)P_{\rm L}(q_2)$$
$$+\int\limits_{\vec{q}_1,\vec{q}_2} e^{i\vec{q}_{12}.\vec{x}_{12}}\left[-2\lambda_1^2\frac{\mu_1\mu_2}{q_1q_2}F_2(\vec{q}_1,\vec{q}_2)+4\lambda_1\lambda_2\frac{i\mu_1}{q_1}F_2(\vec{q}_1,\vec{q}_2)\right]P_{\rm L}(q_1)P_{\rm L}(q_2) \tag{B.15}$$
$$+\int\limits_{\vec{q}_1,\vec{q}_2} e^{i\vec{q}_1.\vec{x}_{23}}\left[4(\lambda_1+\lambda_2)^2\frac{\mu_2\mu_{12}}{q_2q_{12}}G_2(\vec{q}_1,\vec{q}_2)+4\lambda_2(\lambda_1+\lambda_2)\left(-\frac{i\mu_2}{q_2}F_2(\vec{q}_1,\vec{q}_2)+\frac{i\mu_{12}}{q_{12}}G_2(\vec{q}_1,\vec{q}_2)\right)\right]\times$$
$$P_{\rm L}(q_1)P_{\rm L}(q_2)+\int\limits_{\vec{q}_1,\vec{q}_2} e^{i\vec{q}_{12}.\vec{x}_{23}}\left[-2(\lambda_1+\lambda_2)^2\frac{\mu_1\mu_2}{q_1q_2}F_2(\vec{q}_1,\vec{q}_2)+4\lambda_2(\lambda_1+\lambda_2)\frac{i\mu_1}{q_1}F_2(\vec{q}_1,\vec{q}_2)\right]\times$$
$$P_{\rm L}(q_1)P_{\rm L}(q_2)-2\lambda_1(\lambda_1+\lambda_2)\int\limits_{\vec{q}_1,\vec{q}_2} e^{i\vec{q}_1.\vec{x}_{13}}e^{i\vec{q}_2.\vec{x}_{23}}\frac{\mu_1\mu_{12}}{q_1q_{12}}\Big[2G_2(\vec{q}_1,\vec{q}_2)P_{\rm L}(q_1)P_{\rm L}(q_2)$$
$$+2F_2(\vec{q}_1,-\vec{q}_{12})P_{\rm L}(q_1)P_{\rm L}(q_{12})+2G_2(\vec{q}_2,-\vec{q}_{12})P_{\rm L}(q_2)P_{\rm L}(q_{12})\Big]+\lambda_2^2\langle\,\delta_2u_2^2\rangle\,,$$

$$\langle(\lambda_{123}\Delta u_{123})^2\delta_3\rangle_{\rm tree} =$$

$$\int_{\vec{q}_1,\vec{q}_2} e^{i\vec{q}_1.\vec{x}_{13}}\Big[4\lambda_1^2\big(\frac{\mu_1\mu_2}{q_1q_2}F_2(\vec{q}_1,\vec{q}_2)+(\frac{\mu_2}{q_2}-\frac{\mu_1}{q_1})\frac{\mu_{12}}{q_{12}}G_2(\vec{q}_1,\vec{q}_2)\big)+4\lambda_1\lambda_2\big(\frac{\mu_1\mu_2}{q_1q_2}F_2(\vec{q}_1,\vec{q}_2)$$

$$-\frac{\mu_1\mu_{12}}{q_1q_{12}}G_2(\vec{q}_1,\vec{q}_2)\big)\Big]P_{\rm L}(q_1)P_{\rm L}(q_2)-\int_{\vec{q}_1,\vec{q}_2} e^{i\vec{q}_{12}.\vec{x}_{13}}\Big[2\lambda_1^2\big(\frac{\mu_1\mu_2}{q_1q_2}F_2(\vec{q}_1,\vec{q}_2)+2\frac{\mu_1\mu_{12}}{q_1q_{12}}G_2(\vec{q}_1,\vec{q}_2)\big)$$

$$+4\lambda_1\lambda_2\frac{\mu_1\mu_{12}}{q_1q_{12}}G_2(\vec{q}_1,\vec{q}_2)\Big]P_{\rm L}(q_1)P_{\rm L}(q_2)+\int_{\vec{q}_1,\vec{q}_2} e^{i\vec{q}_1.\vec{x}_{23}}\Big[4\lambda_2^2\big(\frac{\mu_1\mu_2}{q_1q_2}F_2(\vec{q}_1,\vec{q}_2) \tag{B.16}$$

$$+(\frac{\mu_2}{q_2}-\frac{\mu_1}{q_1})\frac{\mu_{12}}{q_{12}}G_2(\vec{q}_1,\vec{q}_2)\big)+4\lambda_1\lambda_2\big(\frac{\mu_1\mu_2}{q_1q_2}F_2(\vec{q}_1,\vec{q}_2)-\frac{\mu_1\mu_{12}}{q_1q_{12}}G_2(\vec{q}_1,\vec{q}_2)\big)\Big]P_{\rm L}(q_1)P_{\rm L}(q_2)$$

$$-\int_{\vec{q}_1,\vec{q}_2} e^{i\vec{q}_{12}.\vec{x}_{23}}\Big[2\lambda_2^2\big(\frac{\mu_1\mu_2}{q_1q_2}F_2(\vec{q}_1,\vec{q}_2)+2\frac{\mu_1\mu_{12}}{q_1q_{12}}G_2(\vec{q}_1,\vec{q}_2)\big)+4\lambda_1\lambda_2\frac{\mu_1\mu_{12}}{q_1q_{12}}G_2(\vec{q}_1,\vec{q}_2)\Big]P_{\rm L}(q_1)P_{\rm L}(q_2)$$

$$-2\lambda_1\lambda_2\int_{\vec{q}_1,\vec{q}_2} e^{i\vec{q}_1.\vec{x}_{13}}e^{i\vec{q}_2.\vec{x}_{23}}\frac{\mu_1\mu_2}{q_1q_2}\Big[2F_2(\vec{q}_1,\vec{q}_2)P_{\rm L}(q_1)P_{\rm L}(q_2)+2G_2(\vec{q}_1,-\vec{q}_{12})P_{\rm L}(q_1)P_{\rm L}(q_{12})$$

$$+2G_2(\vec{q}_2,-\vec{q}_{12})P_{\rm L}(q_2)P_{\rm L}(q_{12})\Big]+(\lambda_1+\lambda_2)^2\langle\,\delta_3u_3^2\rangle\,,$$

$$\langle\lambda_{123}\Delta u_{123}\delta_1\delta_2\rangle_{\rm tree} =$$

$$2(\lambda_1-\lambda_2)\int_{\vec{q}_1,\vec{q}_2} e^{i\vec{q}_1.\vec{x}_{12}}\Big[\frac{i\mu_2}{q_2}F_2(\vec{q}_1,\vec{q}_2)-\frac{i\mu_{12}}{q_{12}}G_2(\vec{q}_1,\vec{q}_2)\Big]P_{\rm L}(q_1)P_{\rm L}(q_2) \tag{B.17}$$

$$-2(\lambda_1-\lambda_2)\int_{\vec{q}_1,\vec{q}_2} e^{i\vec{q}_{12}.\vec{x}_{12}}\frac{i\mu_1}{q_1}F_2(\vec{q}_1,\vec{q}_2)P_{\rm L}(q_1)P_{\rm L}(q_2)-(\lambda_1+\lambda_2)\int_{\vec{q}_1,\vec{q}_2} e^{i\vec{q}_1.\vec{x}_{13}}e^{i\vec{q}_2.\vec{x}_{23}}\frac{i\mu_{12}}{q_{12}}\times$$

$$\Big[2G_2(\vec{q}_1,\vec{q}_2)P_{\rm L}(q_1)P_{\rm L}(q_2)+2F_2(\vec{q}_1,-\vec{q}_{12})P_{\rm L}(q_1)P_{\rm L}(q_{12})+2F_2(\vec{q}_2,-\vec{q}_{12})P_{\rm L}(q_2)P_{\rm L}(q_{12})\Big]$$

$$\langle \lambda_{123}\Delta u_{123}\delta_1\delta_3\rangle_{\rm tree} =$$

$$2(2\lambda_1+\lambda_2)\int_{\vec{q}_1,\vec{q}_2} e^{i\vec{q}_1.\vec{x}_{13}}\left[\frac{i\mu_2}{q_2}F_2(\vec{q}_1,\vec{q}_2)-\frac{i\mu_{12}}{q_{12}}G_2(\vec{q}_1,\vec{q}_2)\right]P_{\rm L}(q_1)P_{\rm L}(q_2) \tag{B.18}$$

$$-2(2\lambda_1+\lambda_2)\int_{\vec{q}_1,\vec{q}_2} e^{i\vec{q}_{12}.\vec{x}_{13}}\frac{i\mu_1}{q_1}F_2(\vec{q}_1,\vec{q}_2)P_{\rm L}(q_1)P_{\rm L}(q_2)-\lambda_2\int_{\vec{q}_1,\vec{q}_2} e^{i\vec{q}_1.\vec{x}_{13}}e^{i\vec{q}_2.\vec{x}_{23}}\frac{i\mu_2}{q_2}\times$$

$$\left[2F_2(\vec{q}_1,\vec{q}_2)P_{\rm L}(q_1)P_{\rm L}(q_2)+2G_2(\vec{q}_1,-\vec{q}_{12})P_{\rm L}(q_1)P_{\rm L}(q_{12})+2F_2(\vec{q}_2,-\vec{q}_{12})P_{\rm L}(q_2)P_{\rm L}(q_{12})\right]$$

$$\langle \lambda_{123}\Delta u_{123}\delta_2\delta_3\rangle_{\rm tree} = 2(2\lambda_2+\lambda_1)\int_{\vec{q}_1,\vec{q}_2} e^{i\vec{q}_1.\vec{x}_{23}}\left[\frac{i\mu_2}{q_2}F_2(\vec{q}_1,\vec{q}_2)-\frac{i\mu_{12}}{q_{12}}G_2(\vec{q}_1,\vec{q}_2)\right]P_{\rm L}(q_1)P_{\rm L}(q_2)$$

$$-2(2\lambda_2+\lambda_1)\int_{\vec{q}_1,\vec{q}_2} e^{i\vec{q}_{12}.\vec{x}_{23}}\frac{i\mu_1}{q_1}F_2(\vec{q}_1,\vec{q}_2)P_{\rm L}(q_1)P_{\rm L}(q_2)-\lambda_1\int_{\vec{q}_1,\vec{q}_2} e^{i\vec{q}_1.\vec{x}_{13}}e^{i\vec{q}_2.\vec{x}_{23}}\frac{i\mu_1}{q_1}\times \tag{B.19}$$

$$\left[2F_2(\vec{q}_1,\vec{q}_2)P_{\rm L}(q_1)P_{\rm L}(q_2)+2F_2(\vec{q}_1,-\vec{q}_{12})P_{\rm L}(q_1)P_{\rm L}(q_{12})+2G_2(\vec{q}_2,-\vec{q}_{12})P_{\rm L}(q_2)P_{\rm L}(q_{12})\right].$$

The last expectation value in Eqs. (B.6) and (B.14)-(B.16) can be written as $\langle\,\delta(x)\,u_z(x)^2\rangle = \gamma\langle\,\delta(x)\,u_z(x)^2\rangle_{\rm PT}$ where $\langle\,...\rangle_{\rm PT}$ is its value in perturbation theory:

$$\langle\,\delta(x)\,u_z(x)^2\rangle_{\rm PT} = \int_{\vec{q}_1,\vec{q}_2}\left[-2\frac{\mu_1\mu_2}{q_1q_2}F_2(\vec{q}_1,\vec{q}_2)+4\frac{\mu_1\mu_{12}}{q_1q_{12}}G_2(\vec{q}_1,\vec{q}_2)\right]P_{\rm L}(q_1)P_{\rm L}(q_2) \tag{B.20}$$

and γ parameterizes any deviation from that. In general, the contribution of this term to the bispectrum is tiny even if γ is $O(10)$.

Finally, we need to calculate expectation values involving merely velocities which appear in velocity difference generating functions. The relevant functions are:

$$\langle u_m u_n\rangle_{\rm lin} = \int_{\vec{q}_1} e^{i\vec{q}_1.\vec{x}_{mn}}\frac{\mu_1^2}{q_1^2}P_{\rm L}(q_1)\,, \tag{B.21}$$

$$\langle u_m u_n \rangle_{1\mathrm{L}} = \tag{B.22}$$
$$\int_{\vec{q}_1} e^{i\vec{q}_1.\vec{x}_{mn}} \frac{\mu_1^2}{q_1^2} \left[2 \int_{\vec{q}_2} G_2(\vec{q}_1 - \vec{q}_2, \vec{q}_2)^2 P_{\mathrm{L}}(|\vec{q}_1 - \vec{q}_2|) P_{\mathrm{L}}(q_2) + 6 P_{\mathrm{L}}(q_1) \int_{\vec{q}_2} G_3(\vec{q}_1, -\vec{q}_2, \vec{q}_2) P_{\mathrm{L}}(q_2) \right]$$

$$\langle u^2 \rangle_{\mathrm{lin}} = \int_{\vec{q}_1} \frac{\mu_1^2}{q_1^2} P_{\mathrm{L}}(q_1)\,, \tag{B.23}$$

$$\langle u^2 \rangle_{1\mathrm{L}} = \tag{B.24}$$
$$\int_{\vec{q}_1} \frac{\mu_1^2}{q_1^2} \left[2 \int_{\vec{q}_2} G_2(\vec{q}_1 - \vec{q}_2, \vec{q}_2)^2 P_{\mathrm{L}}(|\vec{q}_1 - \vec{q}_2|) P_{\mathrm{L}}(q_2) + 6 P_{\mathrm{L}}(q_1) \int_{\vec{q}_2} G_3(\vec{q}_1, -\vec{q}_2, \vec{q}_2) P_{\mathrm{L}}(q_2) \right],$$

$$\langle u_m^2 u_n \rangle_{\mathrm{tree}} = 2i \left[2 \int_{\vec{q}_1, \vec{q}_2} e^{i\vec{q}_1.\vec{x}_{mn}} \frac{\mu_1 \mu_2 \mu_{12}}{q_1 q_2 q_{12}} G_2(\vec{q}_1, \vec{q}_2) P_{\mathrm{L}}(q_1) P_{\mathrm{L}}(q_2) \right. \tag{B.25}$$
$$\left. - \int_{\vec{q}_1, \vec{q}_2} e^{i\vec{q}_{12}.\vec{x}_{mn}} \frac{\mu_1 \mu_2 \mu_{12}}{q_1 q_2 q_{12}} G_2(\vec{q}_1, \vec{q}_2) P_{\mathrm{L}}(q_1) P_{\mathrm{L}}(q_2) \right],$$

$$\langle u_1 u_2 u_3 \rangle_{\mathrm{tree}} = -i \int_{\vec{q}_1, \vec{q}_2} e^{i\vec{q}_1.\vec{x}_{13}} e^{i\vec{q}_2.\vec{x}_{23}} \frac{\mu_1 \mu_2 \mu_{12}}{q_1 q_2 q_{12}} \left[2 G_2(\vec{q}_1, \vec{q}_2) P_{\mathrm{L}}(q_1) P_{\mathrm{L}}(q_2) \right.$$
$$\left. + 2 G_2(\vec{q}_1, -\vec{q}_{12}) P_{\mathrm{L}}(q_1) P_{\mathrm{L}}(q_{12}) + 2 G_2(\vec{q}_2, -\vec{q}_{12}) P_{\mathrm{L}}(q_2) P_{\mathrm{L}}(q_2) \right]. \tag{B.26}$$

Bibliography

[1] Abbott, T., Aguena, M., Alarcon, A., Allam, S., Allen, S., Annis, J., Avila, S., Bacon, D., Bechtol, K., Bermeo, A., and et al. (2020). Dark energy survey year 1 results: Cosmological constraints from cluster abundances and weak lensing. *Physical Review D*, 102(2).

[2] Alcock, C. and Paczynski, B. (1979). An evolution free test for non-zero cosmological constant. *Nature*, 281:358.

[3] Amendola, L. et al. (2018). Cosmology and fundamental physics with the Euclid satellite. *Living Reviews in Relativity*, 21(1):2.

[4] Baldauf, T. (2020). Effective Field Theory of Large-Scale Structure. *in: Effective Field Theory in Particle Physics and Cosmology, Edited by: Sacha Davidson, Paolo Gambino, Mikko Laine, Matthias Neubert and Christophe Salomon, Oxford University Press.*

[5] Baldauf, T., Seljak, U., Desjacques, V., and McDonald, P. (2012). Evidence for quadratic tidal tensor bias from the halo bispectrum. *Physical Review D*, 86(8):083540.

[6] Benisty, D. (2020). Reducing the σ_8 tension with the Redshift Space Distortion data set. *arXiv e-prints*, page arXiv:2005.03751.

[7] Bergstrom, L. and Goobar, A. (1999). *Cosmology and particle astrophysics.*

[8] Bernal, J. L., Bellomo, N., Raccanelli, A., and Verde, L. (2020). Beware of commonly used approximations. Part II. Estimating systematic biases in the best-fit parameters. *JCAP*, 2020(10):017.

[9] Bernardeau, F., Colombi, S., Gaztañaga, E., and Scoccimarro, R. (2002). Large-scale structure of the Universe and cosmological perturbation theory. *Physics Reports*, 367(1-3):1–248.

[10] Bertacca, D., Bartolo, N., Bruni, M., Koyama, K., Maartens, R., Matarrese, S., Sasaki, M., and Wands, D. (2015). Galaxy bias and gauges at second order in general relativity. *Classical and Quantum Gravity*, 32(17):175019.

[11] Bertacca, D., Maartens, R., and Clarkson, C. (2014). Observed galaxy number counts on the lightcone up to second order: I. Main result. *JCAP*, 2014(9):037.

[12] Bertacca, D., Maartens, R., Raccanelli, A., and Clarkson, C. (2012). Beyond the plane-parallel and Newtonian approach: wide-angle redshift distortions and convergence in general relativity. *JCAP*, 2012(10):025.

[13] Bertacca, D., Raccanelli, A., Bartolo, N., Liguori, M., Matarrese, S., and Verde, L. (2018). Relativistic wide-angle galaxy bispectrum on the light cone. *Physical Review D*, 97(2):023531.

[14] Beutler, F., Castorina, E., and Zhang, P. (2019). Interpreting measurements of the anisotropic galaxy power spectrum. *JCAP*, 2019(3):040.

[15] Beutler, F. and Di Dio, E. (2020). Modeling relativistic contributions to the halo power spectrum dipole. *JCAP*, 2020(7):048.

[16] Beutler, F. et al. (2014). The clustering of galaxies in the SDSS-III Baryon Oscillation Spectroscopic Survey: testing gravity with redshift space distortions using the power spectrum multipoles. *MNRAS*, 443(2):1065–1089.

[17] Bharadwaj, S. (1999). Radial Redshift Space Distortions. *ApJ*, 516(2):507–518.

[18] Bharadwaj, S., Mazumdar, A., and Sarkar, D. (2020). Quantifying the redshift space distortion of the bispectrum I: primordial non-Gaussianity. *MNRAS*, 493(1):594–602.

[19] Bianchi, D., Gil-Marín, H., Ruggeri, R., and Percival, W. J. (2015). Measuring line-of-sight-dependent Fourier-space clustering using FFTs. *MNRAS*, 453(1):L11–L15.

[20] Blake, C. et al. (2011a). The WiggleZ Dark Energy Survey: measuring the cosmic expansion history using the Alcock-Paczynski test and distant supernovae. *MNRAS*, 418(3):1725–1735.

[21] Blake, C. et al. (2011b). The WiggleZ Dark Energy Survey: testing the cosmological model with baryon acoustic oscillations at z= 0.6. *MNRAS*, 415(3):2892–2909.

[22] Bonvin, C. and Durrer, R. (2011). What galaxy surveys really measure. *Physical Review D*, 84(6):063505.

[23] Bruni, M., Crittenden, R., Koyama, K., Maartens, R., Pitrou, C., and Wands, D. (2012). Disentangling non-Gaussianity, bias, and general relativistic effects in the galaxy distribution. *Physical Review D*, 85(4):041301.

[24] Camera, S., Maartens, R., and Santos, M. G. (2015). Einstein's legacy in galaxy surveys. *MNRAS*, 451:L80–L84.

[25] Castorina, E. and Di Dio, E. (2022). The observed galaxy power spectrum in General Relativity. *JCAP*, 2022(1):061.

[26] Castorina, E. and White, M. (2018a). Beyond the plane-parallel approximation for redshift surveys. *MNRAS*, 476(4):4403–4417.

[27] Castorina, E. and White, M. (2018b). The Zeldovich approximation and wide-angle redshift-space distortions. *MNRAS*, 479(1):741–752.

[28] Castorina, E. and White, M. (2020). Wide-angle effects for peculiar velocities. *MNRAS*, 499(1):893–905.

[29] Challinor, A. and Lewis, A. (2011). Linear power spectrum of observed source number counts. *Physical Review D*, 84(4):043516.

[30] Chan, K. C., Scoccimarro, R., and Sheth, R. K. (2012). Gravity and large-scale nonlocal bias. *Physical Review D*, 85(8):083509.

[31] Chuang, C.-H. et al. (2016). The clustering of galaxies in the SDSS-III Baryon Oscillation Spectroscopic Survey: single-probe measurements from CMASS anisotropic galaxy clustering. *MNRAS*, 461(4):3781–3793.

[32] Clarkson, C., de Weerd, E. M., Jolicoeur, S., Maartens, R., and Umeh, O. (2019). The dipole of the galaxy bispectrum. *MNRAS*, 486(1):L101–L104.

[33] Cole, S., Fisher, K. B., and Weinberg, D. H. (1995). Constraints on Omega from the IRAS redshift surveys. *MNRAS*, 275(2):515–526.

[34] Contreras, D., Johnson, M. C., and Mertens, J. B. (2019). Towards detection of relativistic effects in galaxy number counts using kSZ tomography. *JCAP*, 2019(10):024.

[35] Dalal, N., Doré, O., Huterer, D., and Shirokov, A. (2008). Imprints of primordial non-Gaussianities on large-scale structure: Scale-dependent bias and abundance of virialized objects. *PhysRevD*, 77(12):123514.

[36] D'Amico, G., Lewandowski, M., Senatore, L., and Zhang, P. (2022). Limits on primordial non-Gaussianities from BOSS galaxy-clustering data. *arXiv e-prints*, page arXiv:2201.11518.

[37] de la Torre, S. et al. (2013). The VIMOS Public Extragalactic Redshift Survey (VIPERS) . Galaxy clustering and redshift-space distortions at z $\simeq$ 0.8 in the first data release. *AAP*, 557:A54.

[38] DESI Collaboration, Aghamousa, A., Aguilar, J., et al. (2016). The DESI Experiment Part I: Science,Targeting, and Survey Design. *arXiv e-prints*, page arXiv:1611.00036.

[39] Desjacques, V., Jeong, D., and Schmidt, F. (2018a). Large-scale galaxy bias. *Physics Reports*, 733:1–193.

[40] Desjacques, V., Jeong, D., and Schmidt, F. (2018b). Large-scale galaxy bias. *Physics Reports*, 733:1–193.

[41] Desjacques, V., Jeong, D., and Schmidt, F. (2018c). The galaxy power spectrum and bispectrum in redshift space. *JCAP*, 2018(12):035.

[42] Di Dio, E. and Beutler, F. (2020). The relativistic galaxy number counts in the weak field approximation. *Journal of Cosmology and Astroparticle Physics*, 2020(9):058.

[43] Di Dio, E., Durrer, R., Maartens, R., Montanari, F., and Umeh, O. (2019). The full-sky angular bispectrum in redshift space. *JCAP*, 2019(4):053.

[44] Di Dio, E. and Seljak, U. (2019). The relativistic dipole and gravitational redshift on LSS. *JCAP*, 2019(4):050.

[45] Doré, O. et al. (2014). Cosmology with the SPHEREX All-Sky Spectral Survey. *arXiv e-prints*, page arXiv:1412.4872.

[46] Durrer, R., Jalilvand, M., Kothari, R., Maartens, R., and Montanari, F. (2020). Full-sky bispectrum in redshift space for 21cm intensity maps. *JCAP*, 2020(12):003.

[47] eBOSS Collaboration, Alam, S., Aubert, M., et al. (2020). The Completed SDSS-IV extended Baryon Oscillation Spectroscopic Survey: Cosmological Implications from two Decades of Spectroscopic Surveys at the Apache Point observatory. *arXiv e-prints*, page arXiv:2007.08991.

[48] Eggemeier, A., Scoccimarro, R., Crocce, M., Pezzotta, A., and Sánchez, A. G. (2020). Testing one-loop galaxy bias: Power spectrum. *PhysRevD*, 102(10):103530.

[49] Eggemeier, A., Scoccimarro, R., and Smith, R. E. (2019). Bias loop corrections to the galaxy bispectrum. *Physical Review D*, 99(12):123514.

[50] Eggemeier, A., Scoccimarro, R., Smith, R. E., Crocce, M., Pezzotta, A., and Sánchez, A. G. (2021). Testing one-loop galaxy bias: Joint analysis of power spectrum and bispectrum. *Physical Review D*, 103(12):123550.

[51] Elkhashab, M. Y., Porciani, C., and Bertacca, D. (2022). The large-scale monopole of the power spectrum in a Euclid-like survey: wide-angle effects, lensing, and the 'finger of the observer'. *MNRAS*, 509(2):1626–1645.

[52] Euclid Collaboration, Blanchard, A., et al. (2020). Euclid preparation. VII. Forecast validation for Euclid cosmological probes. *Astronomy and Astrophysics*, 642:A191.

[53] Garcia, K. and Slepian, Z. (2020). Improving the Line of Sight for the Anisotropic 3-Point Correlation Function of Galaxies: Centroid and Unit-Vector-Average Methods Scaling as $O(N^2)$. *arXiv e-prints*, page arXiv:2011.03503.

[54] Gaztanaga, E., Bonvin, C., and Hui, L. (2017). Measurement of the dipole in the cross-correlation function of galaxies. *JCAP*, 01:032.

[55] Gil-Marín, H. et al. (2020). The Completed SDSS-IV extended Baryon Oscillation Spectroscopic Survey: measurement of the BAO and growth rate of structure of the luminous red galaxy sample from the anisotropic power spectrum between redshifts 0.6 and 1.0. *arXiv e-prints*, page arXiv:2007.08994.

[56] Grasshorn Gebhardt, H. S. and Jeong, D. (2020). Nonlinear redshift-space distortions in the harmonic-space galaxy power spectrum. *PhysRevD*, 102(8):083521.

[57] Grieb, J. N., Sánchez, A. G., Salazar-Albornoz, S., and Dalla Vecchia, C. (2016). Gaussian covariance matrices for anisotropic galaxy clustering measurements. *MNRAS*, 457(2):1577–1592.

[58] Grimm, N., Scaccabarozzi, F., Yoo, J., Biern, S. G., and Gong, J.-O. (2020). Galaxy power spectrum in general relativity. *JCAP*, 2020(11):064.

[59] Hahn, C. and Villaescusa-Navarro, F. (2021). Constraining M_ν with the bispectrum. Part II. The information content of the galaxy bispectrum monopole. *JCAP*, 2021(4):029.

[60] Hahn, C., Villaescusa-Navarro, F., Castorina, E., and Scoccimarro, R. (2020). Constraining M_ν with the bispectrum. Part I. Breaking parameter degeneracies. *JCAP*, 2020(3):040.

[61] Hamilton, A. J. S. (1992). Measuring Omega and the Real Correlation Function from the Redshift Correlation Function. *ApJL*, 385:L5.

[62] Hashimoto, I., Rasera, Y., and Taruya, A. (2017). Precision cosmology with redshift-space bispectrum: A perturbation theory based model at one-loop order. *Physical Review D*, 96(4):043526.

[63] Hwang, J.-c., Noh, H., Jeong, D., Gong, J.-O., and Biern, S. G. (2015). Non-linear power spectra in the synchronous gauge. *JCAP*, 2015(5):055–055.

[64] Jeong, D. and Schmidt, F. (2019). The Odd-Parity Galaxy Bispectrum. *arXiv e-prints*, page arXiv:1906.05198.

[65] Jeong, D., Schmidt, F., and Hirata, C. M. (2012). Large-scale clustering of galaxies in general relativity. *Physical Review D*, 85(2):023504.

[66] Jolicoeur, S., Maartens, R., De Weerd, E. M., Umeh, O., Clarkson, C., and Camera, S. (2021). Detecting the relativistic bispectrum in 21cm intensity maps. *JCAP*, 2021(6):039.

[67] Kaiser, N. (1987). Clustering in real space and in redshift space. *MNRAS*, 227(1):1–21.

[68] Karagiannis, D., Lazanu, A., Liguori, M., Raccanelli, A., Bartolo, N., and Verde, L. (2018). Constraining primordial non-Gaussianity with bispectrum and power spectrum from upcoming optical and radio surveys. *MNRAS*, 478(1):1341–1376.

[69] Kehagias, A., Dizgah, A. M., Noreña, J., Perrier, H., and Riotto, A. (2015). A consistency relation for the observed galaxy bispectrum and the local non-Gaussianity from relativistic corrections. *JCAP*, 2015(8):018–018.

[70] Lahav, O. and Liddle, A. R. (2024). The Cosmological Parameters (2023). *arXiv e-prints*, page arXiv:2403.15526.

[71] Lazeyras, T., Wagner, C., Baldauf, T., and Schmidt, F. (2016). Precision measurement of the local bias of dark matter halos. *JCAP*, 2016(2):018.

[72] Lorenz, C. S., Alonso, D., and Ferreira, P. G. (2018). Impact of relativistic effects on cosmological parameter estimation. *Physical Review D*, 97(2):023537.

[73] Ma, C.-P. and Bertschinger, E. (1995). Cosmological perturbation theory in the synchronous and conformal newtonian gauges. *The Astrophysical Journal*, 455:7.

[74] Maartens, R., Jolicoeur, S., Umeh, O., De Weerd, E. M., and Clarkson, C. (2021). Local primordial non-Gaussianity in the relativistic galaxy bispectrum. *JCAP*, 2021(4):013.

[75] Maartens, R., Jolicoeur, S., Umeh, O., De Weerd, E. M., Clarkson, C., and Camera, S. (2020). Detecting the relativistic galaxy bispectrum. *JCAP*, 2020(3):065.

[76] Matsubara, T. (2000). The Correlation Function in Redshift Space: General Formula with Wide-Angle Effects and Cosmological Distortions. *ApJ*, 535(1):1–23.

[77] Mazumdar, A., Bharadwaj, S., and Sarkar, D. (2020). Quantifying the redshift space distortion of the bispectrum II: induced non-Gaussianity at second-order perturbation. *MNRAS*, 498(3):3975–3984.

[78] McDonald, P. (2009). Gravitational redshift and other redshift-space distortions of the imaginary part of the power spectrum. *JCAP*, 2009(11):026.

[79] Mitsou, E., Yoo, J., and Magi, M. (2023). Infrared (in)sensitivity of relativistic effects in cosmological observable statistics. *arXiv e-prints*, page arXiv:2302.00427.

[80] Moradinezhad Dizgah, A., Biagetti, M., Sefusatti, E., Desjacques, V., and Noreña, J. (2021). Primordial non-Gaussianity from biased tracers: likelihood analysis of real-space power spectrum and bispectrum. *JCAP*, 2021(5):015.

[81] Noorikuhani, M. and Scoccimarro, R. (2023). Wide-angle and relativistic effects in Fourier-space clustering statistics. *Physical Review D*, 107(8):083528.

[82] Oddo, A., Rizzo, F., Sefusatti, E., Porciani, C., and Monaco, P. (2021). Cosmological parameters from the likelihood analysis of the galaxy power spectrum and bispectrum in real space. *JCAP*, 2021(11):038.

[83] Oddo, A., Sefusatti, E., Porciani, C., Monaco, P., and Sánchez, A. G. (2020). Toward a robust inference method for the galaxy bispectrum: likelihood function and model selection. *JCAP*, 2020(3):056.

[84] Pápai, P. and Szapudi, I. (2008). Non-perturbative effects of geometry in wide-angle redshift distortions. *MNRAS*, 389(1):292–296.

[85] Pardede, K., Di Dio, E., and Castorina, E. (2023). Wide-angle effects in the galaxy bispectrum. *arXiv e-prints*, page arXiv:2302.12789.

[86] Peacock, J. A. and Dodds, S. J. (1994). Reconstructing the Linear Power Spectrum of Cosmological Mass Fluctuations. *MNRAS*, 267:1020.

[87] Peacock, J. A. and Dodds, S. J. (1996). Non-linear evolution of cosmological power spectra. *MNRAS*, 280(3):L19–L26.

[88] Peebles, P. (1980). *The large-scale structure of the universe*. Princeton University Press.

[89] Peebles, P. J. E. (1993). *Principles of Physical Cosmology*.

[90] Philcox, O. H. E., Ivanov, M. M., Cabass, G., Simonović, M., Zaldarriaga, M., and Nishimichi, T. (2022). Cosmology with the redshift-space galaxy bispectrum monopole at one-loop order. *Physical Review D*, 106(4):043530.

[91] Raccanelli, A., Bertacca, D., Jeong, D., Neyrinck, M. C., and Szalay, A. S. (2018). Doppler term in the galaxy two-point correlation function: Wide-angle, velocity, Doppler lensing and cosmic acceleration effects. *Physics of the Dark Universe*, 19:109–123.

[92] Raccanelli, A. et al. (2013). Testing gravity using large-scale redshift-space distortions. *MNRAS*, 436(1):89–100.

[93] Raccanelli, A., Samushia, L., and Percival, W. J. (2010). Simulating redshift-space distortions for galaxy pairs with wide angular separation. *MNRAS*, 409(4):1525–1533.

[94] Reid, B. A. et al. (2012). The clustering of galaxies in the SDSS-III Baryon Oscillation Spectroscopic Survey: measurements of the growth of structure and expansion rate at z = 0.57 from anisotropic clustering. *MNRAS*, 426(4):2719–2737.

[95] Reimberg, P., Bernardeau, F., and Pitrou, C. (2016). Redshift-space distortions with wide angular separations. *JCAP*, 2016(1):048.

[96] Ruggeri, R., Castorina, E., Carbone, C., and Sefusatti, E. (2018). DEMNUni: massive neutrinos and the bispectrum of large scale structures. *JCAP*, 2018(3):003.

[97] Sachs, R. K. and Wolfe, A. M. (1967). Perturbations of a Cosmological Model and Angular Variations of the Microwave Background. *ApJ*, 147:73.

[98] Samushia, L., Branchini, E., and Percival, W. J. (2015). Geometric biases in power-spectrum measurements. *Monthly Notices of the Royal Astronomical Society*, 452(4):3704–3709.

[99] Samushia, L. et al. (2014). The clustering of galaxies in the SDSS-III Baryon Oscillation Spectroscopic Survey: measuring growth rate and geometry with anisotropic clustering. *MNRAS*, 439(4):3504–3519.

[100] Sánchez, A. G. et al. (2014). The clustering of galaxies in the SDSS-III Baryon Oscillation Spectroscopic Survey: cosmological implications of the full shape of the clustering wedges in the data release 10 and 11 galaxy samples. *MNRAS*, 440(3):2692–2713.

[101] Sánchez, A. G., Scoccimarro, R., Crocce, M., Grieb, J. N., Salazar-Albornoz, S., Dalla Vecchia, C., Lippich, M., Beutler, F., Brownstein, J. R., Chuang, C.-H., Eisenstein, D. J., Kitaura, F.-S., Olmstead, M. D., Percival, W. J., Prada, F., Rodríguez-Torres, S., Ross, A. J., Samushia, L., Seo, H.-J., Tinker, J., Tojeiro, R., Vargas-Magaña, M., Wang, Y., and Zhao, G.-B. (2017). The clustering of galaxies in the completed SDSS-III Baryon Oscillation Spectroscopic Survey: Cosmological implications of the configuration-space clustering wedges. *MNRAS*, 464(2):1640–1658.

[102] Scaccabarozzi, F., Yoo, J., and Biern, S. G. (2018). Galaxy two-point correlation function in general relativity. *JCAP*, 2018(10):024.

[103] Scoccimarro, R. (2004). Redshift-space distortions, pairwise velocities, and nonlinearities. *Physical Review D*, 70(8).

[104] Scoccimarro, R. (2015). Fast estimators for redshift-space clustering. *Physical Review D*, 92(8):083532.

[105] Scoccimarro, R. (2024). Pairwise velocities at infinity and the redshift-space power spectrum. *In progress*.

[106] Scoccimarro, R., Couchman, H. M. P., and Frieman, J. A. (1999). The Bispectrum as a Signature of Gravitational Instability in Redshift Space. *ApJ*, 517(2):531–540.

[107] Shiraishi, M., Akitsu, K., and Okumura, T. (2021a). Alcock-Paczynski effects on wide-angle galaxy statistics. *PhysRevD*, 103(12):123534.

[108] Shiraishi, M., Taruya, A., Okumura, T., and Akitsu, K. (2021b). Wide-angle effects on galaxy ellipticity correlations. *MNRAS*, 503(1):L6–L10.

[109] Slepian, Z. and Eisenstein, D. J. (2017). Modelling the large-scale redshift-space 3-point correlation function of galaxies. *MNRAS*, 469(2):2059–2076.

[110] Slosar, A., Hirata, C., Seljak, U., Ho, S., and Padmanabhan, N. (2008). Constraints on local primordial non-Gaussianity from large scale structure. *JCAP*, 2008(8):031.

[111] Spergel, D., Gehrels, N., Baltay, C., Bennett, D., et al. (2015). Wide-Field InfrarRed Survey Telescope-Astrophysics Focused Telescope Assets WFIRST-AFTA 2015 Report. *arXiv e-prints*, page arXiv:1503.03757.

[112] Szalay, A. S., Matsubara, T., and Landy, S. D. (1998). Redshift-Space Distortions of the Correlation Function in Wide-Angle Galaxy Surveys. *ApJL*, 498(1):L1–L4.

[113] Szapudi, I. (2004). Wide-Angle Redshift Distortions Revisited. *ApJ*, 614(1):51–55.

[114] Tansella, V., Bonvin, C., Durrer, R., Ghosh, B., and Sellentin, E. (2018). The full-sky relativistic correlation function and power spectrum of galaxy number counts. Part I: theoretical aspects. *JCAP*, 2018(3):019.

[115] Taruya, A., Saga, S., Breton, M.-A., Rasera, Y., and Fujita, T. (2020). Wide-angle redshift-space distortions at quasi-linear scales: cross-correlation functions from Zel'dovich approximation. *MNRAS*, 491(3):4162–4179.

[116] Tellarini, M., Ross, A. J., Tasinato, G., and Wands, D. (2016). Galaxy bispectrum, primordial non-Gaussianity and redshift space distortions. *JCAP*, 2016(6):014.

[117] Viljoen, J.-A., Fonseca, J., and Maartens, R. (2021). Multi-wavelength spectroscopic probes: biases from neglecting light-cone effects. *JCAP*, 2021(12):004.

[118] Wadekar, D. and Scoccimarro, R. (2020). Galaxy power spectrum multipoles covariance in perturbation theory. *PhysRevD*, 102(12):123517.

[119] Wang, M. S., Beutler, F., and Bacon, D. (2020). Impact of relativistic effects on the primordial non-Gaussianity signature in the large-scale clustering of quasars. *MNRAS*, 499(2):2598–2607.

[120] Yamamoto, K., Nakamichi, M., Kamino, A., Bassett, B. A., and Nishioka, H. (2006). A Measurement of the Quadrupole Power Spectrum in the Clustering of the 2dF QSO Survey. *Publications of the Astronomical Society of Japan*, 58:93–102.

[121] Yankelevich, V. and Porciani, C. (2019). Cosmological information in the redshift-space bispectrum. *MNRAS*, 483(2):2078–2099.

[122] Yoo, J. (2009). Complete treatment of galaxy two-point statistics: Gravitational lensing effects and redshift-space distortions. *PhysRevD*, 79(2):023517.

[123] Yoo, J. (2010). General relativistic description of the observed galaxy power spectrum: Do we understand what we measure? *Physical Review D*, 82(8):083508.

[124] Yoo, J., Fitzpatrick, A. L., and Zaldarriaga, M. (2009). New perspective on galaxy clustering as a cosmological probe: General relativistic effects. *Physical Review D*, 80(8):083514.

[125] Yoo, J. and Gong, J.-O. (2016). Exact analytic solution for non-linear density fluctuation in a ΛCDM universe. *JCAP*, 2016(7):017.

[126] Yoo, J. and Seljak, U. (2015). Wide-angle effects in future galaxy surveys. *MNRAS*, 447(2):1789–1805.

[127] Yoo, J. and Zaldarriaga, M. (2014). Beyond the linear-order relativistic effect in galaxy clustering: Second-order gauge-invariant formalism. *Physical Review D*, 90(2):023513.

[128] Zhang, Y. et al. (2020). Testing General Relativity on cosmological scales at redshift $z \sim 1.5$ with quasar and CMB lensing. *arXiv e-prints*, page arXiv:2007.12607.

[129] Zhang, Y., Pullen, A. R., and Maniyar, A. S. (2021). Joint analyses of 2D CMB lensing and 3D galaxy clustering in the spherical Fourier-Bessel basis. *PhysRevD*, 104(10):103523.

[130] Zheng, Z., Coil, A. L., and Zehavi, I. (2007). Galaxy Evolution from Halo Occupation Distribution Modeling of DEEP2 and SDSS Galaxy Clustering. *The Astrophysical Journal*, 667(2):760–779.